

Computational Material Science of Carbon/Carbon Composites based on Carbonaceous Mesophase Matrices

Gaurav Gupta

Master of Engineering

Department of Chemical Engineering

McGill University

Montreal, Quebec

August 2005

A thesis submitted to the Faculty of Graduate Studies and Research in Partial fulfillment
of the requirements for the degree of Master of Engineering

©Gaurav Gupta 2005 All rights reserved



Library and
Archives Canada

Bibliothèque et
Archives Canada

Published Heritage
Branch

Direction du
Patrimoine de l'édition

395 Wellington Street
Ottawa ON K1A 0N4
Canada

395, rue Wellington
Ottawa ON K1A 0N4
Canada

Your file *Votre référence*
ISBN: 978-0-494-22646-9
Our file *Notre référence*
ISBN: 978-0-494-22646-9

NOTICE:

The author has granted a non-exclusive license allowing Library and Archives Canada to reproduce, publish, archive, preserve, conserve, communicate to the public by telecommunication or on the Internet, loan, distribute and sell theses worldwide, for commercial or non-commercial purposes, in microform, paper, electronic and/or any other formats.

The author retains copyright ownership and moral rights in this thesis. Neither the thesis nor substantial extracts from it may be printed or otherwise reproduced without the author's permission.

AVIS:

L'auteur a accordé une licence non exclusive permettant à la Bibliothèque et Archives Canada de reproduire, publier, archiver, sauvegarder, conserver, transmettre au public par télécommunication ou par l'Internet, prêter, distribuer et vendre des thèses partout dans le monde, à des fins commerciales ou autres, sur support microforme, papier, électronique et/ou autres formats.

L'auteur conserve la propriété du droit d'auteur et des droits moraux qui protègent cette thèse. Ni la thèse ni des extraits substantiels de celle-ci ne doivent être imprimés ou autrement reproduits sans son autorisation.

In compliance with the Canadian Privacy Act some supporting forms may have been removed from this thesis.

Conformément à la loi canadienne sur la protection de la vie privée, quelques formulaires secondaires ont été enlevés de cette thèse.

While these forms may be included in the document page count, their removal does not represent any loss of content from the thesis.

Bien que ces formulaires aient inclus dans la pagination, il n'y aura aucun contenu manquant.


Canada

To my parents ,
for their unconditional love and support

ABSTRACT

Carbon/Carbon composites belong to the generic class of fiber reinforced composites and are widely used because of their high strength as well as chemical and thermal stability. Like other fiber reinforced composites they consist of the fibers which act as reinforcements and matrix which acts as a glue that binds the fibers. c/c composites from pitch based precursor are unique since the matrix in this case is a liquid crystal or mesophase. This makes them remarkable in the sense that unlike c/c composites from other precursors such as PAN, rayon etc. they have extremely high degree of molecular orientation and exhibit texture. An important characteristic of their textures is the presence of topological defects. It is hence of great interest to understand and elucidate the principles that govern the formation of textures so as to optimize their properties. In this work we present a computational study of structure formation in carbon-carbon composites that describes the emergence of topological defects due to the distortions in the oriented matrix created by the presence of fiber matrix interaction. Dynamical and structural features of texture formation were characterized using gradient elasticity and defect physics.

ABRÉGÉ

Les composites carbone/carbone appartiennent à la classe générique des composites renforcés par fibres et sont couramment utilisés à cause de leur grande solidité ainsi que leur stabilité chimique et thermal. Comme d'autres composites renforcés par fibres, ils consistent de fibres agissant comme renforçant et d'une matrice qui agit comme une colle reliant les fibres. Les composites c/c basés sur des précurseurs pitch sont uniques étant donné que la matrice est dans ce cas un cristal liquide ou mésophase. Ceci les rends remarquable dans le sens qu'à la différence de composites c/c obtenu avec d'autres précurseur tel que PAN, rayon etc. ils ont un très grand degré d'alignement moléculaire et ils exhibent des textures. Une importante caractéristique de ces textures est la présence de défauts topologiques. Il est donc d'un grand intérêt de comprendre et d'élucider les principes gouvernant la formation des textures pour en optimiser les propriétés. Dans ce travail nous présentons une étude numérique de la formation de structures dans les composites carbone/carbones qui décrit l'émergence de défauts topologiques du aux distorsions dans la matrice orienté créés par la présence d'interaction matrice-fibres. Les caractéristiques dynamiques et structurelles de la formation de textures ont été caractérisées en utilisant la physique des gradients d'élasticités et des défauts.

FOREWORD

The present author chooses the manuscript-based thesis option according to the Guidelines for Thesis Preparation given by the Faculty of Graduate Studies and Research. The following is excerpts from the Guidelines for thesis preparation.

As an alternative to the traditional thesis format, the thesis can consist of a collection of papers of which the student is an author or co-author. These papers must have a cohesive, unitary character making them a report of a single program of research. Candidates have the option of including, as part of the thesis, the text of one or more papers submitted, or to be submitted, for publication, or the clearly-duplicated text (not the reprints) of one or more published papers. These texts must conform to the "Guidelines for Thesis Preparation" with respect to font size, line spacing and margin sizes and must be bound together as an integral part of the thesis. (Reprints of published papers can be included in the appendices at the end of the thesis.) The thesis must be more than a collection of manuscripts. All components must be integrated into a cohesive unit with a logical progression from one chapter to the next. In order to ensure that the thesis has continuity, connecting texts that provide logical bridges preceding and following each manuscript are mandatory.

When previously published copyright material is presented in a thesis, the candidate must include signed waivers from the publishers and submit these to the Graduate and Postdoctoral Studies Office with the final deposition, if not submitted previously. The candidate must also include signed waivers from any co-authors of unpublished manuscripts.

Contribution of Authors

Contents of Chapter 3 to 5 of the present thesis are adopted or revised from the papers that have been published or submitted for publication in scientific journals under the normal supervision of my research supervisor, Professor A. D. Rey, who is also a co-author. In

Chapter 3, Mr. Dae Kun Hwang pursued optical modeling to validate computational results for periodic lattices in carbonaceous mesophases, and he is the co-author of the corresponding paper.

Dear Gaurav Gupta:

Thank you for requesting permission to reproduce material from American Institute of Physics publications.

Permission is granted for the following article: Journal of Chemical Physics 122, (3): 034902-11 (2005),

to be included as part of your thesis.

Please be sure to include an appropriate credit line referencing the original source of the material.

Sincerely,

Susann Brailey

Office of the Publisher, Journals and Technical Publications

Rights & Permissions

American Institute of Physics

Suite 1NO1

2 Huntington Quadrangle

Melville, NY 11747-4502

516-576-2268 TEL

516-576-2450 FAX

rights@aip.org



ELSEVIER

25 July 2005

425-125

YEARS OF PUBLISHING
TRADITION | EXCELLENCE

We commemorate the founding
of the House of Elsevier in 1580
and celebrate the establishment
of the Elsevier company in 1880.

Our ref: HG/HDN/JUL05/J094

Gaurav Gupta
McGill University
Dept of Chemical Engineering
Montreal, H3A 2B2
Canada

Dear Sir/Madam

CARBON, Vol 43, No 7, 2005, pp 1400 – 1406, G Gupta, "Texture..."

As per your letter dated 21st July 2005, we hereby grant you permission to reprint the aforementioned material at no charge in your thesis subject to the following conditions:

1. If any part of the material to be used (for example, figures) has appeared in our publication with credit or acknowledgement to another source, permission must also be sought from that source. If such permission is not obtained then that material may not be included in your publication/copies.
2. Suitable acknowledgment to the source must be made, either as a footnote or in a reference list at the end of your publication, as follows:

"Reprinted from Publication title, Vol number, Author(s), Title of article, Pages No., Copyright (Year), with permission from Elsevier".
3. Reproduction of this material is confined to the purpose for which permission is hereby given.
4. This permission is granted for non-exclusive world English rights only. For other languages please reapply separately for each one required. Permission excludes use in an electronic form. Should you have a specific electronic project in mind please reapply for permission.
5. This includes permission for the National Library of Canada to supply single copies, on demand, of the complete thesis. Should your thesis be published commercially, please reapply for permission.

Yours sincerely

Helen Gainford
Rights Manager

Your future requests will be handled more quickly if you complete the online form at www.elsevier.com/locate/permissions

ACKNOWLEDGEMENTS

I would like to express my sincere gratitude to Professor A. D. Rey for his support, guidance and patience during the project. I was very lucky to work with him since he has an exceptional ability to relate complex physical problems to their quantitative meaning, making him an excellent choice to do computational research. Professor Rey is highly dedicated towards research and is an excellent motivator. I am especially grateful to him for encouraging and supporting me not only for the project but also during my personnel struggles.

My stay at complex fluid group was made easier and enjoyable by the amazing group we have. Benjamin Wincure helped me in the initial stages of the project by providing his detailed notes. I always found my discussions with him very helpful in improving my understanding of the project. Thanks are due to Rillar and Gino for being faithful beer buddies. Life would have been very dull without our occasional outings. I am also thankful to Susanta Das a post doc in the group for helping me with so many issues. I express my gratitude towards Dana, Luiz, Majid, Samir, Malena and Ae-Gyeong who made my stay here a pleasant one. Outside lab I made a great friend Ian. I will miss our squash and soccer outings and i wish him the best in life.

I would like to thank my sister Goldie and brother Shantanu who religiously called me and I apologize for not being able to return their calls as often as I would have liked. And finally my parents who have always supported me in whatever i chose to do and provided solid advice throughout my life.

TABLE OF CONTENTS

DEDICATION	ii
ABSTRACT	iii
ABRÉGÉ	iv
ACKNOWLEDGEMENTS	xi
LIST OF TABLES	xiv
LIST OF FIGURES	xv
1 Introduction	1
1.1 Thesis Motivation	1
1.2 Carbonaceous Mesophase Pitches	5
1.2.1 Description of the mesophase	5
1.2.2 Formation of the Mesophase	7
1.2.3 Textures in Carbonaceous Mesophase based c/c composites	8
1.2.4 Disclinations = Line Defects	10
1.2.5 Processing of c/c composites	12
1.3 Introduction to Liquid Crystals	14
1.3.1 Classification of Liquid Crystals [14]	14
1.4 Experimental Observations related to the Thesis	16
1.5 Thesis Objective	22
1.6 Thesis Methodology	22
1.7 Thesis Organization	23
1.8 References	25
2 Theory and Methodology	27
2.1 Introduction	27
2.2 State of the art in modeling liquid crystalline systems, [7]	27
2.3 Order Parameter	28
2.4 Landau-de Gennes Theory [16]	31
2.5 Carbonaceous Mesophase texture modeling: theory and derivation	34
2.6 Texture Equation for Carbonaceous Mesophase	36

2.7	Computational Modeling	37
2.8	Validation Methodology	41
2.9	References	43
3	Optical and structural modeling of disclination lattices in carbonaceous mesophase	45
3.1	Abstract	45
3.2	Introduction	45
3.3	Microstructural, Optical and Computational Modeling	50
	3.3.1 Microstructural Model for Carbonaceous Mesophases	50
	3.3.2 Optical Modeling	64
3.4	Results and Discussions:	68
	3.4.1 Disclination Lattice Microstructure	68
	3.4.2 Computational Reflection Polarized Optical Microscopy	72
3.5	Conclusions	75
3.6	Acknowledgements	76
3.7	References	77
4	Texture Modeling in Carbon-Carbon Composites based on Mesophase Precursor Matrices	80
4.1	Abstract	80
4.2	Introduction	80
4.3	Theory and Modeling	85
	4.3.1 Microstructure Modeling	85
	4.3.2 Textures in Carbon-Mesophase Carbon Composites	89
4.4	Computational Results and Discussion	92
4.5	Conclusions	95
4.6	Acknowledgments	96
4.7	References	97
5	Texture Rules for Concentrated Filled Nematics	99
5.1	Abstract	99
5.2	Introduction and Discussion	99
6	Conclusions	112
	APPENDIX A	114

LIST OF TABLES

<u>Table</u>		<u>page</u>
5-1	Experimental Textures [13] for c/c composites	101

LIST OF FIGURES

<u>Figure</u>		<u>page</u>
1-1	Schematic showing superior strength and light weighted-ness of the composites. Taken from; http://www.composites-by-design.com/advanced-composites.htm	2
1-2	Shows some of the possible arrangements of fibers inside the matrix. The first is random arrangement of fibers and the next two have fibers aligned in a particular fashion.	2
1-3	Mechanical properties of three c/c composites (A, B, C) and graphite (G). From Ref. kato . (A=pitch based, B=PAN, C=Rayon, D=graphite).	3
1-4	Shows a comparison of carbon fiber composite with phenolic resin and carbonaceous mesophase as the matrices. When light is shone through the samples, isotropic liquid shows black whereas anisotropic substance shows birefringence and show optical response. The c/c composites with mesophase show texture whereas the phenolic resin is isotropic and there is no orientation. Adapted from [3].	4
1-5	Schematic of disk shaped CM molecules. The director n is the average orientation of the unit normals u to the disklike molecules in a discotic nematic phase.	6
1-6	Schematic model of stacking of carbonaceous mesophase molecules adapted from [5]	6
1-7	Some model structure for mesophase-forming molecules, adapted from [5]	7
1-8	Picture showing growth of carbonaceous mesophase spheres known as spherules. Taken from http://www.shanshantech.com/eptoduct-a.htm	8
1-9	Experimental picture reference [7] indicating the presence of texture in carbonaceous mesophase. The picture is section of the composite transverse to the axis of the fiber bundle, mapped by polarized-light micrography with immersion oil.	9

1-10	Top row shows schematics of defects textures in liquid crystals. Bottom pictures are SEM images of disclination observed in carbonaceous mesophase taken from reference reference [5].	11
1-11	The optical microscope picture showing defects in a nematic liquid crystal. .	12
1-12	Processing of c/c composites. From reference [13]	13
1-13	Schematic representation of rodlike and disklike molecules in space in a nematic liquid crystal.	15
1-14	Schematic representation of cholesteric. Rodlike molecules are represented by small segments lying on a series of equidistant planes. The structure is continuous and P here represents the pitch.	16
1-15	schematic representation of Smectic A structure.	16
1-16	The schematic illustrates different length scales observed in a c/c composite. It is of great interest to control both the meso (R and L1) and nano (defect cores) scales of the system to optimize the performance of these systems.	18
1-17	Schematic of a c/c composite showing two different defect core structures. Adapted from reference [7].	19
1-18	Schematic design of spinneret with the screen modification for controlling the texture of the mesophase. Adapted from reference, [17].	20
1-19	Effect of manipulating the mesophase texture from reference [16]. These pictures are optical micrographs(a) No manipulation was done. (b) Manipulation was done by passing through a 200 mesh screen.	21
1-20	A more detailed picture of the disclination lattice adapted from reference [16]. The arrows indicate the presence of different defect types.	22
2-1	Schematic of a disklike molecule.	29
2-2	Schematic showing the molecular arrangement for different phases. Liquid crystalline systems have intermediate scalar order parameter values and show birefringence.	30
2-3	The free energy density as a function of scalar order parameter for different values of temperature. Magnified image of the left figure is presented on the right. The parameters a,b,c etc. were taken from reference [7]	34
2-4	Schematic of transverse section of c/c composite.	34

2-5	(a) Experimental observations ref indicate that the mesophase molecules align face-on along the fiber surface. This type of “homeotropic anchoring” causes what is popularly known as the <i>sheath effect</i> . (b) Close to the fiber the molecules are aligned homeotropically whereas away from the fiber surface the alignment is more uniform.	36
2-6	The figure shows mesh at two different time steps in the problem. The first one is at initial time step and the second one is at a later time step. . . .	39
3-1	Definition of the director orientation of uniaxial discotic nematic liquid crystals. The director n is the average orientation of the unit normals to the disk-like molecules in a discotic nematic phase.	46
3-2	A map of regular array of +2 and - wedge disclinations formed by mesophase flow through a 200-mesh screen in an experiment to control the microstructure of mesophase pitch conducted by Fathollahi at al. Reprinted from [16] with permission of Taylor and Francis. The dark dots correspond to +2 ($s=+1$) disclinations, and the two disclinations along the diagonals of a unit square lattice are ($s=-1/2$) wedge disclinations.	48
3-3	Schematic of the computational domain used for simulating the stable super-disclination array shown in Figure 3-2. The cylindrical inclusions arranged in a square array pattern have strong homeotropic anchoring mimicking the +2 disclinations as in the experiments of Fathollahi [15, 16]. The size of the unit square is $L^*=5$. The radius of each fiber is $H^*=0.05$	64
3-4	(a) Computed gray scale plot of steady state scalar order parameter for the super-disclination array with $U=3.55$, $\frac{\xi}{H}=0.01$. In the plot the low scalar order parameter ($S_0 \approx 0$) is black and high order parameter ($S_0 \approx S_{eq}$) is gray. (b) Zoomed view of the director profile for a square cell.	69
3-5	Computed visualizations of (a) scalar order parameter field S and (b) zoomed director field nat at time $t^*=130$, for the same parametric conditions as in fig. 3-4.	71
3-6	Dynamic evolution of dimensionless gradient and total energy.	72
3-7	The optical textures (a) The experimental optical textures [16] reprinted with permission of Taylor and Francis (b) Simulated optical textures using the Berreman method based on the simulated director profiles shown in Fig.(3-4	74

4-1	Schematic of carbon fiber embedded in a carbonaceous mesophase matrix at different anchoring regimes: (a) strong anchoring with face-on interfacial orientation, when $l_{extrapolation} < R$, and (b) weak anchoring, when $l_{extrapolation} > R$. The lines in both plots represent a side-view of the molecular planes; see Figure 4-2 for an actual composite structure under the strong anchoring regime.	83
4-2	Alignment of mesophase layers in a random arrangement of fibers. Disclinations of $-\pi$ and -2π are found in the matrix with $-\pi$ having a discontinuous core whereas -2π have continuous cores. Adapted from [5]. Reprinted with permission of Elsevier.	84
4-3	(a) Computed gray scale plot of steady state scalar order parameter with $U=3.5$, $\frac{\xi}{H} = 0.0033$. In the plot the low scalar order parameter ($S_0 \approx 0$) is black and high order parameter ($S_0 \approx S_{seq}$) is gray. (b) Computed director field, where the lines represent the average molecular orientation, which is normal to the molecular planes.	92
4-4	Computed director field for the triangular symmetry extracted from fig.4-3b. Each triangular arrangement is accompanied by a $-\pi$ ($s = -1/2$) in the center.	93
4-5	Computed director field for the square configuration extracted from fig.4-3b. The square configuration has a -2π ($s = -1$) disclination in the center with an escaped core.	94
5-1	(a) Particle arrangements in a carbon fiber-mesophase carbon composites; the circles are cross-section of the carbon fibers. The outlined areas denote different polygonal networks: $N=3, 4, 5$, and 6 . (b). Shows fibers in an infinite triangular lattice, here number of polygon sides $N=3$ and the coordination number for this lattice $Z=6$	100
5-2	Summary of computational results for submicron (left column) and micron fiber results. Different scales are selected for clarity. See text.	105
5-3	Dimensionless gradient elasticity as a function of dimensionless fiber radius R^* , for $N=4$, $U=3.5$. See text.	107
5-4	(a) Computed enlarged view of a $s = -3/2$ singular disclination line, for $N=5$, $U=3.5$, at intermediate time $t^* = 600$. See text. (b) Dimensionless splitting time as a function of nematic potential U . The slow-down is driven by proximity to the nematic-isotropic transition temperature. . . .	108

CHAPTER 1 Introduction

1.1 Thesis Motivation

Composites materials are composed of two or more materials that are mechanically combined together [1]. This combination is done to tailor unique and desirable properties like achieve superior strength, greater thermal resistance, lighter weight etc. These composites then have superior properties which cannot be offered by the components individually. For example, polymer/ceramic composites have a greater young's modulus than the polymer component but aren't as brittle as ceramics. Figure 1-1 highlights two of the most important properties of the composites, strength and light weighted-ness. While a single component can offer one of these properties but to achieve both is difficult, however a composite can offer both of these properties at the same time.

The two components in a composite are fillers and matrix. The matrix is the component that takes up the majority of the composite volume. In a composite, fillers are dispersed inside the matrix. While the fillers provide the required reinforcement; the matrix plays a crucial role in acting as the glue and provides load transfer between the fillers. Commonly used fillers are fibers and particles. Examples of the composites include Fiber Glass (glass fibers and polyesters), Kevlar and natural composite such as wood which contains cellulose fibers.

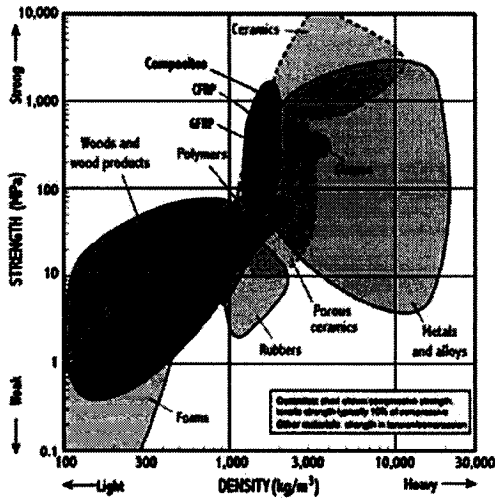


Figure 1-1: Schematic showing superior strength and light weighted-ness of the composites. Taken from; <http://www.composites-by-design.com/advanced-composites.htm>

In a typical composite, the fibers can be randomly positioned inside the matrix or they can be aligned. A few possible configurations are depicted in figure 1-2. The choice of the arrangement of the fibers is based on tailoring of specific material properties. A part of this thesis focuses on understanding arrangement of fibers inside the matrix to achieve optimum properties.

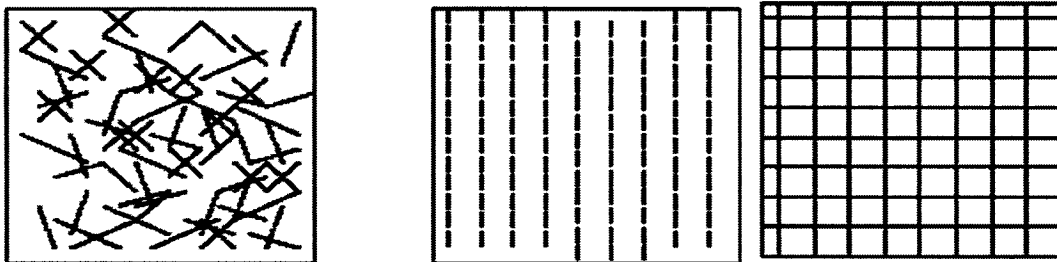


Figure 1-2: Shows some of the possible arrangements of fibers inside the matrix. The first is random arrangement of fibers and the next two have fibers aligned in a particular fashion.

This thesis will concentrate on one of the widely used composites; carbon/carbon composites. In these composites the fillers are carbon fibers which are dispersed inside a carbon matrix. Both the carbon fibers and carbon matrix can be made from different materials also known as precursors. Most commonly used precursors include petroleum pitch and PAN (Polyacrylonitrile) [2]. Experiments have indicated that type of matrix obtained from either PAN or pitch based precursors plays a pivotal role in determining the mechanical properties of the composite material [3]. For example figure 1-3 compares the mechanical properties of three carbon/carbon composites (labeled A, B, C) and an isostatically molded fine-grain petroleum coke graphite (labeled G).

	A ^a	B ^b	C ^c	G
Bulk density (g/cm ³)	1.68	1.77	1.57	1.76
Young's modulus (GPa)	13.5	26.3	17.0	10.5
Vickers hardness ^d (MPa)	135	163	-	172
Bending strength (MPa)	65.7	96.9	-	39.6
Tensile strength (MPa)	R.T. 35.7	55.4	68	28
	800°C 43.4	65.4	88	30
	1600°C 42.0	50.4	102	37
	2400°C 62.7	83.0	111	44
Fracture toughness (MPa.m ^{1/2})	R.T. 2.96	3.44	4.0	0.8
	800°C 2.82	3.58	5.5	0.8
	1600°C 4.64	6.75	6.1	1.0
	2400°C 5.30	12.9	7.0	1.9
Thermal diffusivity (mm ² /sec)	62.4	56.6	-	48.0
Thermal shock resistance (W/mm)	~148	~155	~171	50 ± 6
Thermal shock fracture toughness (W/mm ^{1/2})	~779	~805	~856	33 ± 3

^aPitch carbon-carbon composite.
^bPAN carbon-carbon composite.
^cTwo-dimensional rayon carbon-carbon composite.
^dLoad 5 kg.

Figure 1-3: Mechanical properties of three c/c composites (A, B, C) and graphite (G). From Ref.[4]. (A=pitch based, B=PAN, C=Rayon, D=graphite).

The present work focuses on petroleum pitch as the matrix for making c/c composite. This petroleum pitch based matrix is known as carbonaceous mesophase pitch [5]. Composites made from carbonaceous mesophase pitch as the matrix are unique in that they

exhibit texture. Texture means the presence of orientation and defects [6] as shown in the figure 1-4. Orientation indicated by lines in the figure depicts alignment of molecules along a preferred direction known as the director [6] (this would be made clearer in the next section). Defects are created by mismatch in orientation.

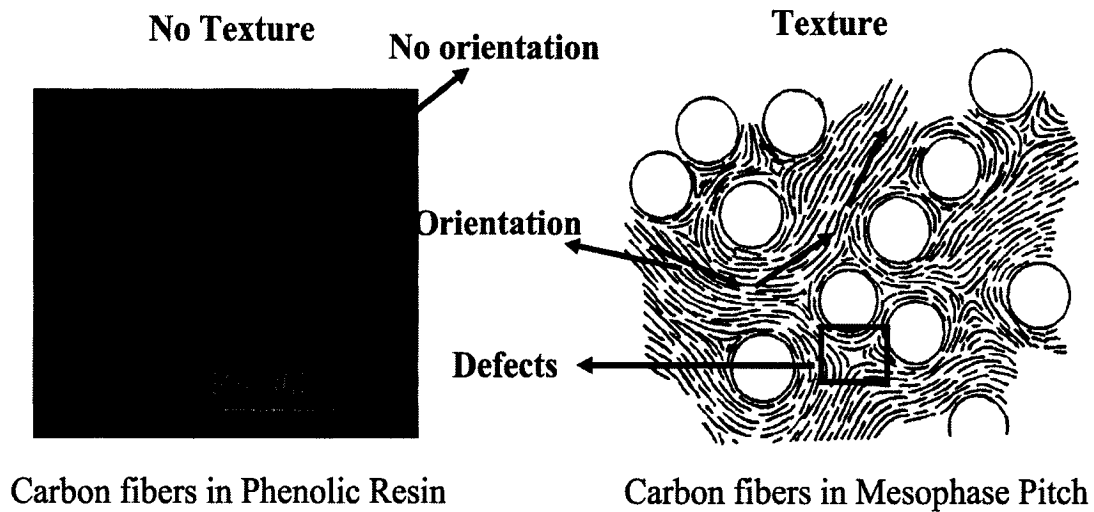


Figure 1-4: Shows a comparison of carbon fiber composite with phenolic resin and carbonaceous mesophase as the matrices. When light is shone through the samples, isotropic liquid shows black whereas anisotropic substance shows birefringence and show optical response. The c/c composites with mesophase show texture whereas the phenolic resin is isotropic and there is no orientation. Adapted from [3].

The presence of texture as shown above (orientation + defects) is of interest to material scientists as it arises from high order of molecular orientation and hence it is desirable to retain and manipulate this ordering to achieve superior mechanical properties [5]. These c/c composites with mesophase pitch are perhaps one of the most advanced forms of carbon, and are extremely strong, tough and are thermally resistant. In fact the low density of the carbon ensures their superior specific strength, specific modulus and specific thermal resistance among composites [3]. Due to their exceptional properties they find

usage in specialty applications and are used extensively in aerospace industry to make aircraft brakes, heat pipe, reentry vehicles and also in rocket motor nozzles, hip replacements, biomedical implants and electronic heat sinks [3]. On the downside these composites have poorer mechanical strength compared to PAN based c/c composites. They tend to be expensive, hence optimization and tailoring their property becomes an essential component rather than a choice to justify the investment.

Previously a lot of emphasis has been laid on understanding material properties of Carbon fiber/Carbon mesophase (CF/CM) composites [3], however in all these studies the matrix is considered dormant. But as explained before the matrix is actually a dynamic system exhibiting orientation and defects. Previous experimentation [7] has shown that understanding the matrix texture is important since defects are found to affect the fracture behavior of these materials [8]. This thesis focuses on understanding the dynamic process of texture formation in CF/CM composites using modeling and simulation and hence provide scientific pathways to improve the performance of these composites.

1.2 Carbonaceous Mesophase Pitches

As previously outlined mesophase pitch based carbon/carbon composites are unique in the sense that they exhibit molecular ordering and hence have texture. The texture of mesophase pitch based carbon/carbon composites influences the physical changes that take place during processing and affects the final composite mechanical properties [8]. The following section gives an overview of the CM matrix.

1.2.1 Description of the mesophase

One question that comes to mind is why do mesophase pitch based composites have texture? The answer to this question comes from the fact that carbonaceous mesophase (CM) is a *discotic liquid crystal*. The word discotic [9] means that CM consists of disklike molecules. Figure 1-5 shows a schematic depicting molecular geometry, positional order,

and orientational order of discotic nematic liquid crystals. The partial orientational order of the molecular unit \mathbf{u} is along the average orientation or director \mathbf{n} ($\mathbf{n} \cdot \mathbf{n} = 1$). The name discotic distinguishes the molecular geometry and the name nematic identifies the type of liquid crystalline order.

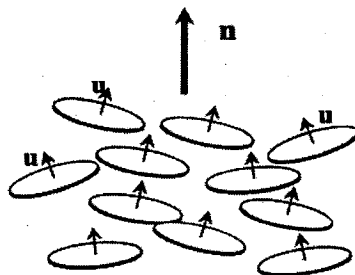


Figure 1-5: Schematic of disk shaped CM molecules. The director \mathbf{n} is the average orientation of the unit normals \mathbf{u} to the disklike molecules in a discotic nematic phase.

These molecules display *long range orientational order* in the sense that the molecules lie approximately parallel to each other. The parallel stacking of molecules is shown in Figure 1-6.

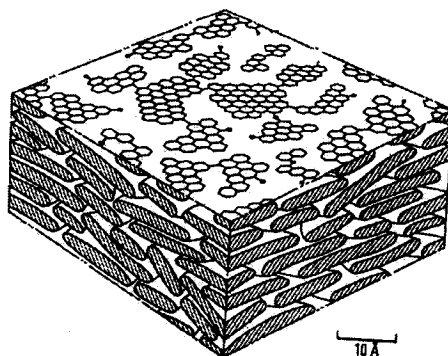


Figure 1-6: Schematic model of stacking of carbonaceous mesophase molecules adapted from [5]

The fact that the molecules in CM have disklike structure provides it with physical properties that are different from other nematic liquid crystals which contain rodlike molecules. Precise determination of the constituent molecules and their distribution in the carbonaceous mesophase is complicated by the wide range of molecular sizes and shapes. Infrared spectroscopy, NMR and vapor pressure osmometry can be used to estimate the structural configuration of the disklike aromatic molecules in the carbonaceous mesophase [5]. Few of the model structures for the molecules are shown in figure 1-7.

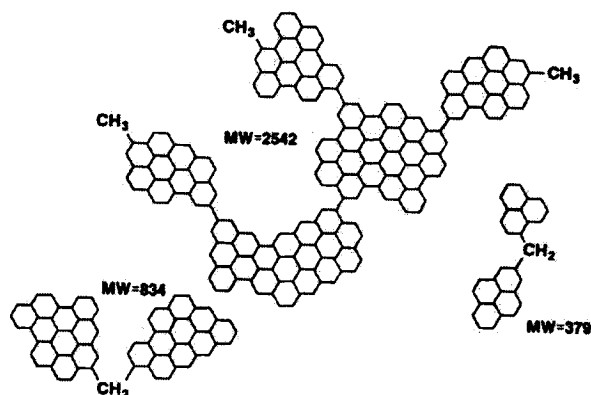


Figure 1-7: Some model structure for mesophase-forming molecules, adapted from [5]

1.2.2 Formation of the Mesophase

The mesophase formation has been observed for many aromatic compounds, but the present work focuses solely on mesophase formation from the pyrolysis of petroleum and coal tar pitches. A general scheme for the formation of mesophase can be shown as:



In the absence of air, the organic component melts in heating and becomes an isotropic pitch or liquid. As the temperature rises over 400°C , optically anisotropic spheres, known as spherules [10], appear in the isotropic petroleum pitch matrix [10]. Figure 1-8 shows

an experimental picture of spherule formation. This formation of carbonaceous mesophase is a nucleation and growth process. Attractive forces among the spherules give rise to droplet coalescence and overall growth of the mesophase. As the polymerization reaction continues, the molecules get larger and the mesophase becomes more viscous. This growth phenomenon is commonly termed as "Brooks Taylor Morphology" [10] and has been identified in spherules as small as a few microns. These spherules seldom grow beyond $50\mu\text{m}$ without developing complex internal structures. As the pyrolysis proceeds, these spherules then coalesce and produce large regions of bulk mesophase.



Figure 1-8: Picture showing growth of carbonaceous mesophase spheres known as spherules. Taken from <http://www.shanshantech.com/eptoduct-a.htm>

1.2.3 Textures in Carbonaceous Mesophase based c/c composites

The emphasis of this thesis is on identifying and characterizing the textures in the CM, in particular for c/c composites. Figure 1-9 shows a typical texture observed in CM in a c/c composite with CM as the matrix.

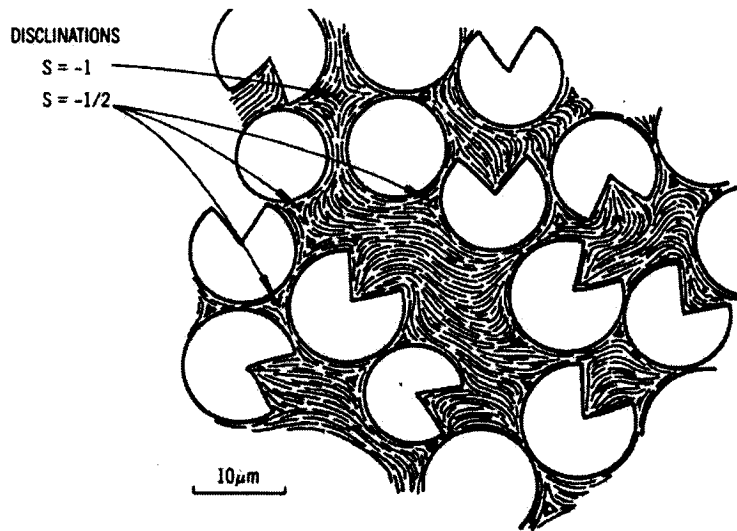


Figure 1-9: Experimental picture reference [7] indicating the presence of texture in carbonaceous mesophase. The picture is section of the composite transverse to the axis of the fiber bundle, mapped by polarized-light micrography with immersion oil.

The above figure 1-9 is an optical micrograph obtained by taking a section transverse to the fiber bundles, which are then polished and observed under immersion oil with cross polarized light. The characteristics of the texture can be described by two things. Firstly, the disklike molecules tend to lie parallel to the surface of the fibers and form a circular sheath several microns in thickness, this is known as the "sheath effect" [5]. Secondly the disclinations or defects are observed in abundance in this system and is of practical importance as it affects the fracture behavior of the material [5]. These defects are essentially discontinuities in the parallel stacking of layers owing to freedom of preferred orientation of splay, twist and bend [11] similar to that of other nematic liquid crystals; details of defects are presented next.

To perfect the composite properties understanding the study of textures is essential thus

studies are required to optimize defects and enhance structures resistive to crack propagation.

1.2.4 Disclinations = Line Defects

Disclinations [11] or defects [12] appear in system as a result of incompatibility or breakage of symmetry. These defects are common in liquid crystalline systems and have been studied quite extensively [12]. Defects play an important role in such phenomena as response to external stresses and the nature and type of phase transitions. For example the defects formed in CM in CF/CM composites are found to be related to the fracture behavior of the composite [8]. The presence of these defects can be attributed to control of boundary conditions, external fields, or surface conditions. As already explained the term texture refers to orientation of the liquid crystal molecules (CM molecules) in the vicinity of the surface. Each liquid crystalline material can form its own characteristic textures, which are useful in its identification. A nematic phase exhibits broken symmetry when compared to the isotropic phase because it is defined by the average molecular orientation, \mathbf{n} [6]. Because any orientation of \mathbf{n} is possible the degeneracy leads to the possibility of defects or spatial discontinuities of \mathbf{n} . Defects are classified in terms of strength (S) and dimensionality (D). The strength captures the degree of rotational discontinuity when encircling the defect, whereas the dimension refers the points, lines, and walls. The spatial arrangement of defects is called texture. The strength S of a defect is equal to the number of rotations the director experiences on a path encircling the defect. Points are D=0 defects, disclinations are D=1 line defects, and walls are D=2 defects. The core of disclinations can be singular or non singular; $S = \pm\frac{1}{2}$ (or $\pm\pi$) have singular cores whereas $S = \pm 1$ (or $\pm 2\pi$) disclinations can have either. Singular and non singular cores are explained in detail in chapter 4. Figure 1-10 shows some disclinations that are commonly observed in CM in c/c composite.

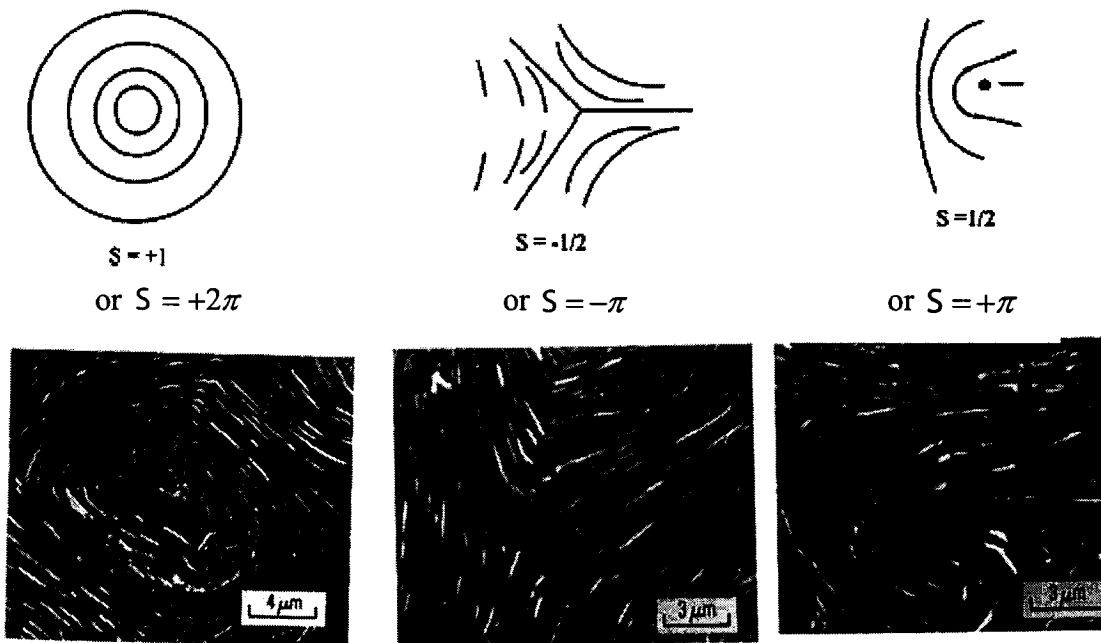


Figure 1-10: Top row shows schematics of defects textures in liquid crystals. Bottom pictures are SEM images of disclination observed in carbonaceous mesophase taken from reference reference [5].

Since Liquid crystals are anisotropic materials they exhibit birefringence. That is they demonstrate double refraction. Light that is parallel to the director \mathbf{n} has a different refraction (travels with a different speed) than the light polarized perpendicular to the director. Because these two components travel at different speeds, the waves get out of phase. And when they combine together on exiting the liquid crystal sample the polarization state has changed because of this phase difference. Figure 1-11 is a microscope picture of a nematic liquid crystal, taken between cross polarizers. Some of the regions are dark whereas others appear lighter. The light and dark regions denote differences in the director orientation \mathbf{n}

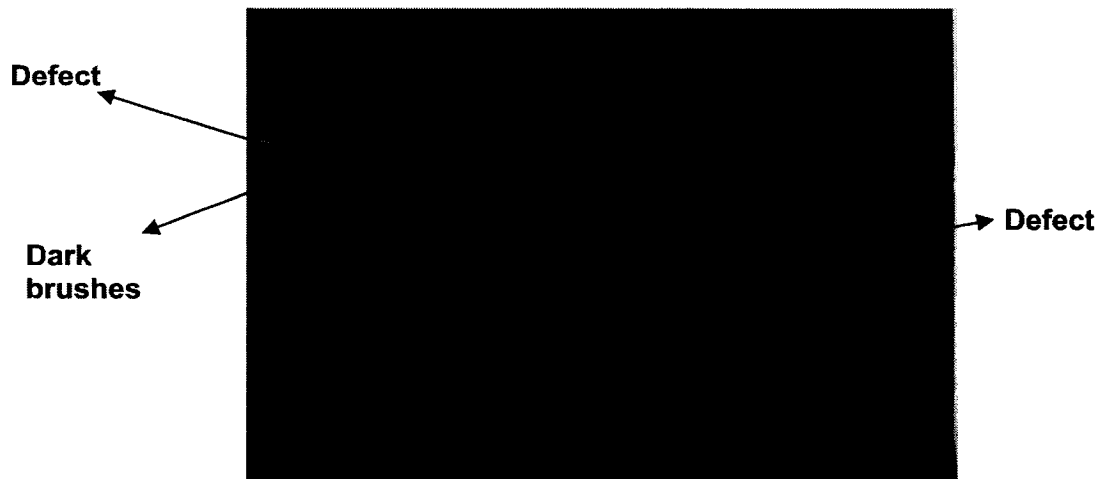


Figure 1-11: The optical microscope picture showing defects in a nematic liquid crystal.

The dark lines are known as brushes. Notice that the above figure shows dark lines ending in a point. These points are defects in the sample. As a general rule the strength of the defect S is equal to number of dark brushes divided by four. That is $S = \pm \frac{N}{4}$. The sign positive or negative comes from the sense of rotation [6]. For example, a point with four dark lines emanating out is a defect of strength $S = \pm 1, \left(\frac{4 \text{ dark brushes}}{4} \right)$. This makes it easy to identify location and type of defect in a sample by looking at its optical picture.

1.2.5 Processing of c/c composites

c/c composites are fabricated using four different methods, namely (1) liquid phase impregnation (LPI), (2) hot isostatic pressure impregnation carbonization (HIPIC), (3) hot pressing, and (4) chemical vapor infiltration (CVI). A schematic of the processing of c/c composite is shown in figure 1-12. In all the methods a prepreg is first prepared by combining the carbon fibers with pitch or resin. This pre-impregnation cycle is then followed by a second stage involving carbonization at about 350-850⁰C. Usually carbonization causes

shrinking of the pitch and resin and hence additional pitch or resin has to be impregnated to make up for the loss. The carbon yield that is obtained after carbonization is dependent on the type of matrix (pitch based or resin) the process (LPI, HIPIC, CVI) and also the Pressure. The mesophase pitch typically offers a higher carbon yield during carbonization hence the use of mesophase pitch offers the advantage of fewer impregnation cycles. The next stage is the graphitization which is the conversion of the carbon to graphite at excessive temperatures; the specifics are given in figure 1-12.

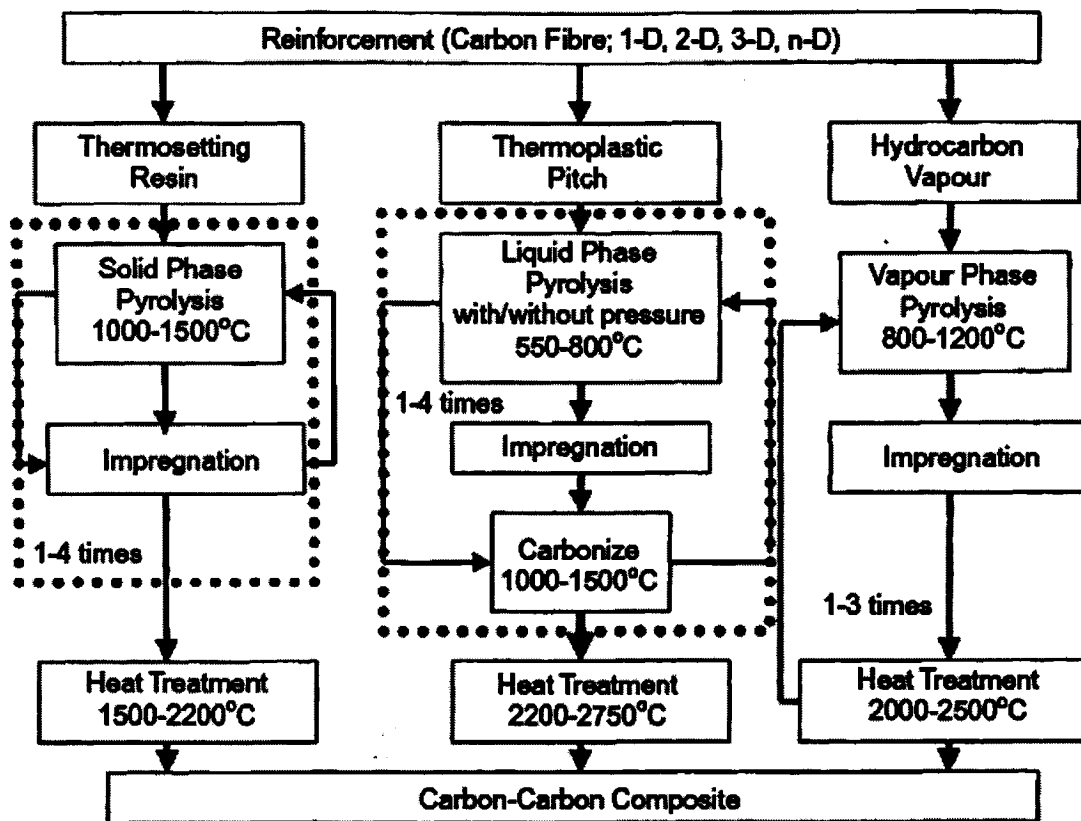


Figure 1-12: Processing of c/c composites. From reference [13]

1.3 Introduction to Liquid Crystals

For many organic compounds the phase transition from solid state and the liquid state is not a single phase transition, and an intermediate state called mesophase exists between solid and liquid. Mesomorphic materials possess both liquid like fluidity and solid like molecular order. They contain order between that of a solid and a liquid. The shape of a molecule is an important factor for mesomorphism to occur. Two types of liquid crystalline compounds characterized by their shape and size are most widely studied, the rodlike liquid crystal and the disklike liquid crystals known as discotic liquid crystals. As previously mentioned the carbonaceous mesophase pitch belongs to the class of discotic liquid crystals.

1.3.1 Classification of Liquid Crystals [14]

Phase transition to the ordered fluid state (mesophase) can be effected through changes temperature (thermotropic liquid crystal) or concentration (lyotropic liquid crystals). The molecular ordering in these systems can be best achieved with molecular shapes that are disk-, lath-, or rod-like. Based on symmetry a classification can be done into three main classes of liquid crystals: nematic, cholesteric, and smectic.

Nematic Liquid Crystals

The nematic phase is characterized by a long range orientational order (the long axis tend to align along a preferred direction known as the director \mathbf{n}) and an absence of positional order (there is no specific arrangement of molecules in space). Figure 1-13 shows two types of nematogens rodlike and disklike along a preferred direction \mathbf{n} and the molecules themselves seem to have no spatial arrangement in space.

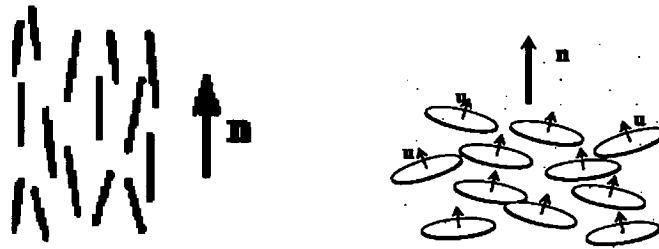


Figure 1-13: Schematic representation of rodlike and disklike molecules in space in a nematic liquid crystal.

Cholesteric Liquid Crystals

Cholesteric liquid crystals are constituted of chiral molecules (molecules without mirror images). The cholesteric phase lacks positional order, like the nematic phase but the director follows helical path. The strong modulation of refractive index due to helical deformation causes Bragg scattering of various colors of light, a property that is exploited in the use of liquid crystals as temperature sensors. Figure 1-14 shows layers from a three dimensional assembly. In each layer the molecules have a uniform orientation (notice the molecules are orientated along a certain direction). However, from one layer to the next the orientation changes by a slight angle leading to a periodic configuration characterized by a length scale denoted by p (pitch).

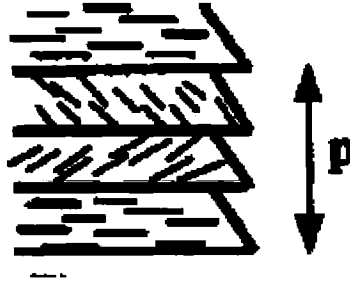


Figure 1-14: Schematic representation of cholesteric. Rodlike molecules are represented by small segments lying on a series of equidistant planes. The structure is continuous and P here represents the pitch.

Smectic Liquid Crystals

Smectic liquid crystals have stratified structures which makes them the most ordered and viscous mesophases. Molecules stand on series of equidistant parallel layers which are free to move. Approximately 12 different types of smectic liquid crystals have been identified to this day. However the best known are A and C. Figure 1-15 shows a schematic of a typical smectic A.



Figure 1-15: schematic representation of Smectic A structure.

1.4 Experimental Observations related to the Thesis

- a Multiple Length Scales: A *c/c* composite mesophase pitch composite, as shown in figure 1-9, exhibits important features at different length scales. These have been characterized in great detail in experiments [5]. Figure 1-16 illustrates a schematic of

a c/c composite which highlights this multiscale phenomenon. The radius of the fibers (R) and the distance between them (L1) can be thought of as macro variables (these are of the order of microns [5,7,8]). On the other hand the defects that arise in the system as previously explained are nano-scale phenomena. Experimental evidence suggests that the size of these defects is of the order of 10nm [15]. As previously pointed out the presence of fibers influences how the molecules assemble inside the matrix thus creating a macro level assembly. This macro level assembly has broken symmetries (defects) which are nanoscopic. So changes in macro level (changing fiber size or their arrangement) can cause changes at the nano scale. And since the nano sized defects are found to affect mechanical properties, such as the fracture behavior of these systems [8], it thus becomes important to understand the relationship and effect of different scales. This length scale relationship study forms an important part of this thesis.

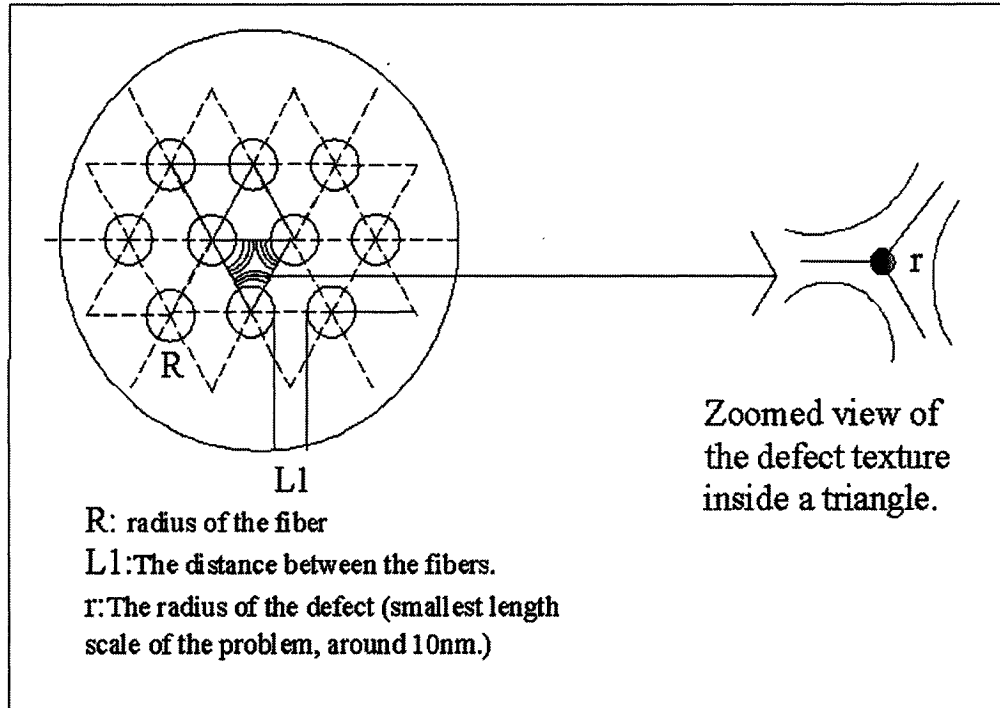


Figure 1-16: The schematic illustrates different length scales observed in a c/c composite. It is of great interest to control both the meso (R and L1) and nano (defect cores) scales of the system to optimize the performance of these systems.

b Defect Core Structures: Previously it was pointed that c/c composites have defects. However not all the defects that arise in these material systems are identical. C/C composites are found to contain variety of defects [7]. Some of these defects were mentioned in section 1.2.4. Experiments [7] have indicated that controlling the configuration of fibers inside the mesophase influences the type of defects. For example in the work of [7,8] it was shown that an arrangement of fibers in triangular configuration leads to $S = -\frac{1}{2}$ defect but a square arrangement of fibers leads to the creation of $S = -1$ defect. This is illustrated in figure 1-17. The -1 defect is an escaped core

defect and is non singular in nature whereas the $-1/2$ defect is singular defect. To identify what type of defect is created under influences of fiber configuration or fiber size forms another section of this thesis.

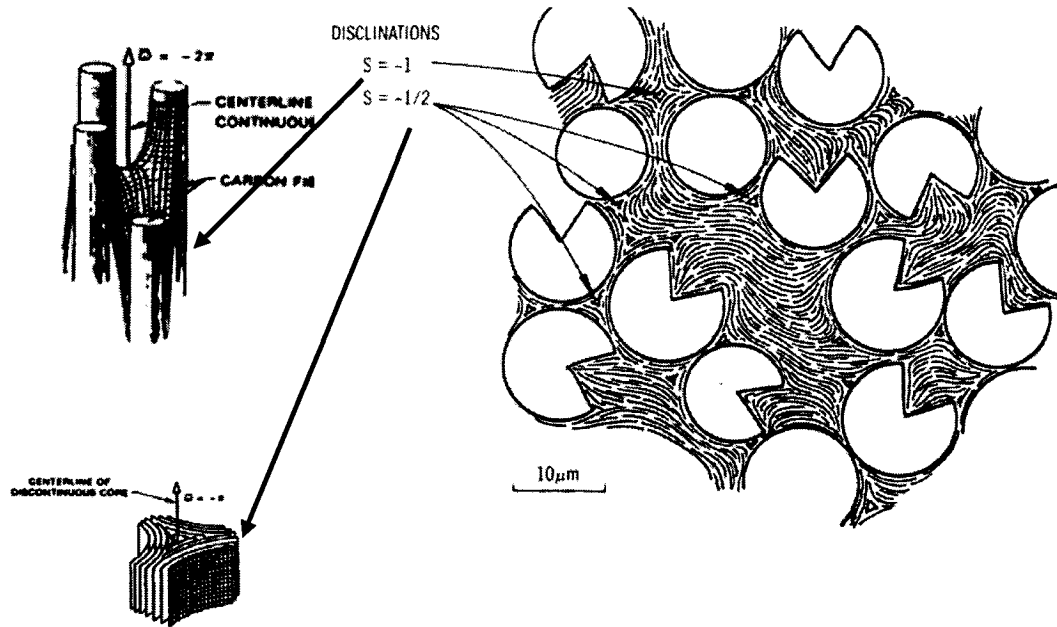


Figure 1-17: Schematic of a c/c composite showing two different defect core structures. Adapted from reference [7].

c Stability of Defect Lattices: Experimentalists [16, 17] over the years have tried to manipulate the texture of carbonaceous mesophase during the fiber spinning process. This manipulation process is known as mesophase miniaturization. They manipulate the mesophase flow to produce a desired texture at a workable scale. One of the ways to manipulate the texture is the use of wire screens. Figure 1-18 shows a schematic design of this manipulation process. Here wire screens are added to the spinning apparatus used for making fibers. The effect of the screens can be seen in figure 1-19.

Figure 1-19a shows the texture when no screen was used in the spinning apparatus. The texture is random and there is no periodicity in the texture. However when screens are used a regular array of $+2\pi$ and $-\pi$ defects are created shown in figure 1-19b. This periodic pattern is shown clearly in figure 1-20. The identification of defects is done by looking at the number of brushes which was discussed in section 1.2.4. These defects lattice structures as they have come to be known [17] are stable structures. The possibility of achieving desired texture in the mesophase also forms an important part of this thesis. Details about possible control of mesophase to obtain experimentally observed periodic defect structures will be presented in detail in chapter 3.

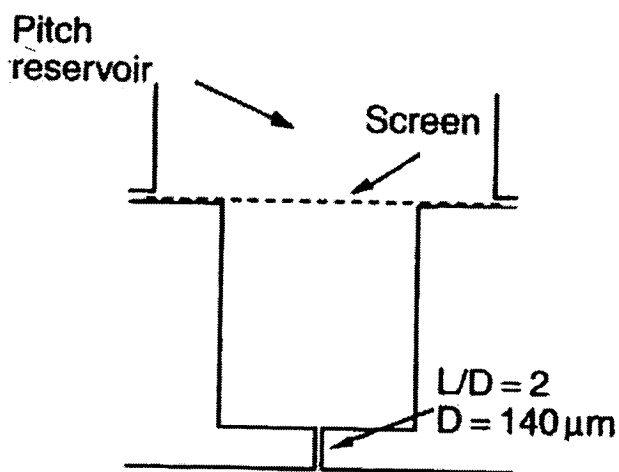


Figure 1-18: Schematic design of spinneret with the screen modification for controlling the texture of the mesophase. Adapted from reference, [17].

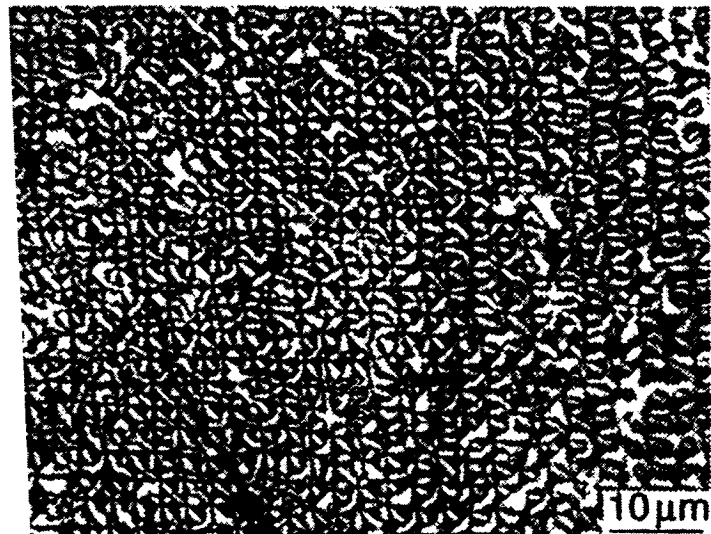
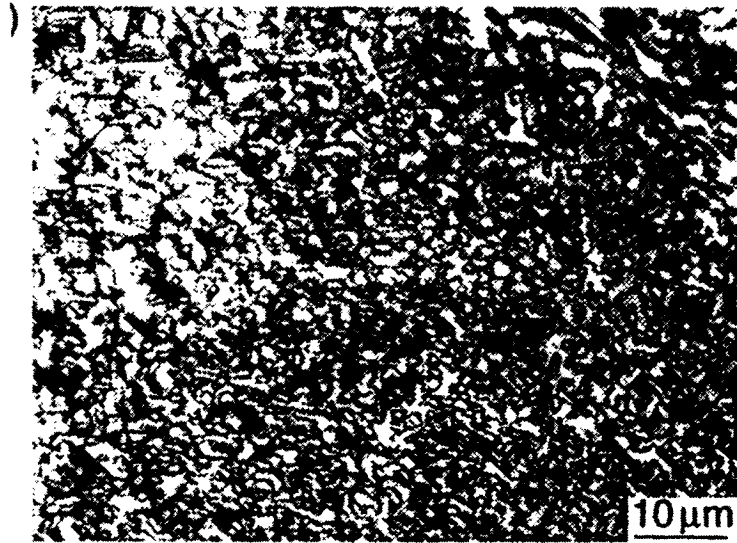


Figure 1-19: Effect of manipulating the mesophase texture from reference [16]. These pictures are optical micrographs (a) No manipulation was done. (b) Manipulation was done by passing through a 200 mesh screen.

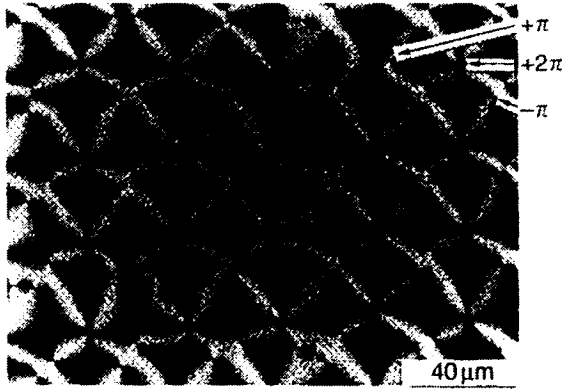


Figure 1–20: A more detailed picture of the disclination lattice adapted from reference [16]. The arrows indicate the presence of different defect types.

1.5 Thesis Objective

- i Establish a suitable mathematical framework for c/c composites using the Landau de Gennes theory of liquid crystals.
- ii Validate the relevance of using the Landau de Gennes theory in modeling carbon-based material systems.
- iii Use the developed model to understand the texture selection process in CF/CM composites and elucidate the main mechanisms that control texture formation.
- iv Identify geometric parameters (fiber arrangement and size) and processing conditions (temperature) that lead to experimentally observed material architectures.

1.6 Thesis Methodology

In order to analyze and understand the texturing process in a c/c composite a standard multilevel modeling methodology of (a) Theory (b) Modeling, (c) Validation is adopted.

- a Previous theory and Modeling Work: Previous work done by Rey and coworkers [18,19,20,21,22] has demonstrated that liquid crystal theories can be applied successfully to describe key texture features of the mesophase. These theories have been

successfully used by them to characterize texture development in the fiber spinning process [19,20], model the rheology of carbonaceous mesophases [18, 21] and simulate the texture of mesophase under pressure driven flows [22]. This thesis will build on previous modeling approaches and adapt the liquid crystal theory for CF/CM composites. This involves introducing geometric constraints that arise from the presence of fibers in the system and processing conditions for these materials.

- b Multiscale modeling: As explained above, fiber size, fiber-fiber distance and presence of defect cores introduce multiscale phenomena into the system. Modeling these material systems requires robust large scale computational modeling tools that can resolve all these length scales. To tackle this issue, computational methods have to be developed and used with utmost care. In this thesis a large effort has been devoted to take care of the disparate length scales using grid adaptation and numerical techniques. The numerical approach based on finite element method is presented in chapter 2.
- c Validation: Validation of simulation is a crucial step in process modeling. Abundant experimental data is available for c/c composites with mesophase pitch as the precursor [5,7,8,16,17] and will be used to validate the results.

1.7 Thesis Organization

This thesis is organized as follows:

- i Chapter 1 presents a general background of the thesis including motivation, introduction to textures in CF/CM composites, properties of carbonaceous mesophase and a general outlook of liquid crystals. It also presents thesis objectives.
- ii Chapter 2 focuses on formalism and adaptation of Landau de Gennes theory for liquid crystals for CF/CM composite systems. It also presents multiscale modeling

technique and formulation of finite element based method for solving the governing equations.

- iii Chapter 3 focuses on understanding flow-based periodic texturing of mesophases to control the mesophase texture. It provides an alternative route based on particle dispersion inside the mesophase to obtain textures similar to those observed in experiments.
- iv Chapter 4 focuses on CF/CM composites and presents computational modeling study of texture formation in these systems. The modeling predictions on texture formation and defects are validated with experiments. The role of fiber configurations inside the mesophase is the key element of this chapter.
- v Chapter 5 presents the effect of varying fiber size and their configurations inside the mesophase on the texture of the composite. The predictions are compared with experimental observations in a similar study.
- vi Chapter 6 presents the main conclusions of this thesis.

1.8 References

- 1 S. Kalpakjian, *Manufacturing Engineering and Technology* , Addison Wesley; 1998.
- 2 Buckley JD. *Carbon-carbon Composites* . In: Peter ST, editor. *Handbook of composites* (2nd Edition). London, U.K.: Kluwer Academic Publishers, 1997; 333-351.
- 3 D.D.L. Chung, *Carbon fiber Composites*, Washington, Butterworth-Heinemann; 1994.
- 4 S. Sato, A. Kurumada, H. Iwaki, and Y. Komatsu, *Carbon* **27** (6), 791-801 (1989).
- 5 J.E. Zimmer and J. L. White, *Advances in Liquid Crystals*, **5** , 157-213 (1982).
- 6 de Gennes PG, Prost J. *The physics Of Liquid Crystals* , 2nd edition. Oxford: Clarendon Press. 1993.
- 7 J.E. Zimmer and J. L. White, *Carbon*, **27** (6), 791-801 (1989).
- 8 J. E. Zimmer and R. L. Weitz, *Extended Abstracts 16th biennial conf. on Carbon*, American Carbon Society; 92-3 (1983).
- 9 S Chandrasekhar et al., *J. Phys. (Paris) Colloq.*, **40** , C3-120 (1979).
- 10 J. D. Brook and G. H. Taylor, *Carbon*, **3** , 185 (1965).
- 11 F. C. Frank, *Discussion of Faraday Society*, **25** , 19-28 (1958).
- 12 J. Friedel, *Dislocations*, Oxford, Pergamon; 1967.
- 13 L. M. Manocha, *Sadhana* **28** , 349 (2003).
- 14 A.D. Rey and M. M. Denn, *Annu. Rev. Of Fluid Mechanics*, **34** , 233 (2002).
- 15 H. Stark. *Phys. Reports* , **351** , 387 (2001).
- 16 J. L. White, B. Fathollahi, and X. Bourrat, in *Fibers and Composites* , 1 st edition, edited by D. Pierre (Taylor and Francis, 2003), Chap. 1, p.3-23.
- 17 J. J. McHugh and D. D. Edie, *Carbon* **34** (11), 1315-1322 (1996).
- 18 T. Tsuji and A. D. Rey, *J. Non-Newtonian Fluid Mech* . **73** , 127 (1997).
- 19 J. Yan and A. D. Rey, *Phys. Rev. E* **65** , 031713 (2002).
- 20 D. Sharma and A. D. Rey, *Liquid Crystals* **30** , 377-389 (2003).

21 D. Grecov and A. D. Rey, *Rheologica Acta* **44** , 135-149 (2004).

22 de Andrade Lima and A. D. Rey, *J. Rheology* **48** , 1067-1084 (2004).

CHAPTER 2 Theory and Methodology

2.1 Introduction

The processing of c/c composites is a complex process involving viscous, elastic and thermal processes [1]. Previously, theoretical approach has been successfully applied to model textures in carbon fibers [2,3] and carbonaceous mesophase [4]. Both experiments [5,6] and simulation [2,3] indicate that carbonaceous mesophase texturing process follows a liquid crystalline self assembly process. This chapter presents the theoretical approach to modeling these systems. First an overview of present state of the art in theoretical modeling is given followed by the derivation of the model used to simulate this system.

2.2 State of the art in modeling liquid crystalline systems, [7]

Theories that describe the liquid crystalline phases can be divided into two general classes [8]: molecular and phenomenological. The molecular theories take into consideration the interaction between the individual molecules. This approach is useful since information at macro scale is obtained from microscopic molecular interactions. However this approach requires a large group of molecules which are computationally expensive. Approximate theories are needed to overcome this problem and hence simplify the approach. Popular theories such as Onsager's hard rod model with purely steric repulsion [9] considers molecules as cylindrical rods and the interactions between them are hard, like billiard balls: the rods cannot penetrate or deform each other but they don't feel each other until they touch. This is a simplification since in reality the molecules could be flexible. Other popular simplified theories include Maier-Saupe's mean field theory [10] and

approach proposed by Telo da Gama et al. [11]. Recently lot of effort [12,13,14,15] has also concentrated on numerically solving the problem using efficient Monte Carlo algorithm and molecular dynamics studies. In this method the nature of liquid crystal mediated effective interactions is studied by Monte Carlo method based on the combination of canonical expanded ensemble simulations and a density-of-states formalism.

The phenomenological approach, on the other hand starts with a suitable macroscopic order parameter and then expanding the free energy density of a liquid crystalline system in the vicinity of phase transition (isotropic-nematic) as a power series of the order parameter [16]. The minimum of free energy at each temperature and pressure is evaluated as a function of the order parameter and corresponds to the state of equilibrium.

The present work on carbonaceous mesophase texturing in c/c composites is based on phenomenological model of Landau-de Gennes theory. In section 2.2 the concept of order parameter is introduced. The basic theory is presented in section 2.3. In section 2.4 the theory is derived for carbonaceous mesophase and their ordering due to the presence of carbon fibers, and finally section 2.5 discusses the numerical approach used.

2.3 Order Parameter

The concept of order parameter was first introduced by Landau [17] for the purpose of a phenomenological description of phase transitions. This is used for the description of *long-range* order of the structural or thermodynamic properties, that repeats uniformly in a given system and *short-range* order that takes into account the spatial thermodynamic fluctuations.

Let us consider a disk like molecule with unit vector \mathbf{u} along the axis of the molecule. \mathbf{n} as was mentioned previously is the director which is the average direction of the molecules and θ is the angle between \mathbf{u} and \mathbf{n} .

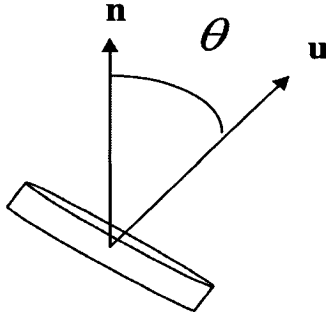


Figure 2-1: Schematic of a disklike molecule.

If it is assumed that the distribution function¹ is cylindrically symmetric about \mathbf{n} and the directions \mathbf{n} and $-\mathbf{n}$ are fully equivalent, i.e., the preferred axis is non polar. Subject to these two conditions the degree of alignment was first introduced by Tsvetkov [18]

$$S = \frac{1}{2} \langle 3 \cos^2 \theta - 1 \rangle \quad (2.1)$$

S is known as Maier-Saupe or Scalar order parameter [16]. This function gives an indication of the distribution of molecular orientation \mathbf{u} along the director \mathbf{n} . Figure 2-2 shows the different degree of ordering and consequently the variation of scalar order parameter with change in phase.

¹ Distribution function also known as the probability density functions describe the probability with which one can expect the molecules to occupy the available energy in a given system.

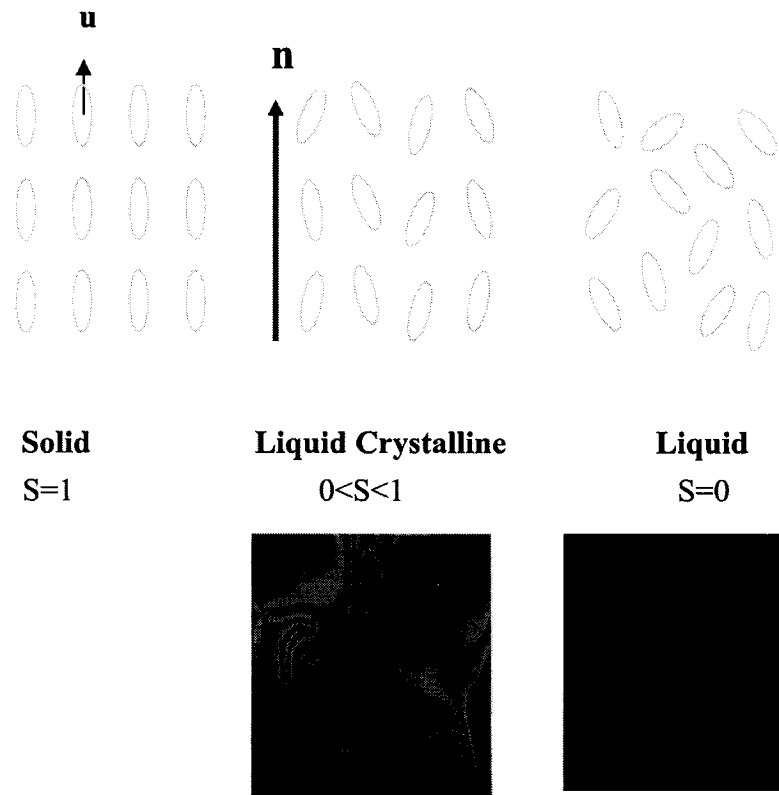


Figure 2–2: Schematic showing the molecular arrangement for different phases. Liquid crystalline systems have intermediate scalar order parameter values and show birefringence.

For a perfectly ordered phase the unit directors of the molecule \mathbf{u} are along the director \mathbf{n} making θ equal to zero and hence $S = 1$ from equation (2.1). In the isotropic phase or liquid phase, the molecules are randomly distributed. From the calculation of distribution function it gives $S = 0$. For a Liquid Crystalline phase there is an average orientation along a certain preferred direction \mathbf{n} and hence the scalar order parameter for a typical nematic phase corresponds to $S \approx 0.3 - 0.6$. Optically, due to the alignment of the liquid crystalline molecules birefringence is observed in these systems whereas for an

isotropic liquid no image is obtained when light is shone through the sample due to the random orientation of the molecules.

The director \mathbf{n} only gives the preferred orientation and the scalar order parameter S gives the degree of alignment. To combine these two concepts together a second order tensor \mathbf{Q} was introduced [16]. It is defined as:

$$\mathbf{Q} = S \left[\mathbf{n} \cdot \mathbf{n} - \frac{1}{3} \delta \right] \quad (2.2)$$

Notice here that \mathbf{Q} is a function of both the scalar order parameter and the director and hence is suitable to describe a uniaxial nematic phase. δ is the kronecker delta function. Biaxial ordering is introduced by using a more general form:

$$\mathbf{Q} = S(\mathbf{nn} - \frac{1}{3}\delta) + \frac{1}{3}P(\mathbf{mm} - \mathbf{ll}) \quad (2.3)$$

Where P is the biaxial order parameter. It is important to note that \mathbf{Q} is always a symmetric and traceless tensor [16]. Biaxial states are important when describing defect cores [16], but in the bulk of the nematic phase, the ordering is uniaxial. The uniaxial director \mathbf{n} corresponds to the maximum eigenvalue $\mu_{\mathbf{n}} = \frac{2}{3}S$, the biaxial director \mathbf{m} corresponds the second largest eigenvalue $\mu_{\mathbf{m}} = -\frac{1}{3}(S - P)$, and the second biaxial director $\mathbf{l} (= \mathbf{n} \times \mathbf{m})$ corresponds to the smallest eigenvalue $\mu_{\mathbf{l}} = -\frac{1}{3}(S + P)$. The orientation is defined completely by the orthogonal director triad $(\mathbf{n}, \mathbf{m}, \mathbf{l})$.

2.4 Landau-de Gennes Theory [16]

The tensor order parameter can be used to construct a Landau expansion of the free energy density in the vicinity of the phase transition [16].

$$f_h = \frac{1}{2}a_0 \left(T - T^{ref} \right) (\mathbf{Q} : \mathbf{Q}) - \frac{1}{3}b\mathbf{Q} : (\mathbf{Q} \cdot \mathbf{Q}) + \frac{1}{4}c(\mathbf{Q} : \mathbf{Q})^2 \quad (2.4)$$

here a_0, b, c are material dependent parameters and T^{ref} are independent of temperature whereas T is the temperature. Using the uniaxial definition of \mathbf{Q} from equation (2.2), and assuming liquid crystal molecules are aligned along the x axis ($n_x=1$ and $n_y= n_z=0$) gives:

$$f_h = \frac{1}{3}a_0 \left(T - T^{ref} \right) (S)^2 - \frac{2}{27}b(S)^3 + \frac{1}{9}c(S)^4 \quad (2.5)$$

Equation (2.5), is a power series in scalar order parameter S , also higher order terms are neglected since S is smaller than one. At equilibrium the free energy of the system is minimum. The problem requires minimization of the free energy f_h , so in essence we are interested in minimizing the free energy of the system under constraints of material properties, processing conditions and boundary conditions.

In order to understand the phase transitions from isotropic state to nematic state consider figure 2-3. The figure is a phase diagram obtained from the solution of equation (2.5). [7] .The are six regions in the figure:

$T > T^{**}$ there is only one minimum corresponding to $S=0$, which means at this temperature the liquid crystalline material has the properties of isotropic fluid.

$T^{**} > T > T_{NI}$ as we lower the temperature to this region a second minimum appears. This minimum corresponds to a metastable nematic phase since f_h at this point is larger than that at $S=0$ (the global minimum). Also T^{**} is defined as the highest temperature at

which liquid crystals can be found in metastable nematic phase and is referred to as the *highest superheating temperature of the nematic phase*.

$T = T_{NI}$ at this temperature the values of f_h corresponding to the isotropic and nematic phase are equal indicating that the probability of finding the system in isotropic phase is equal to the probability of finding it in the nematic phase and hence is known as the *phase transition temperature*.

$T_{NI} > T > T^{ref}$ in this region the isotropic phase becomes metastable and the nematic phase becomes stable.

$T = T^{ref}$ at this point the minimum at $S=0$ disappears. This temperature corresponds to the lowest temperature at which metastable isotropic phase exists and is known as the *supercooling temperature of the isotropic phase*.

$T < T^{ref}$ beyond this point the free energy has only one minimum corresponding to the nematic phase.

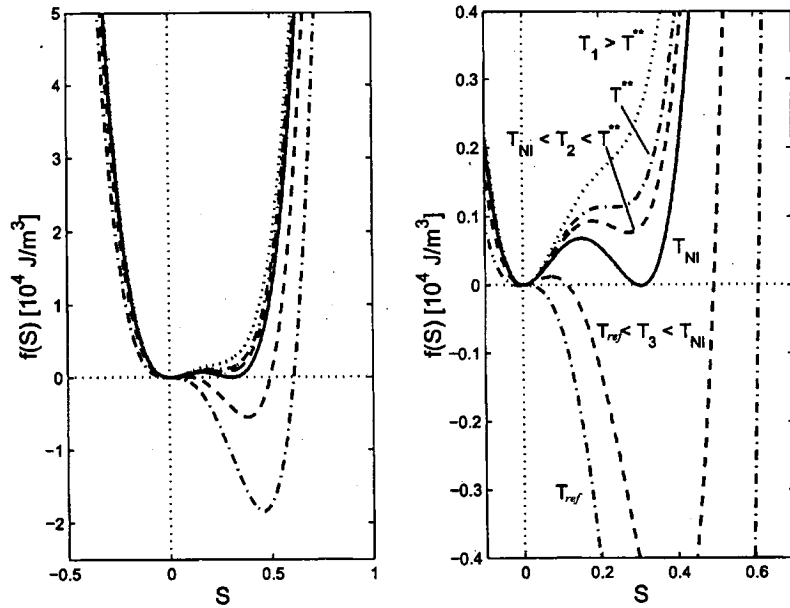


Figure 2-3: The free energy density as a function of scalar order parameter for different values of temperature. Magnified image of the left figure is presented on the right. The parameters a,b,c etc. were taken from reference [7]

2.5 Carbonaceous Mesophase texture modeling: theory and derivation

This section is devoted to carbonaceous mesophase above the phase transition temperature T_{NI} . The texture in these systems has been experimentally studied by White and coworkers [5,6] and lately modeling of these materials in carbon fibers has also been accomplished by Rey and coworkers [2,3]. However till now the effect of carbon fibers on the bulk mesophase texturing process was not studied and forms the basis of this thesis.

The c/c composite consists of a randomly positioned and axially aligned set of cylindrical carbon fibers of equal radius embedded in a textured carbonaceous mesophase matrix, shown in figure 2-4.

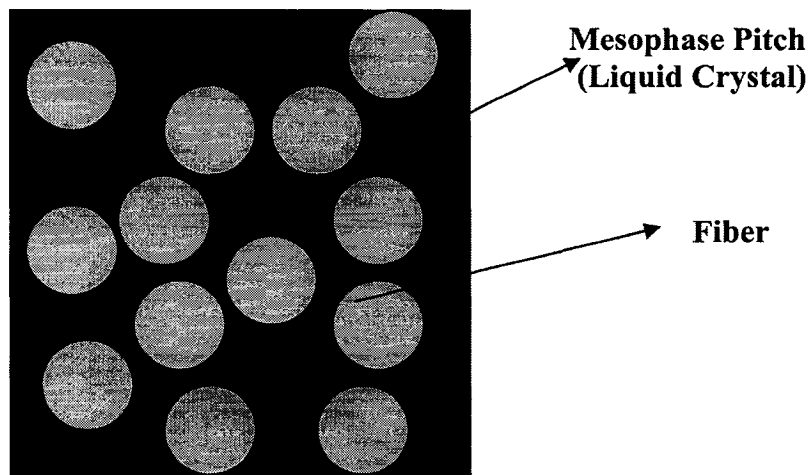


Figure 2-4: Schematic of transverse section of c/c composite.

In actual systems the fibers maybe weaved or arranged in two-dimensional or three dimensional configurations which were depicted in figure 1-2, however as a starting point in modeling these composites as well as to validate the simulations with the experiments of White et al. [5,6], a transverse cross-section along the fiber radius was studied. Experimentally [5,6] it is known that the presence of fibers induces homeotropic anchoring where the disk like molecules lie face-on onto the fiber surface. This is illustrated schematically in figure 2-5a. The present work only deals with this type of surface anchoring consistent with experimental observations. In fact experiments [5,6] indicate that the effect of the fibers is so strong that molecules tend to align homeotropically around the fiber up to few microns outside the fiber periphery causing what is known as the “sheath effect”. The presence of these fibers in the mesophase causes a disruption near the vicinity of the surface of these fibers leading to orientation and defects that were discussed before. For example consider figure 2-5b, shows a single fiber inside the mesophase. Since the molecules closer to the fiber will tend to align homeotropically to the fiber surface, however as we move away from the fiber surface this effect will reduce and in the bulk the molecules will be unaffected by the fibers. This forms the boundary condition for the problem. This would create an incompatibility between the molecules that are close to the fibers and that are in bulk, creating defects.

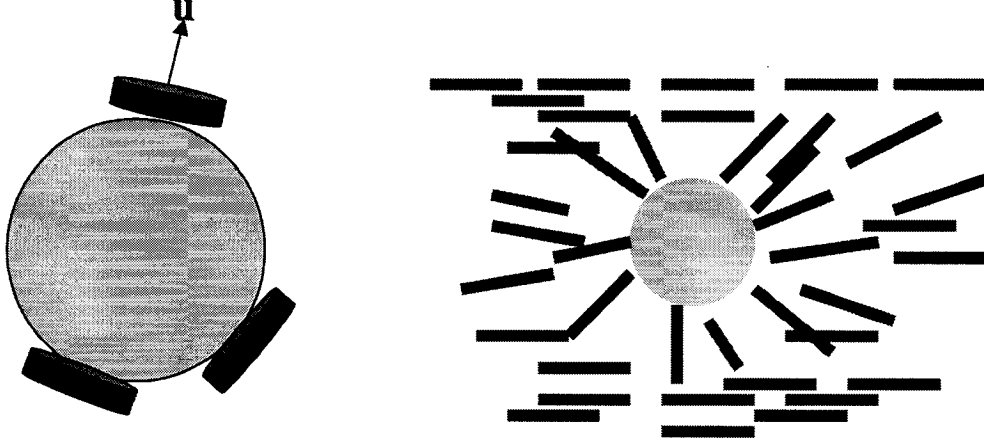


Figure 2-5: (a) Experimental observations ref indicate that the mesophase molecules align face-on along the fiber surface. This type of “homeotropic anchoring” causes what is popularly known as the *sheath effect* . (b) Close to the fiber the molecules are aligned homeotropically whereas away from the fiber surface the alignment is more uniform.

2.6 Texture Equation for Carbonaceous Mesophase

In the previous section it was mentioned that the presence of fibers inside the mesophase causes disruption. In this case the average preferred orientation of the molecules, given by director \mathbf{n} varies from point to point in the material (close to the fiber surface the anchoring is homeotropic whereas away from the surface it is uniform). This requires that additional terms be added to the free energy of the bulk liquid crystal equation (2.4) (as previously the equation only accounted for phase transition but not spatial variation of director). Thus the generalized equation becomes

$$\begin{aligned}
 f = & \frac{1}{2}a_0 (T - T^{\text{ref}}) (\mathbf{Q} : \mathbf{Q}) - \frac{1}{3}b\mathbf{Q} : (\mathbf{Q} \cdot \mathbf{Q}) + \frac{1}{4}c(\mathbf{Q} : \mathbf{Q})^2 \\
 & + \frac{1}{2}L_1 \nabla_\alpha \mathbf{Q}_{\beta\gamma} \nabla_\alpha \mathbf{Q}_{\beta\gamma} + \frac{1}{2}L_2 \nabla_\alpha \mathbf{Q}_{\alpha\gamma} \nabla_\beta \mathbf{Q}_{\beta\gamma} + \frac{1}{2}L_3 \mathbf{Q}_{\alpha\beta} \nabla_\alpha \mathbf{Q}_{\gamma\delta} \nabla_\beta \mathbf{Q}_{\gamma\delta}
 \end{aligned} \tag{2.6}$$

where the parameters L_1 , L_2 and L_3 are elastic parameters independent of temperature and concentration. These added terms take into account the distortion of mesophase due to

the elasticity of the material. The transient evolution of texturing in the mesophase can be obtained by solving a torque balance equation:

$$- \underbrace{\gamma(\mathbf{Q}) \frac{\partial \mathbf{Q}}{\partial t}}_{\text{viscous resistance}} = \underbrace{\left(\frac{\delta F}{\delta \mathbf{Q}} \right)^{[s]}}_{\text{elastic driving force}} = \left[\frac{\partial F}{\partial \mathbf{Q}} - \nabla \cdot \frac{\partial F}{\partial \nabla \mathbf{Q}} \right]^{[s]} \quad (2.7)$$

where the left hand side represents the viscous resistance, and the right hand side is the driving force; the symbol [s] denotes symmetric and traceless condition that arise because \mathbf{Q} is symmetric and traceless. The viscous resistance is due to the rotational viscosity $\gamma(\mathbf{Q})$ of the mesophase and the driving force originates from a decrease in the total elastic free energy F of the system:

$$F = \int_V f dV \quad (2.8)$$

Equation (2.7) is the governing equation and consists of five coupled parabolic non-linear partial differential equations. The solution vector is space-time dependent $\mathbf{Q}(\mathbf{x}, t)$.

2.7 Computational Modeling

During the last two decades modeling has played unquestionably a significant role in engineering. It has replaced the old trial and error system specific methods that prototype engineers once used in design, research and development with science-based computational modeling based on finite element, finite volume and finite difference analysis. In fact modeling has been successfully applied to problems in biology, geology, chemical, and mechanical with the aid of the laws of physics, in terms of algebraic differential or integral equations. The fact that very few equations have an exact solution leads one to approximate methods such as finite elements. The present thesis uses finite elements for the approximation and solution of the governing equation (2.7).

In essence finite elements method (FEM) approximates a partial differential equation (PDE) with a problem that has finite number of unknown parameters. This process is known as *discretization* of the original problem.

- The first step in solving a PDE using finite elements is the generation of mesh. This means that the geometry is partitioned into small units of simple shape like triangles in 2D and prisms or cubes in 3D. These elements only approximate the geometry and the more elements that one takes the better this approximation gets. Figure 2-6 below shows a typical mesh that was used in the computation. An important point to note regarding the mesh is that since the radius of the defect core is 10nm [19] the coarsest mesh size should be smaller than this number. This creates difficulty as the fiber size is in micron range. This large scaling difference creates computational resource problem and using a uniform mesh is inadequate. To overcome this challenge, adaptive grids were used. For the present problem the mesh was adapted manually. Simulation was stopped at an intermediate time step and then the domain was remeshed according to the spatial gradients in \mathbf{Q} . The higher the gradients in \mathbf{Q} the higher the density of elements. Figure 2-6 shows the mesh design at two different time steps.

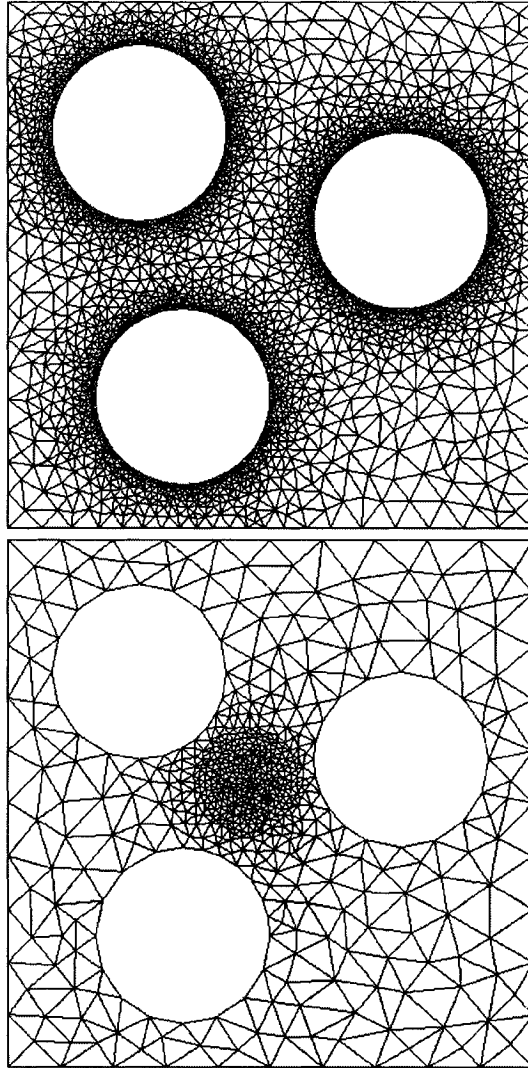


Figure 2–6: The figure shows mesh at two different time steps in the problem. The first one is at initial time step and the second one is at a later time step.

Initially, the mesh density is higher near the fiber surface because the directors start to arrange homeotropically near the fiber surface. At a later stage in the problem the mesh density decreases near the fiber surface as everything is already aligned and so the mesh becomes coarser there. Since FEMLAB at present didn't have automatic

grid adaptation, the remeshing was done manually. The simulation were stopped at an intermediate time step and the problem was remeshed based on the spatial gradients in \mathbf{Q} . At a later stage in the research due to the availability of improved computational resources, the same results were compared with a uniform mesh. The two results were found to be in excellent agreement.

- Once the mesh has been created the dependent variable needs to be approximated. The idea is to approximate the dependent variable with a function. This approximation of the dependent variable when introduced into the weak form [20] of the equation generated a system of algebraic equations. The governing equation (2.7) has \mathbf{Q} as

$$\text{the dependent variable, where the tensors order parameter } \mathbf{Q} = \begin{pmatrix} Q_{11} & Q_{12} & Q_{13} \\ Q_{21} & Q_{22} & Q_{23} \\ Q_{31} & Q_{32} & Q_{33} \end{pmatrix}.$$

These dependent variables for the present simulations were approximated by a quadratic basis function for eg. the variable Q_{11} can be approximated by:

$$Q_{11} = \sum_1^N Q_{11j}(t) \varphi_j(x, y, z) \quad (2.9)$$

Here, $\varphi_j(x, y, z)$ is a quadratic function and we have described the finite element space by using a basis function.

- The third step is the discretization of the equations. The starting point is the formulation of the weak form of the problem. For eg. the weak form of the component Q_{11} is:

$$\int \left(\gamma(\mathbf{Q}) \frac{\partial Q_{11}}{\partial t} + \left[\frac{\partial F}{\partial \mathbf{Q}} - \nabla \cdot \frac{\partial F}{\partial \nabla \mathbf{Q}} \right]_{11}^{[s]} \right) \varphi_i dx dy = 0 \quad (2.10)$$

Now if we use the definition of Q_{11} from equation (2.9) and substitute into equation (2.10) we have:

$$\gamma(\mathbf{Q}) \frac{\partial Q_{11}}{\partial t} \int \varphi_i \varphi_j dx dy = - \int \left(\left[\frac{\partial F}{\partial \mathbf{Q}} - \nabla \cdot \frac{\partial F}{\partial \nabla \mathbf{Q}} \right]_{11}^{[s]} \right) \varphi_i dx dy = A \quad (2.11)$$

this expression can be written in concise form as:

$$Q_{11}(t_{n+1}) = \frac{\Delta t_{n+1}}{\gamma} A \bullet \mathbf{M}^{-1} + Q_{11}(t_n) \quad (2.12)$$

here \mathbf{M} is called the mass matrix

$$M = \int \varphi_i \varphi_j dx dy \quad (2.13)$$

where t_n is the time of n^{th} step and Δt_{n+1} is the time adopted in $n+1$ time step. Similar computations are performed for other components of \mathbf{Q} . The governing sets of equations for all components of \mathbf{Q} equation (2.12) were then solved by using a nonlinear iterative solver through commercial software FEMLAB [21].

- Convergence was monitored by increasing the mesh density, and comparing the solution to get a mesh independent solution.

2.8 Validation Methodology

The approach described in this Chapter was applied to simulate significant textural features relevant to the science and engineering of c/c composites, and results are presented in the next three Chapters. In all cases the computational predictions were validated using available experimental data. The validation procedure was based on the fact that the structural variable \mathbf{Q} is directly observed experimentally using reflection polarized optical microscopy (RPOM) [22]. The computed texture can then be compared with the observed textures. As indicated in Chapter 4, we use the identical fiber structure and overall geometry as in experiments. In addition in Chapter 3 the validation also included

optical computations based on the spatial distribution of \mathbf{Q} . The optical computations were performed by Mr Dae Kun Hwang and the methodology is explained in [23] and Chapter 3.

2.9 References

- 1 J.E. Zimmer and J. L. White, *Advances in Liquid Crystals*, **5** , 157-213 (1982).
- 2 J. Yan and A. D. Rey, *Phys. Rev. E* **65** , 031713 (2002).
- 3 D. Sharma and A. D. Rey, *Liquid Crystals* **30** , 377-389 (2003).
- 4 T. Tsuji and A. D. Rey, *J. Non-Newtonian Fluid Mech .* **73** , 127 (1997).
- 5 J.E. Zimmer and J. L. White, *Carbon*, **27** (6), 791-801 (1989).
- 6 J. E. Zimmer and R. L. Weitz, *Extended Abstracts 16th biennial conf. on Carbon*, American Carbon Society; 92-3 (1983).
- 7 A. Borstnik, Ph. D. Thesis, University of Ljubljana (2000)
- 8 E. B. Priestley, P. J. Wojtowicz, and P. Sheng, *Introduction to Liquid Crystals* , Plenum, New York, (1974)
- 9 L. Onsager, *Ann. N.Y. Acad. Sci.*, 51, 627 (1949)
- 10 W. Maier and A. Saupe, *Z. Naturf. A*, 13, 564 (1958)
- 11 J. H. Thurtell, M. M. Telo da Gama and K. E. Gubbins, *Mol. Phys.*, 54, 312 (1985)
- 12 J. C. Gay and J. Berne, *J. Chem. Phys.*, 74, 3316 (1981)
- 13 J. L. Billeter and R. A. Pelcovits, *Phys. Rev. E*, 62, 711 (2000)
- 14 D. Andrienko, G. Germano and M. P. Allen, *Phys. Rev. E*, 63, 041701 (2001)
- 15 S. Grollau et al., *J. Chem. Phys.* 119 (4), 2444 (2003)
- 16 de Gennes PG, Prost J. *The physics Of Liquid Crystals* , 2nd edition. Oxford: Clarendon Press. 1993.
- 17 L.D. Landau and E. M. Lifshitz, *Course of theoretical Physics; statistical physics* , Butterworth & Heinemann, Oxford, (1999)
- 18 V. N. Tsvetkov and S. P. Krozer, *zh. Tekh. Fiz.* 28, 1444 (1958);[*Sov. Phys.-Tech. Phys.* 3, 1340 (1958)].
- 19 H. Stark. *Phys. Reports* , **351** , 387 (2001).

- 20 B. A. Finlayson, *Nonlinear analysis in Chemical Engineering* ,London: McGraw Hill. 1980.
- 21 Femlab Version 3.0a, Comsol Inc.
- 22 H. Wohler, G. Hass, M. Fritsch, and D. A. Mlynski, *J. Opt. Soc. Am. A* **5** , 1554-1557 (1988).
- 23 Gupta G, Hwang DK, and Rey AD. *Optical and structural modeling of disclination lattices in carbonaceous mesophases. Journal of Chemical Physics* 2005; **122** (3): 034902-11.

CHAPTER 3

Optical and structural modeling of disclination lattices in carbonaceous mesophase

3.1 Abstract

An integrated microstructural and optical model for carbonaceous mesophases is developed and used to explain the principles that govern the formation and stability of experimentally observed disclination lattices. The model is able to capture the orientation features of disclination lattices, including the type and location of disclination lines, and the orientation field in the mesophase matrix. The optical model based on reflection polarized optical microscopy is able to replicate all the details observed in actual observations. The typical brush figures have the proper distribution, orientation, and intensity. The computational predictions offer new science-based routes to create and control desirable material architectures based on carbonaceous mesophase-carbon fiber composites.

3.2 Introduction

Carbonaceous mesophases, such as coal tar and petroleum pitches, are used in the industrial manufacturing of mesophase carbon fiber, carbon foams, carbon fiber-carbon mesophase composites (CFCM), and carbon nanotube-carbon mesophase nanocomposites (CNCM) [1-5]. The thermodynamic phase that describes carbonaceous mesophases is the discotic nematic liquid crystal state [6, 7]. Liquid crystals are intermediate (i.e. mesophase) phases, typically found for anisodiametric organic molecules, which exist between the higher temperature isotropic liquid state and the lower temperature crystalline state. Carbonaceous mesophases are composed of disk-like molecules [7]. Figure 3-1 shows the molecular geometry, positional disorder, and uniaxial orientational order of discotic nematic liquid

crystals. The partial orientational order of the molecular unit normal \mathbf{u} is along the average orientation or director \mathbf{n} ($\mathbf{n} \cdot \mathbf{n} = 1$) [6]. The name discotic distinguishes the molecular geometry and the name nematic identifies the type of liquid crystalline orientational order [6].

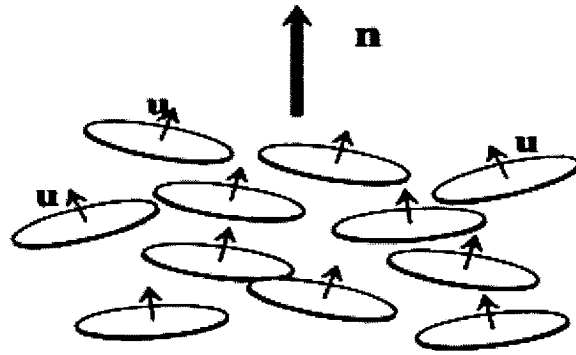


Figure 3-1: Definition of the director orientation of uniaxial discotic nematic liquid crystals. The director \mathbf{n} is the average orientation of the unit normals to the disk-like molecules in a discotic nematic phase.

For anisotropic liquid crystalline phases, processing and product properties are strongly correlated with microstructure since liquid crystallinity implies molecular alignment and macroscopic orientation [8]. Hence thermodynamic, transport, and mechanical properties can be controlled by manipulation of the underlying microstructure [7]. In these materials microstructural features exist at different length scales, from microns to nanometers. As in the case of metals, pure liquid crystals exhibit point, line and wall defects, polydomain or grain textures, and banded patterns [9-14]. In general a defect is specified by a charge (s) and dimensionality (0D, 1D, 2D). The magnitude of s denotes the amount of director rotation when encircling the defect and the sign the sense of this rotation [9-14]. The presence of textures or distributions of defects also offers a way to identify the phases using

polarized optical microscopy [11]. In practice the way to manipulate microstructure to design liquid crystalline materials with specific properties can be classified into: (i) hydrodynamic structuring, (ii) thermodynamic structuring, (iii) interfacial structuring and (iv) particle dispersion structuring. Hydrodynamic structuring can be achieved by flow through meshes [15, 16], and flow in capillaries and dies [17, 18], among others. Thermodynamic structuring is based on phase separation of a second phase in a liquid crystal matrix. These special liquid crystal colloids can organize the second phase in an ordered lattice through the action of long range orientational forces [19]. Interfacial structuring forms the basis of a sensor technology, since surface roughness can be detected by the resulting texture in liquid crystal thin films [20]. Particles and fibers dispersed in liquid crystals interact with the liquid crystalline matrix, giving rise to defect textures in the mesophase matrix [21-23]. Currently significant effort is directed to study filled liquid crystals (FLCs), mesophase-carbon fiber composites [24], and mesophase-carbon nanotube nanocomposites [25].

Hydrodynamics structuring of carbonaceous mesophases has been studied by White and co-workers [15, 16]. The mesophase was pumped through capillary with a metal mesh screen of square symmetry. After traversing the mesh a robust super-disclination structure formed and persisted downstream. The microstructure was characterized using RPOM (reflection polarized optical microscopy) commonly used for anisotropic opaque materials [26]. Figure (3-2) shows the orientation distribution and the optical micrograph.

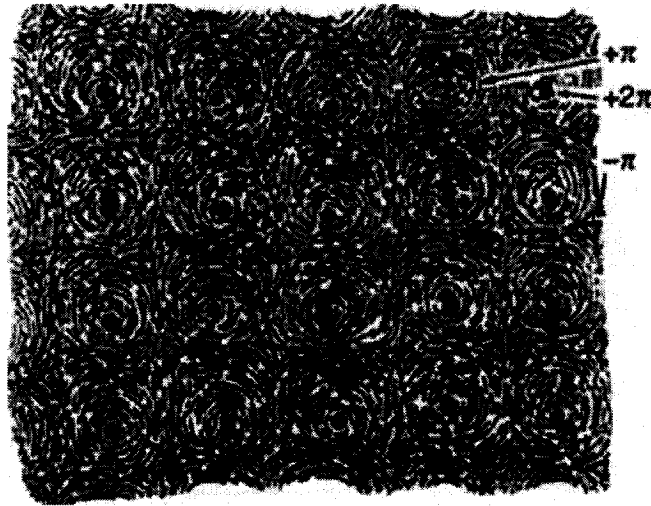


Figure 3-2: A map of regular array of +2 and - wedge disclinations formed by mesophase flow through a 200-mesh screen in an experiment to control the microstructure of mesophase pitch conducted by Fathollahi et al. Reprinted from [16] with permission of Taylor and Francis. The dark dots correspond to +2 ($s=+1$) disclinations, and the two disclinations along the diagonals of a unit square lattice are ($s=-1/2$) wedge disclinations.

The figure shows that hydrodynamic structuring with square meshes produces a square disclination lattice of strength $s=+1$. Along one diagonal of each unit square cell two $s=-1/2$ disclinations are separated by a small distance. The total topological charge of the superdisclination is zero and the superdisclination is stable because all repulsive and attractive interactions are balanced. Hydrodynamic structuring acts through the action of viscous torques, also known as orientation. Since the mesophase can anchor in specific orientations at surfaces, structuring through particle dispersion is another route to create new material architectures.

Particle dispersion structuring is based on interfacial mesophase-particle interactions [7,21]. Under strong interfacial orientational anchoring conditions, the mesophase tends to be oriented along the easy axis [7,26-28]. For circular interfaces the easy axis rotates with

the unit surface normal, and the distortion propagates into the bulk by a distance of the order of the particle size [6]. The distortion is quenched by the nucleation of point, line, or wall defects. For planar orientation, insertion of a circular fiber with their axis normal to the director field under strong anchoring conditions, creates a pair of disclinations of strength $s=-1/2$. A lattice of such fibers would in principle create a lattice of such defects, identical to the superdisclination structure created by White and co-workers [15,16]. This paper seeks to show by computational modeling that immersing a lattice of sufficiently small circular fiber into an isotropic pitch evolves naturally into the super-disclination structure of [15, 16], and demonstrate that particle structuring of carbonaceous mesophases is in addition to hydrodynamics structuring, a route to design new multiscale material architectures. The existence and properties of stable crystals of defects (i.e. superdisclinations) has been discussed and reviewed by Bouligand[13]. It is known that in many mesophases, including water-lipid systems and blue-phases, defects enters the architecture of the unit cell in a three dimensional array, and the mesophase forms a crystal of defects. Hence the super-disclinations observed and simulated in this paper are another example of a large number of defect lattices experimentally found in other liquid crystalline materials.

The specific objectives of this paper are:

- 1 Develop, solve, and validate a computational model of microstructure formation in carbonaceous mesophases-fiber composites.
- 2 Demonstrate that super-disclinations obtained by flow through grids and screens [15,16] are also achievable in principle by inserting periodic arrays of fibers in mesophases.
- 3 Develop, solve, and validate a computational model for reflection polarized microscopy, useful to characterize microstructures in textured carbonaceous materials.

In this work the radius of the fibers inserted into the mesophase is approximately 0.5 μm , a scale intermediate between carbon fibers and nanotubes. No specific claim is made

regarding the applicability of the model to single wall or double wall nanotubes. The key assumption in the paper is that the mesophase strongly orients at the fiber surface, which has been clearly demonstrated for carbon fibers of radius $5\mu\text{m}$ [7].

This paper is organized as follows. In section 3.3 we present the model formulation for microstructural and optical phenomena. Section 3.4 presents, discusses, and validates the microstructural and optical simulations results. Conclusions are given in section 3.5.

3.3 Microstructural, Optical and Computational Modeling

This section presents technical details of the microstructural model, the optical model, and the computational methodology.

3.3.1 Microstructural Model for Carbonaceous Mesophases

The microstructural modeling of carbonaceous mesophases requires spatio-temporal specification of the orientation and degree of molecular order, and their time evolution when driven by viscoelastic processes. This subsection defines the microstructure, the elastic energies involved in molecular and macroscopic distortions, and the microstructure evolution equation that governs the emergence of multiscale patterns and structures. In this work we adopt the Landau-de Gennes liquid crystal modeling formalism to carbonaceous mesophases [6, 29-32].

Description of Microstructure

The Landau-de Gennes theory of liquid crystals [6] describes the viscoelastic behavior of nematic liquid crystals using the second moment of the orientation distribution function, known as the tensor order parameter $\mathbf{Q}(\mathbf{x},t)$, and the velocity field $\mathbf{v}(\mathbf{x},t)$. The tensor order parameter field $\mathbf{Q}(\mathbf{x},t)$ and the velocity field $\mathbf{v}(\mathbf{x},t)$ have independent origins. In the absence of macroscopic flow, $\mathbf{v}=0$, the viscoelasticity of liquid crystals is described by $\mathbf{Q}(\mathbf{x},t)$. This means that spatio-temporal changes in the order parameter may exist even

in the absence of flow. In this paper macroscopic flow does not occur, $\mathbf{v} = 0$, and the state of the liquid crystal is defined solely by $\mathbf{Q}(\mathbf{x}, t)$.

The macroscopic and molecular description of the microstructure defined by the second order symmetric and traceless tensor \mathbf{Q} [6] and is efficiently expressed as:

$$\mathbf{Q} = S(\mathbf{nn} - \frac{1}{3}\delta) + \frac{1}{3}P(\mathbf{mm} - \mathbf{ll}) \quad (3.1a)$$

where the following restrictions apply:

$$\mathbf{Q} = \mathbf{Q}^T \quad (3.1b)$$

$$tr(\mathbf{Q}) = 0 \quad (3.1c)$$

$$-\frac{1}{2} \leq S \leq 1 \quad (3.1d)$$

$$-\frac{3}{2} \leq P \leq \frac{3}{2} \quad (3.1e)$$

$$\mathbf{n} \cdot \mathbf{n} = \mathbf{m} \cdot \mathbf{m} = \mathbf{l} \cdot \mathbf{l} = 1 \quad (3.1f)$$

$$\mathbf{nn} + \mathbf{mm} + \mathbf{ll} = \delta = \begin{bmatrix} 1 & 0 & 0 \\ 0 & 1 & 0 \\ 0 & 0 & 1 \end{bmatrix} \quad (3.1g)$$

Equivalently, the symmetric traceless tensor order parameter \mathbf{Q} can be written as an expansion of its eigenvectors:

$$\mathbf{Q} = \mu_n \mathbf{nn} + \mu_m \mathbf{mm} + \mu_l \mathbf{ll} \quad (3.2a)$$

$$\mu_n + \mu_m + \mu_l = 0 \quad (3.2b)$$

where the uniaxial director \mathbf{n} corresponds to the maximum eigenvalue $\mu_n = \frac{2}{3}S$, the biaxial director \mathbf{m} corresponds the second largest eigenvalue $\mu_m = -\frac{1}{3}(S - P)$, and the second biaxial director $\mathbf{l} (= \mathbf{n} \times \mathbf{m})$ corresponds to the smallest eigenvalue $\mu_l = -\frac{1}{3}(S + P)$.

The orientation is defined completely by the orthogonal director triad $(\mathbf{n}, \mathbf{m}, \mathbf{l})$. The magnitude of the uniaxial scalar order parameter S is the molecular alignment along the uniaxial director \mathbf{n} , and is given by: $S = \frac{3}{2}(\mathbf{n} \cdot \mathbf{Q} \cdot \mathbf{n})$. The magnitude of the biaxial scalar order parameter P is the molecular alignment in a plane perpendicular to the direction of uniaxial director \mathbf{n} , and is given by: $P = \frac{3}{2}(\mathbf{m} \cdot \mathbf{Q} \cdot \mathbf{m} - \mathbf{l} \cdot \mathbf{Q} \cdot \mathbf{l})$. On the principal axes, the tensor order parameter \mathbf{Q} is represented as:

$$\mathbf{Q} = \begin{bmatrix} -\frac{1}{3}(S - P) & 0 & 0 \\ 0 & -\frac{1}{3}(S + P) & 0 \\ 0 & 0 & \frac{2}{3}S \end{bmatrix} \quad (3.3)$$

both S and P are positive for normal disc-like uniaxial nematic liquid crystals. According to equation (3-3), the model is able to describe biaxial ($S \neq 0, P \neq 0$), uniaxial ($S \neq 0, P = 0$), and isotropic ($S = 0, P = 0$) states. The isotropic state is the zero tensor: $\mathbf{Q} = 0$. Defects are regions of molecular size in which orientational order (S, P) sharply changes. These localized disordered regions are in principle captured by mesoscopic models since \mathbf{Q} remains well behaved. The eigenvalues of \mathbf{Q} capture molecular information and the eigenvector describe macroscopic orientation, and hence the Landau-de Gennes model is a multiscale model [9].

Mesophase Elasticity. In the Landau-de Gennes theory the free energy density difference between nematic and isotropic state is expressed in terms of \mathbf{Q} and its spatial gradients $(\nabla \mathbf{Q})$ [30, 31]. The total elastic free energy density f is given by the sum of homogenous f_h and gradient f_g contributions:

$$f = f_h + f_g \quad (3.4)$$

The homogeneous free energy density f_h represents the free energy difference between the liquid crystal and isotropic phases and may be expressed as a power series in \mathbf{Q} [9]:

$$f_h = \frac{1}{2}a_o \left(T - T^{ref} \right) (\mathbf{Q} : \mathbf{Q}) - \frac{1}{3}b\mathbf{Q} : (\mathbf{Q} \cdot \mathbf{Q}) + \frac{1}{4}c(\mathbf{Q} : \mathbf{Q})^2 \quad (3.5)$$

where a_o , b , and c are constants, and T^{ref} is the liquid crystal-isotropic transition temperature [6]. The homogeneous energy describes energy changes due to molecular ordering. The isotropic state corresponds to zero homogeneous energy, while for the stable liquid crystal state corresponds to negative homogeneous energies. The gradient elasticity $f_g(\nabla\mathbf{Q})$ can be decomposed into three contributions:

$$f_g(\nabla\mathbf{Q}) = f_{g1}(\nabla\mathbf{Q}) + f_{g2}(\nabla\mathbf{Q}) + f_{g3}(\mathbf{Q}, \nabla\mathbf{Q}) \quad (3.6)$$

These three contributions arise naturally since mesophases are intrinsically anisotropic[31]. The three contributions can be shown to be [31-33].

$$f_{g1} = \frac{1}{2}L_1 \nabla_\alpha Q_{\beta\gamma} \nabla_\alpha Q_{\beta\gamma} \quad (3.7a)$$

$$f_{g2} = \frac{1}{2}L_2 \nabla_\alpha Q_{\alpha\gamma} \nabla_\beta Q_{\beta\gamma} \quad (3.7b)$$

$$f_{g3} = \frac{1}{2}L_3 Q_{\alpha\beta} \nabla_\alpha Q_{\gamma\delta} \nabla_\beta Q_{\gamma\delta} \quad (3.7c)$$

where $\alpha, \beta, \gamma, \delta = 1, 2, 3$ denote the components along the three orthogonal axes in the Cartesian coordinate system, and ∇_i denotes the partial derivative $\frac{\partial}{\partial x_i}$. All throughout the thesis summation over repeated indices is implied. The coefficients L_1, L_2, L_3 , are constant phenomenological parameters dependent on the liquid crystal. In the one-constant approximation, $L_2=L_3=0$, and the material is assumed to be elastically isotropic. The gradient energy f_g is always non-negative: $f_g \geq 0$. In the presence of defects and distortions the gradient energy is always positive: $f_g > 0$. For spatially homogeneous states the gradient elastic energy vanishes: $f_g = 0$. In the definition of the total energy density (eqn. 3.4), for

the sake of simplicity we have neglected the free energy of the isotropic part, and influence of any external field and any surface energy contributions since we are interested in studying the bulk only.

To discuss and characterize orientation process it is useful to consider the contributions due to orientation gradients. For most relatively low molar mass liquid crystals we can safely set $L_3=0$ without missing any first order process. In the absence of biaxiality ($P=0$) and deviations from equilibrium in the order parameter, the tensor order parameter simplifies to:

$$Q = S_{eq}(\mathbf{nn} - \frac{1}{3}\delta) \quad (3.8)$$

where the equilibrium order parameter is given by:

$$S_{eq} = \frac{b}{4c} \left[1 + \sqrt{1 - \frac{(24a_0c(T - T^{ref}))}{b^2}} \right] \quad (3.9)$$

Using eqns. [3-(6-8)] and the conditions stated above, the elastic energy density due to orientation gradients becomes:

$$f_g = S_{eq}^2 \left\{ \left(L_1 + \frac{1}{2}L_2 \right) (\nabla \cdot \mathbf{n})^2 + L_1 (\mathbf{n} \cdot \nabla \times \mathbf{n})^2 + \left(L_1 + \frac{1}{2}L_2 \right) |\mathbf{n} \times \nabla \times \mathbf{n}|^2 \right\} \quad (3.10)$$

In classical liquid crystal elasticity [6], the elastic free energy density is given by the Frank free energy f_F :

$$2f_F = K_{11} (\nabla \cdot \mathbf{n})^2 + K_{22} (\mathbf{n} \cdot \nabla \times \mathbf{n})^2 + K_{33} |\mathbf{n} \times \nabla \times \mathbf{n}|^2 \quad (3.11)$$

where (K_{11}, K_{22}, K_{33}) are the twist, and bend elastic constants, respectively. Comparing eqns.(3-10) and (3-11) under the assumption of splay-bend isotropy ($K_{11} = K_{33}$) the relations between the Landau-deGennes and Frank constants are [33]:

$$L_1 = \frac{K_{22}}{2S_{eq}^2} \quad (3.12)$$

$$L_2 = \frac{K_{11} - K_{22}}{2S_{\text{eq}}^2} \quad (3.13)$$

The necessary condition for the stability of equilibrium liquid crystal configuration is that the gradient energy must be positive and this restricts the Landau-deGennes coefficients as follows:

$$L_1 > 0; L_1 + \frac{1}{2}L_2 > 0 \quad (3.14)$$

For carbonaceous mesophases it was shown [35] that $L_2 < 0$, and the twist deformation is the most costly. It is thus expected that for most cases, planar splay-bend 2D structures are more favorable than twisted structures.

Microstructure Evolution

To describe the evolution of microstructures in carbonaceous mesophases dynamical equations for the tensor order parameter must be derived. For viscoelastic materials, relaxing the absence of flow, the dynamics obeys the following equation:

$$- \underbrace{\gamma(\mathbf{Q}) \frac{d\mathbf{Q}}{dt}}_{\text{viscous resistance}} = \underbrace{\left(\frac{\delta F}{\delta \mathbf{Q}} \right)^{[s]}}_{\text{elastic driving force}} \quad (3.15)$$

where the viscous resistance is due to the rotational viscosity of the mesophase and the driving force originates from a decrease in the total elastic free energy F of the system:

$$F = \int_V f dV = \int_V (f_h + f_g) dV \quad (3.16)$$

The coefficient γ in eqn.(3.15) is the rotational viscosity, $\delta F / \delta \mathbf{Q}$ is the Volterra variational derivative [36], and the superscript [s] denotes symmetric and traceless property. The evolution equation (3-15) can also be derived using irreversible thermodynamics [6, 30]. The rate of entropy production Δ under isothermal conditions for a relaxing mesophase is

given by [6, 30].

$$\Delta = \frac{d\mathbf{Q}}{dt} : \left(-\frac{\delta F}{\delta \mathbf{Q}} \right)^{[s]} + \mathbf{t} : \nabla \mathbf{v} \quad (3.17)$$

Expanding the fluxes $\left(\frac{d\mathbf{Q}}{dt}, \mathbf{t} \right)$ in terms of forces $\left(\left(-\frac{\delta F}{\delta \mathbf{Q}} \right)^{[s]}, \nabla \mathbf{v} \right)$:

$$\begin{pmatrix} \frac{d\mathbf{Q}}{dt} \\ \mathbf{t} \end{pmatrix} = \begin{pmatrix} \beta_1 & \beta_{12} \\ -\beta_{12} & \beta_2 \end{pmatrix} \begin{pmatrix} \left(-\frac{\delta F}{\delta \mathbf{Q}} \right)^{[s]} \\ \nabla \mathbf{v} \end{pmatrix} \quad (3.18)$$

where the β 's are phenomenological coefficients. In the absence of flow ($\nabla \mathbf{v} = 0$), choosing $\beta_1 = 1/\gamma$ we obtain eqn. (3-15). Nondimensionalization is useful to characterize processes and diminish the number of parameters. The free energy density equation (3-4, 3-6, 3-7) is made dimensionless by using the following parameters [34].

$$f^* = \frac{f}{\varphi k T} \quad (3.19a)$$

$$U = 3 \frac{T^{\text{ref}}}{T} \quad (3.19b)$$

$$a_0 = \varphi k \quad (3.19c)$$

$$b = c = \varphi k T U \quad (3.19d)$$

$$\xi = \sqrt{\frac{L_1}{\varphi k T}} \quad (3.19e)$$

$$\vartheta = \frac{L_2}{L_1} \quad (3.19f)$$

$$\kappa = \frac{L_3}{L_1} \quad (3.19g)$$

$$\overset{*}{\nabla} = \nabla * H; \quad (3.19h)$$

$$S_{\text{eq}} = \frac{1}{4} + \frac{3}{4} \sqrt{1 - \frac{8}{3U}} \quad (3.19i)$$

In the isotropic region $U < 8/3$, for $8/3 < U < 3$ there is biphasic equilibrium where nematic and isotropic regions coexist and for $U > 3$ the phase is uniaxial nematic. φ , k are number density of molecules and Boltzmann's constant respectively. The parameter ξ is the coherence length [6] and is of molecular length size. It is the distance over which the scalar order parameter fluctuations are correlated in the sample of a given volume. H is the external length scale of the system in our case the radius of the cylinders. ϑ , κ are the dimensionless Landau Elastic constants and describe the materials elastic anisotropy.

The dimensionless free energy density thus becomes [34]:

$$f^* = f_h^* + f_g^* \quad (3.20a)$$

$$f_h^* = \frac{1}{2} \left(1 - \frac{U}{3} \right) (\mathbf{Q} : \mathbf{Q}) - \frac{U}{3} \mathbf{Q} : (\mathbf{Q} \cdot \mathbf{Q}) + \frac{U}{4} (\mathbf{Q} : \mathbf{Q})^2 \quad (3.20b)$$

dimensionless short range Energy

$$f_g^* = \frac{\xi^2}{H^2} \left(\frac{1}{2} \nabla_{\alpha}^* \mathbf{Q}_{\beta\gamma} \nabla_{\alpha}^* \mathbf{Q}_{\beta\gamma} + \frac{1}{2} \vartheta \nabla_{\alpha}^* \mathbf{Q}_{\alpha\gamma} \nabla_{\beta}^* \mathbf{Q}_{\beta\gamma} + \frac{1}{2} \kappa \mathbf{Q}_{\alpha\beta} \nabla_{\alpha}^* \mathbf{Q}_{\gamma\delta} \nabla_{\beta}^* \mathbf{Q}_{\gamma\delta} \right) \quad (3.20c)$$

dimensionless long range energy

The total dimensionless free energy of the system can be expressed in terms of dimensionless free energy density (20) for a given sample of volume V as:

$$F^* = \int_V f^* dV \quad (3.21)$$

Using eqns. (3-17, 3-18, 3-20, 3-21) the dynamic equation for \mathbf{Q} becomes [6]:

$$-\gamma(\mathbf{Q}) \frac{d\mathbf{Q}}{dt^*} = \frac{\delta F^*}{\delta \mathbf{Q}} = \left[\frac{\partial F^*}{\partial \mathbf{Q}} - \nabla \cdot \frac{\partial F^*}{\partial \nabla \mathbf{Q}} \right]^{[s]} \quad (3.22a)$$

$$t^* = \varphi k T t \quad (3.22b)$$

The rotational viscosity $\gamma(\mathbf{Q})$ affects only the speed of the transient process and has no effect on the steady-state solution hence in the simulation it was fixed to unity.

Combining (20) and (22) we obtain the 2D dimensionless time evolution equation for the tensor order parameter $Q(x^*, y^*, t^*)$:

$$\begin{aligned}
-\gamma(\mathbf{Q}) \frac{dQ_{ij}}{dt^*} &= \left(1 - \frac{U}{3}\right) Q_{ij} - U Q_{i\alpha} Q_{j\alpha} + \frac{U}{3} Q_{\beta\alpha} Q_{\alpha\beta} \delta_{ij} + U Q_{\alpha\beta}^2 Q_{ij} \\
&+ \frac{\xi^2 \kappa}{2H^2} \left(\overset{*}{\nabla}_i Q_{\gamma\delta} \overset{*}{\nabla}_j Q_{\gamma\delta} \right) - \frac{\xi^2 \kappa}{6H^2} \left(\overset{*}{\nabla}_o Q_{\gamma\delta} \overset{*}{\nabla}_o Q_{\gamma\delta} \right) \delta_{ij} - \overset{*}{\nabla}_l \frac{\xi^2}{H^2} \left(\overset{*}{\nabla}_l Q_{ij} \right) \\
&- \overset{*}{\nabla}_l \frac{\xi^2 \vartheta}{2H^2} \left(\left(\overset{*}{\nabla}_\alpha Q_{\alpha j} \right) \delta_{li} + \left(\overset{*}{\nabla}_\alpha Q_{\alpha i} \right) \delta_{lj} \right) + \overset{*}{\nabla}_l \frac{\xi^2 \vartheta}{3H^2} \left(\left(\overset{*}{\nabla}_\alpha Q_{\alpha o} \right) \delta_{lo} \right) \delta_{ij} \\
&- \overset{*}{\nabla}_l \frac{\xi^2 \kappa}{H^2} \left(Q_{\alpha l} \overset{*}{\nabla}_\alpha Q_{ij} \right)
\end{aligned} \tag{3.23}$$

Since \mathbf{Q} is symmetric and traceless, eqn.(3-11) represents five coupled partial differential equations.

Energies and Forces in Disclination Lines and Disclination Lattices

The objective of this subsection is to provide the necessary background that describes the driving forces behind the formation of the superdisclination shown in Fig.(3-2). Disclination lines are described by singular solutions to the Frank elasticity given in eqn.(3-7). In particular wedge lines are obtained for planar 2D director fields with the disclination line along the axis of rotation of the director. The director \mathbf{n} orientation in the vicinity of a wedge disclination line is best analyzed using a polar cylindrical coordinate system (r, α) . To satisfy the unit length restriction $(\mathbf{n} \cdot \mathbf{n} = 1)$, we parameterize the director as follows:

$$\begin{cases} n_r = \cos\theta(\alpha) \\ n_\alpha = \sin\theta(\alpha) \end{cases} \tag{3.24}$$

assuming that outside the defect cores, the scalar order parameter is constant and equal to its equilibrium value, $S=S_{eq}$ (see equation (3-9)). The gradient free energy density then becomes:

$$f_l = \frac{K}{2} (\nabla\theta)^2 \tag{3.25}$$

where we used eqns.(3-11) and isotropic elasticity assumption ($K=K_{11}=K_{22}=K_{33}$). Replacing this last equation in the governing equation (3-22a), assuming steady state, we get the classical Laplace's equation of orientation elasticity that governs the steady planar (2-D) director field of a nematic liquid crystal in any geometry [6]:

$$\nabla^2\theta = 0 \quad (3.26)$$

A general singular defect solution of the Laplace equation in polar (r, α) coordinates to the director angle θ is [6]:

$$\theta(\alpha) = s\alpha + c \quad (3.27)$$

where c is an arbitrary constant and s is the strength of the defect. This singular solution is independent of the radial coordinate [6]. These singular solutions are known as wedge disclination lines and always observed in nematic liquid crystals [6]. The name nematic means thread and refer to the disclination lines observed under cross polarizer [6]. Since the director orientation angle θ is governed by the linear Laplace operator ∇^2 , the principle of superposition can be used to describe textures with two or more defects. The general solution to the Laplace equation in the presence of arbitrary number N of defects of strength s_i , at a point P_i , is [14]:

$$\theta = \sum_{i=1}^N s_i\alpha_i + c \quad (3.28)$$

where α_i is the polar angle of the ray originating at the defect of strength s_i and ending at point P_i , c is a constant and θ is the director angle at any point P_i . For a 2D disclination lattice with square symmetry, the (x_i, y_i) location of the singular lines obey:

$$x_{i+1} = x_i + H, y_{i+1} = y_i + H \quad (3.29)$$

where H is the lattice spacing.

In a defect lattice at equilibrium the total charge of the network must be zero [9, 13]:

$$\sum_{i=1}^N s_i^+ + \sum_{i=1}^M s_i^- = 0 \quad (3.30)$$

where the superscript denotes the sign of the charge. To satisfy charge neutrality if there are N disclinations of strength $s=+1$, the total negative charge in the system should be:

$$\sum_{i=1}^M s_i^- = -N \quad (3.31)$$

If the negatively charge disclinations are of strength $s=-1$, then $M=N$. As explained below that the preferred negatively charge disclination are of strength $s=-1/2$, and hence $M=2N$. The energy per unit length W of an isolated wedge disclination of strength s in a circular layer of radius R is given by [9]:

$$f_l = \frac{K}{2} (\nabla\theta)^2 \quad (3.32a)$$

$$W = \frac{K}{2} \int (\nabla\theta)^2 dx dy = W_c + \int_0^{2\pi} d\alpha \int_{r_c}^R f_l r dr = W_c + \pi K s^2 \ln \left(\frac{R}{r_c} \right) \quad (3.32b)$$

where r_c is a cut-off radius of molecular size, and W_c is the core energy. As $R \rightarrow \infty$ the energy diverges, $W \rightarrow \infty$, logarithmically. Since W scales with s^2 , defects of strength greater than $\pm 1/2$ will tend to dissociate into $\pm 1/2$ defects. This observation agrees with the data of Fathollahi and White [15, 16], where the $s=-1$ disclination splits into two $s=-1/2$ disclination. For a given equilibrium square lattice of N disclinations of charge $s=+1$, the analytical calculation of the exact location of the balancing $2N$ disclination of charge $s=-1/2$ is a non-trivial problem that is beyond the scope of this work. The experiments of White and co-workers [15,16] for hydrodynamic structuring clearly indicates that the $s=-1/2$ tend to lie on average on one of the two diagonals of the unit square lattice. The selection of this spatial distribution can be argued using disclination-disclination attractive and repulsive

interactions. Following the previous single-defect energy calculation procedure (eqns. (3-32a,b)), the energy per unit length W associated with two defects of strength s_1 and s_2 , separated by a distance r_{12} is readily found [6, 14]:

$$W = W_c + \int_0^{2\pi} d\alpha \int_{r_c}^R f_1 r dr = W_c + \pi K (s_1 + s_2)^2 \ln \left(\frac{R}{r_c} \right) - 2\pi K s_1 s_2 \ln \left(\frac{r_{12}}{2r_c} \right) \quad (3.33)$$

where $r_c \ll r_{12} < R$. Then the interaction force F_{12} per unit length between two defects is then [6, 14]:

$$F_{12} = -\frac{dW}{dr_{12}} = 2\pi K \frac{s_1 s_2}{r_{12}}; r_{12} \gg r_c \quad (3.34)$$

which shows that the force F_{12} is inversely proportional to their separation distance r_{12} , and that defect pairs of like sign repel and defect pairs of opposite sign attract. Hence if we consider a unit cell with $s=+1$ disclinations at the corners and two $s=-1/2$ along the diagonal, mutual repulsion between the negative charges is partially balanced by attractive forces between unequal charges. As shown below by computer simulation, total force balance is achieved by considering interactions with all charges in the network and not only with the nearest neighbours.

Microstructural Computational Modeling

The emergence of the defect lattice is studied by solving the governing dynamical equation (3-23) under the constraints eqn.(3-1). In this paper we report solutions using the one constant approximation ($\vartheta, \kappa = 0$) which is equivalent to $K_{11} = K_{22} = K_{33}$. This simplification does not miss any important physics in the microstructural process described in this paper, as the simulations capture the superdisclination in a self-selected way. Since the defect lattice is a 2D texture, the eigenvalue \mathbf{l} in equation (3-1) is fixed along the z^* direction. The governing equation is a set of five non-linear coupled parabolic reaction-diffusion

equations. The auxiliary data for: (i) computational domain, (ii) boundary conditions, (iii) initial conditions, (iv) parametric values, are as follows.

- i Computational domain: The 2D computational domain consists of the area enclosed by external and internal boundaries (see Fig.3-3). The external boundaries E_b are the unit square. The internal boundary I_b are a lattice of small circular cylinder of dimensionless radius $H^*=0.05$. The fiber lattice has a dimensionless length $L^*=5$.
- ii Boundary Conditions: On the external boundary E_b the boundary conditions are periodic, thus simulating an infinite lattice with no edge effects:

$$\mathbf{Q}(x = -L^*/2) = \mathbf{Q}(x = L^*/2), \frac{\partial \mathbf{Q}}{\partial y} \Big|_{y=-L^*} = \frac{\partial \mathbf{Q}}{\partial y} \Big|_{y=L^*}, \frac{\partial \mathbf{Q}}{\partial x} \Big|_{x=-L^*} = \frac{\partial \mathbf{Q}}{\partial x} \Big|_{x=L^*} \quad (3.35)$$

here L^* represents the dimensionless sample width; in this paper $L^*=5$. This type of boundary condition ensures the periodicity of the structure in space and presents no additional boundary constraints which might affect the system. On the internal boundaries, the following Dirichlet boundary conditions are implemented:

$$t^* > 0, \mathbf{Q} = \mathbf{Q}_0 \quad (3.36a)$$

$$\mathbf{Q}_0 = S_{eq}(\delta_r \delta_r - \frac{1}{3} \delta) \quad (3.36b)$$

where δ_r is a radial unit vector emanating from each fiber. The internal boundary conditions represent a lattice of $+2\pi$ wedge disclinations [15, 16] embedded in the computational domain.

- iii Initial Conditions In the initial state the system was quenched from isotropic state. Mathematically for the bulk mesophase the initial condition can be written as:

$$att^* = 0, \mathbf{Q} = \mathbf{Q}_{ini}, \mathbf{Q}_{ini} = S_0(\mathbf{n}_{ini} \mathbf{n}_{ini} - \frac{1}{3} \delta) \quad (3.37)$$

Here n_{ini} is a random eigenvector and the initial scalar order parameter $S_0 \approx 0$. This initial condition is spatially inhomogeneous, since at each mesh point the both S and \mathbf{n} are randomly selected and hence is a good representation of the isotropic phase.

iv Parametric Values: The parameter vector \mathbf{V} is $V = (\xi/H, U)$. The length scale ratio ξ/H represents the ratio of a defect core diameter to the fiber diameter. In this work we use $\xi/H=0.01$ due to numerical limitations. In actual experiments ξ/H is much smaller, but as shown below this parametric selection captures the essence of defect lattice formation and its stability. The problem has an external length scale L_e and internal length scale L_i defined as:

$$L_e = H, L_i = \xi \quad (3.38)$$

where H is the radius of the cylindrical inclusion. In order to accurately capture the fluctuations in scalar order parameter S , the coarsest mesh size should always be smaller than the correlation length ξ (eqn. 3-19) which is of molecular length scale [6, 9] and is a ratio of the characteristic long range energy density (L_1) and characteristic short range energy density (φkT). The nematic potential U (i.e. dimensionless temperature) was set to $U=3.55$, which gives equivalent scalar order parameter of $S_{eq}=0.62$. Simulations at higher and lower temperatures did not affect the microstructural features of the results.

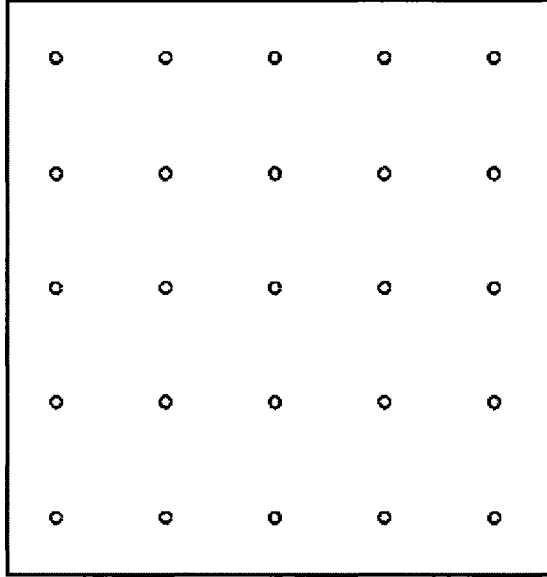


Figure 3–3: Schematic of the computational domain used for simulating the stable super-disclination array shown in Figure 3-2. The cylindrical inclusions arranged in a square array pattern have strong homeotropic anchoring mimicking the +2 disclinations as in the experiments of Fathollahi [15, 16]. The size of the unit square is $L^*=5$. The radius of each fiber is $H^*=0.05$.

The governing equations (3-23) were solved using finite elements method with triangular elements, and quadratic interpolation, and Femlab software [43]. Suitable time integration was implemented and convergence and mesh independence following standard procedure were established.

3.3.2 Optical Modeling

Liquid Crystal Optics

Carbonaceous mesophases are composed of disk-like molecules. The thermodynamic phase of carbonaceous mesophases is the discotic nematic liquid crystal state [1]. The discotic nematic molecules are optically uniaxial and its dielectric anisotropy is negative in the optic axis normal to the molecules in contrast to the classical nematic phase of rod-like

molecules [7]. Furthermore, carbonaceous mesophases are opaque materials which have complex refractive index; therefore in order to investigate textures reflection polarized optical microscopy (RPOM) is commonly used instead of transmission polarized optical microscopy (TPOM).

Matrix-type optical methods based on the stratified approach such as Jones 2×2 method [37, 38] and Berreman method [39-41] have been widely used in order to study optical response of liquid crystals which are optically anisotropic and exhibit different heterogeneous orientations. Matrix-type optical computation methods have been widely used in liquid crystal displays [39] based on thermotropic low-molar mass rod-like nematic liquid crystals. Since thermotropic low-molar mass rod-like nematic liquid crystals are transparent, the transmission of the polarized light between two crossed polarizer's are used. However, Bortchagovsky [37] used the Jones method for reflection polarized light microscopy in order to study optical properties of carbon materials, pyrolytic carbon deposits since this anisotropic material is opaque.

The Jones method is restricted to the normal incident case and it is not able to capture multiple reflections due to existence of different mediums. The Berreman method overcomes the limitation of the Jones method by introducing multiple reflections and oblique incidence cases [39]. However, another major restriction remains in the matrix-type methods due to the assumption that the variation of the dielectric tensor occurs only along the direction of wave propagation. In spite of these limitations on the matrix-type method, these methods are a valuable tool to investigate orientation of optically uniaxial materials in which a slow variation of the dielectric tensor occurs along the transverse directions and they are still widely used due to its simplicity. A complete characterization of all current TPOM methods for low-molar mass thermotropic nematic liquid crystals has been recently performed [42].

In this paper the Berreman method for RPOM adapted to opaque carbonaceous materials of negative electric anisotropy is developed and used to simulate the optical response of disclination lattices in carbonaceous mesophases.

Reflection Polarized Optical Microscopy

The monochromatic incident light $\mathbf{E} = E_o e^{i\omega t}$ is introduced into the computational space; \mathbf{E} is the electric field of amplitude E_o and angular frequency ω and t is elapsed time. The entire medium can be approximated by a stack of homogeneous cubic lattices in which each lattice is assumed to contain be a homogenous medium.

Linear differential equations for the tangential components of the electric and magnetic field can be derived from Maxwell's equations with an assumption that a slow variation of the dielectric tensor occurs along the transverse directions:

$$\frac{d\psi}{dz} = -i \frac{\omega}{c} \Delta(z) \psi \quad (3.39a)$$

$$\psi = (\mathbf{E}_x, \mathbf{H}_y, \mathbf{E}_y, -\mathbf{H}_x)^T \quad (3.39b)$$

where c is the velocity of light in vacuum, z is the propagation direction, $\mathbf{E} = (\mathbf{E}_x, \mathbf{E}_y)$ is electric field vector, and $\mathbf{H} = (\mathbf{H}_x, \mathbf{H}_y)$ is the magnetic field vector. The space-dependent matrix $\Delta(z)$ mainly depends on the dielectric constants, the birefringence, and the Euler angles of the local director \mathbf{n} . The solution vectors for the transmitted and reflected waves based on the solution of the first order linear equation (3-39 a) can be expressed by:

$$\psi_t(d) = \mathbf{F}(i, n)(\psi_i(0) + \psi_r(0)) \quad (3.40a)$$

$$\mathbf{F}(i, n) = \mathbf{p}_{i+n}(h) \mathbf{p}_{i+n-1}(h) \dots \mathbf{p}_{i+1}(h) \mathbf{p}_i(h) \quad (3.40b)$$

The transmitted waves ψ_t and the reflected waves ψ_r are now obtained by use of the total transfer matrix \mathbf{F} with the incident light ψ_i . The polarization, the retardation, absorptions, and the reflection of the polarized incident light due to the variation of the

optic axis and the existence of different media are computed in the total transfer matrix \mathbf{F} which contains information on the refractive index of the materials, within the computation domain in equation (3-40 b). The total transfer matrix \mathbf{F} can be obtained by the multiplication of the local transfer matrix \mathbf{p}_i which representing each homogenous cubic lattice i with the thickness h . Since each cubic lattice is assumed to be homogenous within the thickness, so that the local transfer matrix \mathbf{p}_i can be expressed by the following series:

$$\mathbf{p}_i(h) = \exp(i\frac{\omega}{c}\Delta h) = I + \frac{i\omega h}{c}\Delta + \frac{1}{2!}(\frac{i\omega h}{c})^2\Delta^2 + \frac{1}{3!}(\frac{i\omega h}{c})^3\Delta^3 + \dots \quad (3.41)$$

The incident wave ψ_i , the reflected wave ψ_r , and the transmitted wave ψ_t can be expressed in terms of electric components only since the magnetic components are proportional to the corresponding orthogonal electric components, where the proportionality constant is the refractive index of the medium which must be isotropic and of a nonmagnetic ambient medium. Now, the three waves are given by

$$\psi_t = \begin{bmatrix} Ext \\ n_t Ext \\ Eyt \\ n_t Eyt \end{bmatrix} \quad \psi_i = \begin{bmatrix} Exi \\ n_i Exi \\ Eyi \\ n_i Eyi \end{bmatrix} \quad \psi_r = \begin{bmatrix} -Exr \\ n_r Exr \\ Eyr \\ -n_r Eyr \end{bmatrix} \quad (3.42)$$

where Exi and Eyi are the electric components of the incident wave, Exr , Eyr , Ext and Eyt are the electric tangential components of the reflected and the transmitted waves respectively, and n_t, n_i, n_r indicate the refractive index of transmitted, incident and reflected wave respectively.

In the initial step of the computation for the reflection light, the known incident wave, Exi and Eyi , which are linearly polarized along the x direction, is introduced to the computational space. The solution vectors, the reflected wave and the transmitted wave are spontaneously obtained after solving the equation (3-40a,b). Finally, the intensity of

the reflected wave is obtained by considering the crossed analyzer which is along the y direction. Detailed mathematical description of the Berreman 4×4 method can be found in [40-42].

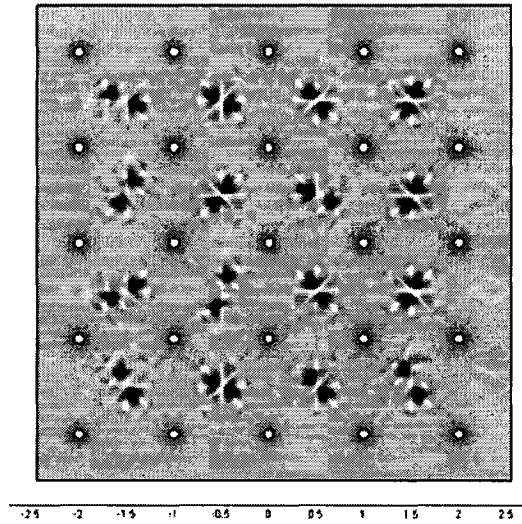
The optical constants chosen for carbonaceous materials are $n_{\perp}=2.15+i1.42$ and $n_{\parallel}=1.81$ with wavelength 546nm [7].

3.4 Results and Discussions:

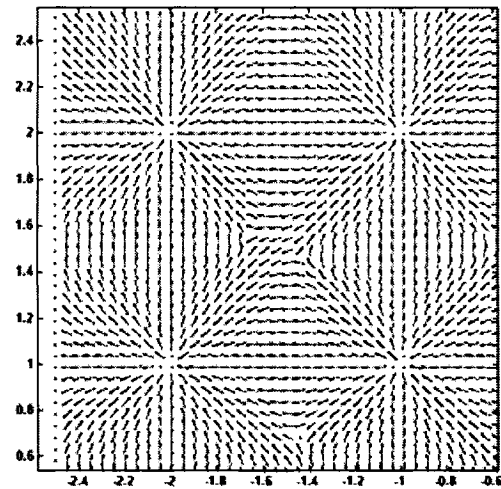
3.4.1 Disclination Lattice Microstructure

As mentioned above White and co-workers [15, 16] observed a regular array of $+2\pi$ and $-\pi$ disclinations in their screen flow experiments with carbonaceous mesophase pitch (fig. 3-2). In order to analyze and study the dynamics of this unique texture in detail we use a regular square arrangement of cylindrical inclusions as shown in Fig.3-3. Each cylinder along with homeotropic boundary condition at their surface as described before indicates a concentric $+2\pi$ disclination. In order to maintain a zero total topological charge, stable negatively charged disclinations must arise in the system due to the distortion in the director field thus forming a superdisclination array [16] of $+2\pi$ and $-\pi$ disclinations.

The initial configuration corresponds to a random state of directors inside the system as in the isotropic state with the initial Scalar Order parameter $S_0 \approx 0$ which happens for $U < 8/3$. The system starts evolving as the temperature reaches the nematic-isotropic phase transition temperature controlled by the parameter U .



(a)



(b)

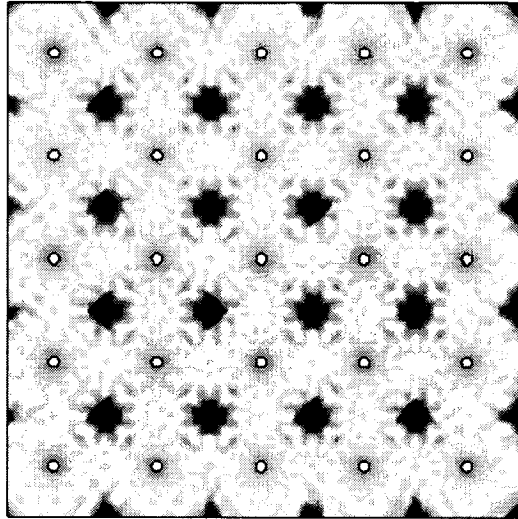
Figure 3-4: (a) Computed gray scale plot of steady state scalar order parameter for the super-disclination array with $U=3.55$, $\frac{\xi}{H}=0.01$. In the plot the low scalar order parameter ($S_0 \approx 0$) is black and high order parameter ($S_0 \approx S_{eq}$) is gray. (b) Zoomed view of the director profile for a square cell.

Fig. 3-4a is the steady state scalar order parameter profile for $U=3.55$, $\frac{\xi}{H}=0.01$, and under isotropic elastic constant assumption. The results indicate the presence of two $-\pi$ defects per square cell formed by four simulated $+2\pi$ disclinations forming a stable array of disclinations. In the figure black regions indicate the $-\pi$ defects and gray region indicate the nematic state. The result matches very well with experiments [15, 16] shown in Fig.3-2.

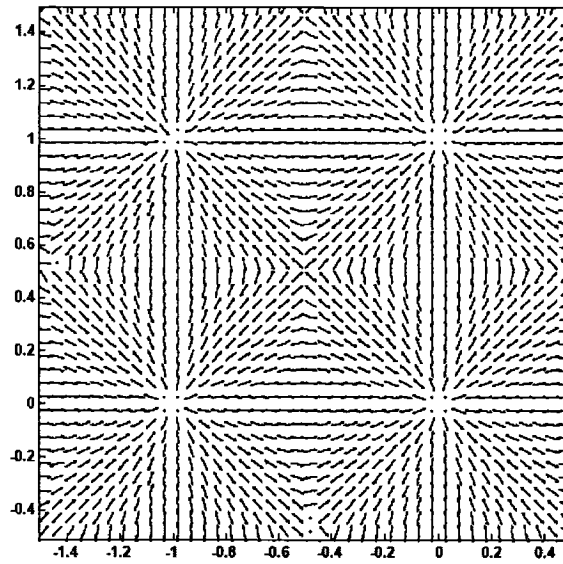
In Fig. 3-4b which is the close view of director profile, the two $-\pi$ defects for every square cell can be seen clearly. These defects lie along one of the diagonals of each square although insignificant deviations do result from finite computational accuracy. The defect array presents complexity in computing an analytical solution for defect separation due to multiple force interactions among the defects however statistically speaking the average defect distance was found to be 0.3616 in dimensionless units.

Fig. 3-5a, b shows the computed visualization of the scalar order parameter and the zoomed director profile for the intermediate state for dimensionless time $t^*=130$.

The simulations suggest that initially the texture goes through a formation of -2π defect. As the time proceeds defect splitting occurs and two $-\pi$ defects form which subsequently start move away from each other due to the repulsive force between them and attractive force with the neighboring $+2\pi$ defects. Eventually the two $-\pi$ defects come to an equilibrium position where the net force is balanced.



(a)



(b)

Figure 3-5: Computed visualizations of (a) scalar order parameter field S and (b) zoomed director field \mathbf{n} at time $t^*=130$, for the same parametric conditions as in fig. 3-4.

Fig. 3-6 shows the time evolution of dimensionless long range and total energy. The equations for long range and total energy can be obtained by integrating eqn. (3-20) over the sample volume. The increase in the long range energy at time $t^*=150$ indicate the transformation from a -2π disclinations. The long range energy then decreases to reduce the gradients. The reason for splitting as explained in detail before is that the long range energy scales with s^2 where s indicates the strength of the disclination. Based on this argument it seems logical that the two disclinations of rotation $-\pi$ and strength $-1/2$ will have lower energy than of a single defect with rotation -2π and strength -1 . The total energy decreases as expected from the minimization theory.

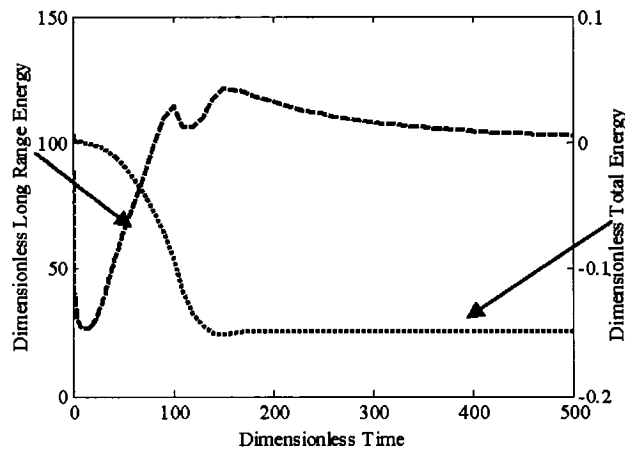


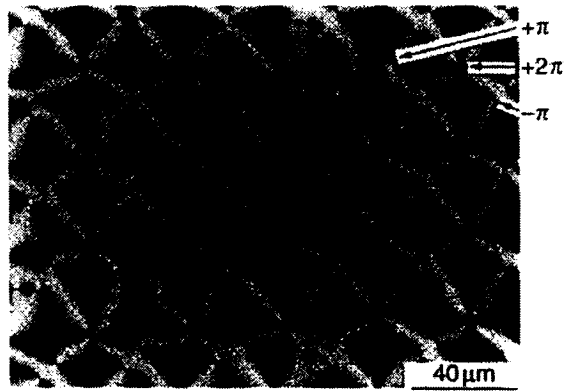
Figure 3-6: Dynamic evolution of dimensionless gradient and total energy.

3.4.2 Computational Reflection Polarized Optical Microscopy

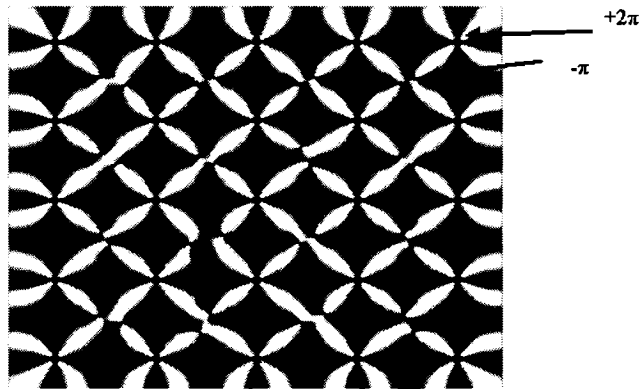
The optical simulations of equilibrium disclination lattices were performed as follows. Firstly, the director profiles were obtained by extracting the main eigenvector of the tensor order parameter corresponding to the equilibrium disclination lattice, shown in Fig. (3-2). Once the director field is known, the space-dependent dielectric tensor is calculated, and then the intensity of reflected light is computed as explained above.

Figure 3-7. shows optical images of the reflected polarized light computed using the Berreman method based on the simulated director structure of the superdisclination. The characteristic feature of this figure is the presence of two and four brush features. The spatial distributions of the centers of the four brush features form a lattice of square symmetry. The two brush features lie on the diagonals of this square lattice. The source of this complex pattern is as follows. As is well known in liquid crystal optics [6], observing wedge disclinations under cross-polars gives rise to typical brush figures. The number of brushes B is related to the wedge disclination strength s by:

$$B = 4s$$



(a)



(b)

Figure 3-7: The optical textures (a) The experimental optical textures [16] reprinted with permission of Taylor and Francis (b) Simulated optical textures using the Berreman method based on the simulated director profiles shown in Fig.(3-4)

Hence $s=+1$ disclinations result in four brushes, while $s=-1/2$ disclinations result in two brushes. The simulated optical images thus correspond to the disclination lattice shown in Fig. (3-4).

3.5 Conclusions

An integrated computational microstructural and optical model of disclination lattices in carbonaceous mesophases filled with small fibers has been developed, solved, and validated with experimental data from hydrodynamic structuring. The microstructural model is used to predict the orientation and defect texture in the discotic nematic ordering in the carbonaceous mesophase. The optical model is used to validate the microstructural model by comparing the optical response with available experimental data.

Inserting micron-sized particles on mesophases creates a disclination network. If the particles display positional ordering (colloidal crystal ordering), the defect network will be a defect lattice. In the present paper we have studied a colloidal crystal of square symmetry, with the aim of characterizing the resulting defect network structure. The microstructural model predicts the formation of a disclination network of square symmetry, composed of a square lattice array of $+2\pi$ disclinations and an array of $-\pi$ disclination lines along the diagonals of the square lattice. The disclination lattice is a robust superstructure that is self-selected and emerges by quenching a disordered isotropic phase.

The most direct way to validate texture modeling of a nematic liquid crystal is polarized optical microscopy. For opaque materials, reflection microscopy is used. In the present paper the reflection optical microscopy model predicts an ordered array of two and four brushes, corresponding to the $+2\pi$ and $-\pi$ disclination array. A comparison between simulations and experiments show excellent quantitative agreement.

In this paper we have shown a pathway to create carbon-based materials with designed micro-architectures. Positional order in filler particles are shown to be translated into defect lattices in the suspending matrix. Defect lattices are a topic of current interest since they arise in a number of natural liquid crystalline phases, including the blue phases of

DNA solutions. In this paper we have shown that disclination lattices are stable hierarchical superstructures that contain positional and orientational order and low symmetry. The dual ordering may be manipulated to design and control high strength/high conductivity materials. The new integrated structural-optical model allows for a complete characterization of carbonaceous mesophases and can be easily extended to flowing systems, and other natural and synthetic liquid crystalline materials.

3.6 Acknowledgements

This work was supported primarily by the ERC program of the National Science Foundation under Award Number EEC-9731680. DKH acknowledges support from the Natural Science and Engineering Research Council of Canada, and the Eugenie Ulmer Lamothe Fund of the Dept. of Chemical Engineering at McGill University. GG acknowledges support from the Eugenie Ulmer Lamothe Fund of the Dept. of Chemical Engineering at McGill University.

3.7 References

- 1 D. M. Riggs, R. J. Shuford, and R. W. Lewis, in *Handbook of Composites* , edited by G Lubin (Van Nostrand Reinhold, New York, 1982), Vol. 1 , p.196-271.
- 2 R. H. Hurt and Z. Y. Chen, *Physics Today* **53** , 39-59 (March 2000).
- 3 L. H. Peebles, Jr., *Carbon Fibers-Formation, Structure, and Properties* (CRC Press, Boca Raton FL, 1995)
- 4 R. Setton, *Carbon Molecules and Materials* (Taylor and Francis, London, 2002)
- 5 D. D. Edie, *Design and Control of Structure of Advanced Carbon Materials for Enhanced Performance* (Kluwer Academic Publishers, 2001), Chap. Carbon fiber processing and strcture/property relations, p.163-181.
- 6 P. G. de Gennes and J Prost, *The Physics of Liquid Crystals* (Clarendon Press, Oxford, 1993).
- 7 J. E. Zimmer and J. L. White, *Advances in Liquid Crystals: Disclination structures in carbonaceous mesophase* **5** , 157-213 (1982).
- 8 A. D. Rey and M. M. Denn, *Annual Review of Fluid Mechanics* **34** , 233-265 (2002).
- 9 M. Kleman and O.D. Lavrentovich, *Soft Matter Physics* (Springer-Verlag, New York, 2003)
- 10 V. P. Mineev, *Topologically Stable Defects and Solitons in Ordered Media* (Harwood Academic Publishers, Amsterdam, 1998)
- 11 I. Dierking, *Textures of Liquid Crystals* (Wiley-VCH, Weinheim,2003).
- 12 L. M. Pismen, *Vortices in Nonlinear Fields* (Oxford Science Publications, Oxford, 1999)
- 13 Y. Bouligand, in *Physical Properties of Liquid Crystals* , edited by D. Demus, J. Goodby and G. W. Gray (Wiley-VCH, Weinheim, 1999), Vol I, Chap. Defects and Textures.

- 14 FRS Chandrashekar, *Liquid Crystals* , 2 nd edition (Cambridge University Press, 1992)
- 15 A. K. Didwania, B. Fathollahi and J. L. White, Extended Abstracts, 24th biennial conf. on carbon, Charleston, South Carolina, 112-113, (1999). American Carbon Society
- 16 J. L. White, B. Fathollahi, and X. Bourrat, in *Fibers and Composites* , 1 st edition, edited by D. Pierre (Taylor and Francis, 2003), Chap. 1, p.3-23.
- 17 J. J. McHugh and D. D. Edie, *Carbon* **34** (11), 1315-1322 (1996).
- 18 J. J. McHugh and D. D. Edie, *Liquid Crystals* **18** (2), 327-225 (1995).
- 19 S. Das and A. D. Rey, *J. Chem. Phys.* **121** , 9733 (2004).
- 20 A. A. Sonin, *The Surface Physics of Liquid Crystals* (Gordon and Breach Publishers, Amsterdam, 1995).
- 21 H. Stark, *Phys. Rep.* **351** , 387-474 (2001).
- 22 R. W. Ruhwandl and E. M. Terentjev, *Phys. Rev. E* **56** , 5561-5565 (1997).
- 23 P. Poulin, H. Stark, and T. C. Lubensky, *Science* **275** , 1770-1773 (1997).
- 24 J. L. White and P. M. Sheaffer, *Carbon* **27** (5), 697-707 (1989).
- 25 K. Christ and K. J. Huttinger, *Carbon* **31** (5), 731-750 (1993).
- 26 P. A. Chollet and F. Kajzar, in *Carbon Molecules and Materials* , edited by R. Setton, P. Bernier and S. Lefrant (Taylor and Francis, 2002), Chap. optical properties of allotropic forms of carbon, p.325-358.
- 27 R. Hurt, G. Krammer, G. Crawford, K. Q. Jian, and C. Rulison, *Chemistry of Materials* **14** (11), 4558-4565 (2002).
- 28 K. Jian, H. S. Shim, D. Tuhs-Dubrow, S. Bernstein, C. Woodward, and M. Pfeffer, *Carbon* **41** , 2073-2083 (2003).
- 29 A. Sonnet and S. Hess, *Phys. Rev. E* **52** (1), 718 (1995).

- 30 T. Tsuji and A. D. Rey, *J. Non-Newtonian Fluid Mech.* **73** , 127 (1997).
- 31 J. Yan and A. D. Rey, *Phys. Rev. E* **65** , 031713 (2002).
- 32 N. Schopohl and T. J. Sluckin, *Phys. Rev. Lett.* , **59** , 2582 (1987).
- 33 K. Schiele and S. Trimper, *Phys. Stat. Sol. (b)* **118** , 267 (1983).
- 34 M. Doi, *J. Polym. Sci. :Pol. Phys. Ed.* **19** , 229-243 (1981).
- 35 A. P. Singh and A. D. Rey, *J. Non-Newtonian Fluid mech.* **94** , 87-111 (2000).
- 36 J. Friedel, *Dislocations* (Pergamon, Oxford, 1967)
- 37 E. G. Bortchagovsky, *J. Appl. Phys.* **95** , 5192-5199 (2004).
- 38 R. C. Jones, *J. Opt. Soc. Am.* **31** , 488-493 (1941).
- 39 D. W. Berreman, *J. Opt. Soc. Am.* **62** , 502-510 (1972).
- 40 A. F. Konstantinova, K. K. Konstantinov, and B. B. Nabatov, *Phys. Prop. Cryst.* **47** , 645-652 (2002).
- 41 H. Wohler, G. Hass, M. Fritsch, and D. A. Mlynski, *J. Opt. Soc. Am. A* **5** , 1554-1557 (1988).
- 42 D. K. Hwang and A. D. Rey, *Liquid Crystals* in press.
- 43 Femlab Version 3.0a, Comsol Inc.

CHAPTER 4

Texture Modeling in Carbon-Carbon Composites based on Mesophase Precursor Matrices

4.1 Abstract

A computational modeling study of texture formation in carbon-carbon composites based on carbon fibers and carbonaceous mesophase precursors is presented. The modeling predictions on texture formation and disclination structures are quantitatively validated with extensive experimental data. The number and type of disclinations displayed by the carbonaceous mesophase matrix is shown to be governed by the elasticity of the mesophase, the carbon fiber-mesophase interfacial energy, the size of the fibers, and positional arrangement of the fibers. The simulations provide new insights on the fundamental principles that govern texturing and disclination nucleation, and on how to control the structure of carbon-carbon composites through fiber concentration, fiber cross-section, and fiber-matrix interaction.

4.2 Introduction

Carbon-carbon composites (C/CC) are industrial materials used in the defense, sports, and transportation industries [1, 2, 3]. Tailoring mechanical property profiles and transport functionality usually leads to uses of different precursors as well as different processing techniques. The use of carbonaceous mesophases (CM) as matrices has the potential to offer advantages in the development of advanced C/C composites, since the matrix microstructure can be manipulated during the formation stage. This paper presents a computational study of texture development during the formation of C/C composites consisting of carbon

fibers embedded in carbonaceous mesophase precursors. Experimental data in C/C composites based on carbon fiber-mesophase carbon precursors, related to the present study, has been widely documented by Zimmer and White [4, 5]. Optimization, control of property profiles and functionality, as well as science-based manufacturing requires a better understanding of the fundamental principles that control microstructural features of the composite. As shown below, a unique feature of using CM precursors is the fact that inserting micron size fibers has a structuring effect on the mesophase. In this paper we simulate textures in the mesophase, while the experimental textures [4, 5] are obtained after carbonization. The premise of the present work is that significant textural features present in the mesophase state are preserved after carbonization. Since the simulation results are in excellent agreement with experimental textures, it is more than reasonable to conclude that our modeling premise is correct. Moreover previous simulations of texture development in the fiber spinning of mesophase precursors [6] are in excellent agreement with experiments, giving additional evidence to the assumption that significant aspects of mesophase texture are retained after carbonization.

Carbonaceous mesophases are discotic nematic liquid crystals, characterized by orientational order and positional disorder. Mesophases flow like viscous liquids but due to their orientational order, they are anisotropic as crystalline solids. A unique characteristic of liquid crystals including CM is their orientational response to surfaces, interfaces, flow fields, and electromagnetic fields. In C/CM composites the carbonaceous mesophase comes in contact with a dispersion of carbon fibers that affect the orientation of the mesophase based on their characteristic size. The intensity of the texturing process, such as the number of disclinations and the orientation gradients in the mesophase, depends on the nature of the fiber-mesophase interface and on the diameter of the fiber. The fiber-mesophase interfacial interaction is characterized by the anchoring coefficient γ_{an} (=[=] energy/area),

whose sign determines whether the mesophase orientation is edge-on ($\gamma_{an} > 0$) or face-on ($\gamma_{an} < 0$). The effect of substrate chemistry on mesophase interfacial orientation has been characterized [7]. For the present case, it has been found that the mesophase orients face-on with respect to the carbon fiber [4, 5]. The orientation gradient elasticity [8] of carbonaceous mesophases is due to basic distortion modes known as splay, bend, and twist [8], and is characterized by the Frank modulus of elasticity K ([=] energy/length). Embedding a circular fiber of radius R in an infinite mesophase will result in an orientational distortion only if:

$$\ell_{extrapolation} = \frac{K}{|\gamma_{an}|} < R \quad (4.1)$$

where $\ell_{extrapolation}$ is the extrapolation length and is a property of the interface (γ_{an}) and the mesophase elasticity (K). The magnitude of the extrapolation length indicates whether the distortion created by immersing an object in the mesophase is absorbed by the bulk or by the interface. When $\ell_{extrapolation} < R$ it is energetically favorable to distort the matrix, and when $\ell_{extrapolation} > R$, it is energetically favorable to distort the relative orientation between the mesophase and the object. The regime $\ell_{extrapolation} < R$ is known as ‘strong anchoring’, and $\ell_{extrapolation} > R$ is known as “weak anchoring” [9]. In addition when $\ell_{extrapolation} < R$ the distortion is usually confined to a close region by the appearance of disclination lines (fibrous objects) or disclination points (spherical objects). Figure 4-1 shows a schematic of a circular carbon fiber embedded in a carbonaceous mesophase for: (a) strong anchoring with face-on interfacial orientation, and (b) weak anchoring, the lines indicate the orientation of the directors. Figure 4-1 shows that under strong anchoring two disclinations arise closer to the interface and the mesophase orientation displays bending distortions. For typical mesophases and micron-thick carbon fibers, experiments (see Figure 4-2) shows that strong anchoring holds, and hence C/C composites will inevitably have a number of disclinations.

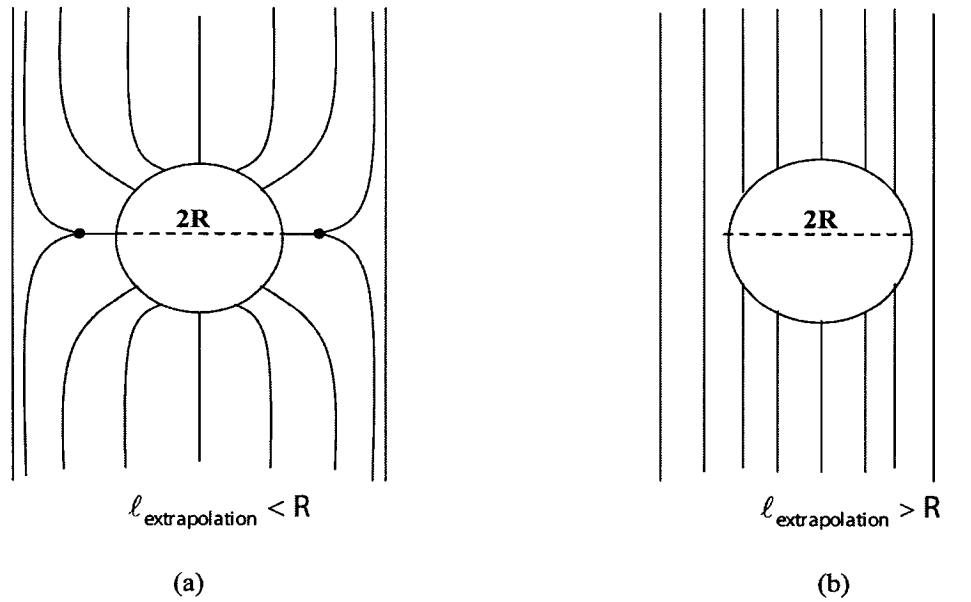


Figure 4-1: Schematic of carbon fiber embedded in a carbonaceous mesophase matrix at different anchoring regimes: (a) strong anchoring with face-on interfacial orientation, when $l_{extrapolation} < R$, and (b) weak anchoring, when $l_{extrapolation} > R$. The lines in both plots represent a side-view of the molecular planes; see Figure 4-2 for an actual composite structure under the strong anchoring regime.

Texturing in C/C composites includes disclination nucleation phenomena from multiple fiber effects. At high fiber density three, four, and higher, multi-fiber clusters encircle mesophase domains and give rise to disclination nucleation from multiple surface anchoring. The rules of disclination nucleation in multiple fiber arrangements have been characterized experimentally [5], and will be discussed in Section 4.2 below. Figure 4-2 shows a typical texture in C/CM composite [5]. The figure shows the random arrangement of circular and wedge carbon fibers and the texture in the mesophase. The figure indicates that according to the type of multi-fiber arrangement different types of disclinations arise; disclination characteristics are discussed in section (4.2) and in the literature [4, 5]. For example on the upper left a four fiber configuration gives rise to a -2π defect [5], while on the lower

left the figure shows that a three fiber configuration gives rise to a $-\pi$ disclination. The dependence of textures on fiber density and fiber arrangement is the focus of this paper.

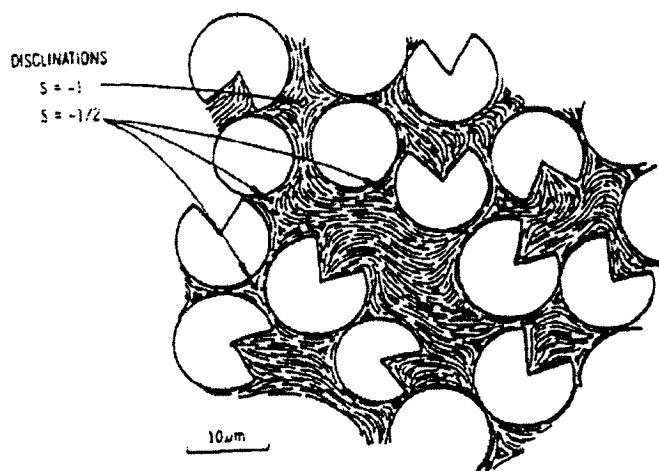


Figure 4-2: Alignment of mesophase layers in a random arrangement of fibers. Disclinations of $-\pi$ and -2π are found in the matrix with $-\pi$ having a discontinuous core whereas -2π have continuous cores. Adapted from [5]. Reprinted with permission of Elsevier.

The specific objectives of this paper are:

(1) Use computational modeling of textural process in C/CM and replicate the main textural features of Figure 4-2, including disclination types.

(2) Provide a fundamental understanding of the processes that govern textures in C/CM composites.

The organization of this paper is as follows.

Section 4.3 presents the theory and model formulation for texture evolution, emphasizing concepts and principles; a detailed discussion of the model has been presented elsewhere [10]. Section 4.4 presents, discusses and validates the microstructural results. Conclusions are given in section 4.5.

4.3 Theory and Modeling

A unique feature of carbon-carbon composites based on mesophase precursors is the distortion of the mesophase in response to the embedded carbon fibers. To assess the textural impact of embedded circular carbon fibers on a carbonaceous mesophase matrix, we develop and solve a model that is able to describe the spatiotemporal behavior of the average molecular orientation of the mesophase. The model is based on the Landau-deGennes theory for liquid crystals, adapted to carbonaceous mesophases. A detailed description of the model and successful applications to microstructural modeling in pitch-based carbon fibers of circular and ribbon shape have been presented before [6, 11]. In the present paper the number, size, and location of the carbon fibers are known and the texture of the mesophase matrix is the unknown.

4.3.1 Microstructure Modeling

The orientational texture of the mesophase is analysed in terms of tensor order parameter \mathbf{Q} [8, 10] defined as

$$\mathbf{Q} = S(\mathbf{nn} - \frac{1}{3}\delta) + \frac{1}{3}P(\mathbf{mm} - \mathbf{ll}) \quad (4.2)$$

The orientation is defined completely by the orthogonal director triad $(\mathbf{n}, \mathbf{m}, \mathbf{l})$ which are the uniaxial director, and the biaxial directors respectively. The scalar order parameter S is a measure of the molecular alignment along the uniaxial director \mathbf{n} and P the biaxial scalar order parameter is the molecular alignment in a plane perpendicular to the direction of uniaxial director \mathbf{n} . The spatiotemporal microstructure evolution of the mesophase is obtained by solving the torque balance equation:

$$- \underbrace{\gamma(\mathbf{Q}) \frac{\partial \mathbf{Q}}{\partial t}}_{\text{viscous resistance}} = \underbrace{\left(\frac{\delta F}{\delta \mathbf{Q}} \right)^{[s]}}_{\text{elastic driving force}} = \left[\frac{\partial F}{\partial \mathbf{Q}} - \nabla \cdot \frac{\partial F}{\partial \nabla \mathbf{Q}} \right]^{[s]} \quad (4.3)$$

where the left hand side represents the viscous resistance, and the right hand size is the driving force; the symbol [s] denotes symmetric and traceless condition. The viscous resistance is due to the rotational viscosity $\gamma(\mathbf{Q})$ of the mesophase and the driving force originates from a decrease in the total elastic free energy F of the system:

$$F = \int_V f dV = \int_V (f_h + f_g) dV \quad (4.4)$$

The steady state solution to equation (4-3) minimizes the total free energy F under the geometric constraints of the C/C composite, such as orientation of the directors at the Carbon Fiber (CF)-CM interface, and number, shape, and locations of the CF's. The free energy F is expressed in terms of \mathbf{Q} and its derivatives $\nabla\mathbf{Q}$ [8, 10], corresponding to the homogenous energy f_h and gradient energy f_g respectively. The gradient terms contribution gives the long range elastic force dominant in the nematic phase (i.e. mesophase matrix) and is expressed in dimensionless form as [10]

$$f_g^* = \frac{\xi^2}{R^2} \underbrace{\left(\frac{1}{2} \nabla_\alpha^* \mathbf{Q}_{\beta\gamma} \nabla_\alpha^* \mathbf{Q}_{\beta\gamma} + \frac{1}{2} \vartheta \nabla_\alpha^* \mathbf{Q}_{\alpha\gamma} \nabla_\beta^* \mathbf{Q}_{\beta\gamma} + \frac{1}{2} \kappa \mathbf{Q}_{\alpha\beta} \nabla_\alpha^* \mathbf{Q}_{\gamma\delta} \nabla_\beta^* \mathbf{Q}_{\gamma\delta} \right)}_{\text{Dimensionless LongRangeEnergy}} \quad (4.5)$$

and the homogenous elastic contribution describes energy changes due to molecular order [8, 10] and is given by:

$$f_h^* = \frac{1}{2} \underbrace{\left(1 - \frac{U}{3} \right) (\mathbf{Q} : \mathbf{Q}) - \frac{U}{3} \mathbf{Q} : (\mathbf{Q} \cdot \mathbf{Q}) + \frac{U}{4} (\mathbf{Q} : \mathbf{Q})^2}_{\text{dimensionless homogeneous range Energy}} \quad (4.6)$$

The nematic potential U is the dimensionless temperature

$$U = 3 \frac{T^*}{T} \quad (4.7)$$

where T^* is the isotropic-liquid crystal transition temperature. In the isotropic (disordered) region $U < 8/3$, for $8/3 < U < 3$ there is biphasic equilibrium where liquid crystal and isotropic

regions coexist, and for $U > 3$ the phase is uniaxial nematic liquid crystal. The parameter ξ is the coherence length [8], and is the characteristic size of a singular disclination; the length scale of ξ is in the nanometer range [8, 9]. R is the external length scale of the system, which in our case is the radius of the fibers. ϑ, κ are the dimensionless Frank elastic constants [10] related to splay, bend and twist distortions [8].

The C/CM composite model geometry has internal surfaces and bounding surfaces. The bounding surfaces are the edges of the bounding rectangle. The internal surfaces are the circular boundaries between the fibers and the mesophase. Since there are internal and external surfaces we implement two types of boundary conditions: (a) external boundary conditions, and (b) internal boundary conditions. For external boundary conditions (i.e. along the outer rectangle) we use periodic boundary conditions, and hence assume that the computational domain is replicated ad-infinitum in the two coordinate directions. The periodic boundary conditions are passive and allow to capture the essence of the whole sample by focusing on a representative unit. In our case the representative unit size was taken from real experiments [5]. For internal boundary conditions we use the so-called Dirichlet condition, where the system state is known. In the present case this means that we specify \mathbf{Q} with a known value. Again the chosen values for \mathbf{Q} are taken in part from real experiments, as explained in what follows. As mentioned above the disk-like molecules of the mesophase pitch tend to align parallel to the surface of the fibers [4, 5], forming a circular sheath around the fibers, hence at the bounding surface assuming uniaxiality ($P=0$), \mathbf{Q} has the form

$$\mathbf{Q}_0 = S_{\text{eq}}(\delta_r \delta_r - \frac{1}{3} \delta) \quad (4.8)$$

where δ_r is a radial unit vector emanating from each fiber, and S_{eq} is the equilibrium scalar order parameter given by [10, 12]

$$S_{eq} = \frac{1}{4} + \frac{3}{4} \sqrt{1 - \frac{8}{3U}} \quad (4.9)$$

Although the boundary values of the scalar order parameter are not known experimentally, the assumed values do not play an essential role in the objectives and/or predictions of the model. It will be confirmed posteriori that condition (4.8) leads to excellent agreement with real experiments (compare Figures (4-2,3)). Eqn. (4.8) represents a strong boundary condition known as homeotropic boundary condition and mimics the tendency of the carbonaceous mesophase layers to align parallel to the surface of the substrates such as fibers, as observed in real experiments [5].

The solution to the model eqn.(4.3) requires initial conditions on the tensor order parameter throughout the computational domain. Since the main objective of this paper is to characterize the texture selection in CF/CM composites, initially we assume that the matrix is isotropic, thus avoiding any biasing.

The geometric, operating conditions and material parameters are as follows:

(a) Geometric Parameters: the number, location, and size of the CF's correspond to the real experiments [5], shown in Fig.4-2. The wedge fibers used in the experiments were replaced by circular fibers in the simulations; this departure causes some differences in the director field but the number and type of disclinations obtained in the simulations are in agreement with experiments. The ratio between a disclination core and the CF radius is $\xi/R = 0.0033$, corresponding to fibers of roughly three micron radius.

(b) Operating conditions: the value of U is chosen to be 3.5 to give an equilibrium scalar order parameter value of $S_{eq} = 0.62$.

(c) Material Properties: in the present work we have imposed the equal elastic constant approximation (Splay = Twist = Bend), which implies $\vartheta, \kappa = 0$.

The governing eqn. (4.3) was solved using the Galerkin Finite Elements Method with triangular elements, quadratic Lagrangean interpolation, and Femlab software [13]. Suitable high order implicit time integration was implemented and convergence and mesh independence were established following standard procedures. Given the length scale ratio of $\xi/H = 0.0033$, sufficient number of triangular elements had to be used, in particular at locations where disclinations appear.

4.3.2 Textures in Carbon-Mesophase Carbon Composites

In this section we summarize the main principles and concepts necessary to characterize the simulations that lead to textures in agreement with Fig.4-2. Qualitatively a mesophase texture is described by a spatial disclination distribution. In more quantitative terms a mesophase texture T can be defined as follows:

$$T : \{\mathbf{x}(CT, s), n(CT, s)\} \quad (4.10)$$

where \mathbf{x} denotes the spatial location of the disclinations, and n denotes the number of disclinations of core type CT and strength s . The strength is quantized as follows:

$$s = \pm 1/2 (\pm\pi), \pm 1 (\pm 2\pi), \pm 3/2 (\pm 3\pi), \pm 2 (\pm 4\pi), \dots \quad (4.11)$$

The sign of s denotes the sense of rotation and the magnitude the amount of rotation when encircling the defect. The quantities in the parenthesis in eqn.(4.11) denote the actual rotation angle; for example a $s=-1/2$ disclination is also known as a $-\pi$ disclination. A rigorous discussion and review of disclination in carbonaceous mesophases has been presented [4]. In general since the energy of a disclination is proportional to s^2 , lower order disclinations are more abundant. On the other hand in C/C composites, anchoring effects

due to several fibers lead to higher order disclinations [5]. Experiments [5] on carbonaceous mesophases laden with carbon fibers and general liquid crystal elasticity theory have shown that disclinations can be of escaped core (EC) or singular core (SC). Experiments [5] on carbonaceous mesophases laden with carbon fibers, under face-on strong anchoring, show that the relation between micron-sized fiber arrangements and disclinations are:

(a) Triangular fiber arrangement: $s=-1/2$, CT: singular

(b) Square fiber arrangement: $s= -1$, CT: escaped

These results indicate that at least locally a charge balance equation that governs the charge of disclination reads:

$$s = - \left(\frac{n-2}{2} \right) \quad (4.12)$$

where n is the number of sides in the fiber configuration. For a triangle $n=3$, and for a square $n=4$. This simple rule describes the defects in Figure 4-2. In the 4-fiber configuration in the upper left we have:

$$s = - \left(\frac{4-2}{2} \right) = -1 \textit{disclination}$$

and in the 3-fiber configuration in the lower left:

$$s = - \left(\frac{3-2}{2} \right) = -\frac{1}{2} \textit{disclination}$$

We next briefly characterize the core type of these disclinations; for an authoritative treatment see the review of Zimmer and White [4].

Singular Core Disclinations

Singular core disclinations commonly observed in carbonaceous mesophase such as $s = \pm \frac{1}{2}$ are singular, with a core of molecular nm size, where the ordering of the mesophase has been eliminated [14]. The energy per unit length W of an isolated singular disclination

of strength s in a circular mesophase layer of radius R is given by [15]

$$f_l = \frac{K}{2} (\nabla\theta)^2 \quad (4.13)$$

$$W = \frac{K}{2} \int (\nabla\theta)^2 dx dy = W_c + \int_0^{2\pi} d\alpha \int_{r_c}^R f_l r dr = W_c + \pi K s^2 \ln\left(\frac{R}{r_c}\right) \quad (4.14)$$

where r_c is the radius of the core of the singular disclination and is of molecular size, W_c is the core energy. As $R \rightarrow \infty$ the energy diverges, $W \rightarrow \infty$, logarithmically. Since W scales with s^2 , defects of strength greater than $\pm 1/2$ will tend to dissociate into $\pm 1/2$ defects, hence we don't expect to see singular high strength disclinations. Cases for singular high strength disclinations have been reported in the literature for rod-like nematic liquid crystals [16], and carbonaceous mesophase [17]. In this paper we only restrict the discussion to $s = -1/2$ singular disclinations, since Fig.4-2 does not show the presence of high order singular disclination lines.

Escaped Core Disclinations

Disclinations of strength $s = \pm 1$ commonly observed in carbonaceous mesophase are non-singular, with a core of macroscopic μm size, where the ordering of the mesophase has been retained. The escape of director along the disclination line can remove the singularity from the core of the disclination [18, 19]. This can happen by the tilting of molecules outside the plane along the disclination line leading to a structure of lower energy. This lower energy configuration allows the possibility of high strength disclinations as confirmed by the observations of Zimmer and White [5]. The energy per unit length of an escaped core does not depend on the external length scale R in our case the radius of the fiber and can be written as [15]:

$$W = 3\pi K |s| \quad (4.15)$$

Comparison of eqn.(4.14) with eqn.(4.15) indicates that for disclinations of strength $|s| > \frac{1}{2}$, escape is generally favored with exceptions when $K_3 \gg K_1$ and $R \approx nm$. In the experiments [5] since the 4-fiber configuration encloses an area A whose characteristic size is of the same order as the fiber diameter ($R \gg nm$), no $s=-1$ disclinations of singular core are observed experimentally.

4.4 Computational Results and Discussion

Figure 4-3a shows a 2D gray-scale visualization of the scalar order parameter S , and Fig.4-3b shows the corresponding director field on the computational domain. In figure 3a, black regions represent low scalar order parameter depicting singular disclinations (negative half integer singular disclinations) whereas grey regions depict regions where $S_0 \approx S_{eq} = 0.62$ (see eqn.(4.9)). The white circles are the carbon fibers. As mentioned above the location and size of the fibers are identical to the experimental case [5].

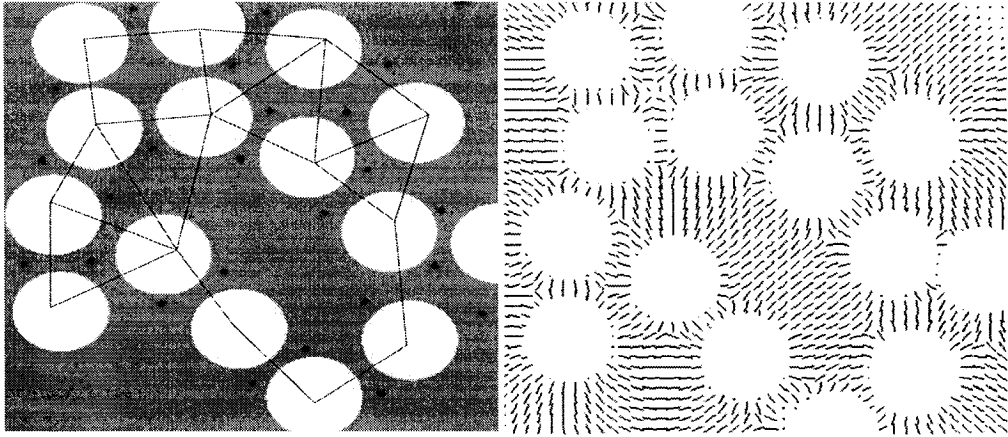


Figure 4-3: (a) Computed gray scale plot of steady state scalar order parameter with $U=3.5$, $\frac{\xi}{H} = 0.0033$. In the plot the low scalar order parameter ($S_0 \approx 0$) is black and high order parameter ($S_0 \approx S_{seq}$) is gray. (b) Computed director field, where the lines represent the average molecular orientation, which is normal to the molecular planes.

The thin lines define the polygonal mesh obtained by uniting neighboring fibers. The computed texture contains twenty four $s=-1/2$ and one $s=-1$. The $s=-1$ escaped core disclination appears in the 4-fiber configuration and each 3-fiber configuration contains singular disclinations of strength $s=-1/2$, as shown in Fig.4-2. Of-center a large 7-sided polygon contains five $s=-1/2$ disclinations. Using equation (4.12) for $n=7$ we get

$$s = -\left(\frac{7-2}{2}\right) = -5\left(\frac{1}{2}\right)$$

which is consistent with the simulations. Figure 4-3b shows the orientation distortion in the matrix as well as the singular and non-singular disclinations. When the fibers are clustered together distortions increase. In the large 7-sided polygon distortions are weaker.

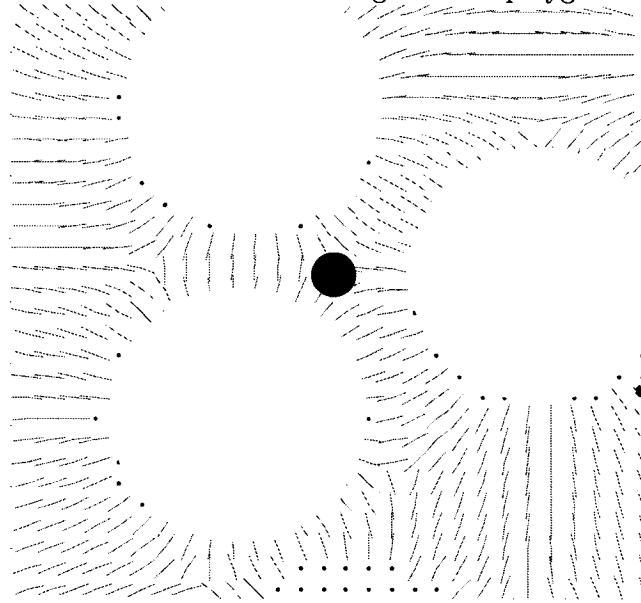


Figure 4-4: Computed director field for the triangular symmetry extracted from fig.4-3b. Each triangular arrangement is accompanied by a $-\pi$ ($s = -1/2$) in the center.

Figure 4-4 shows a computed visualization of the director field of the 3-fiber configuration extracted from the lower left triangle in Figure 4-3; the large dot denotes the singular

core. The triangular array of fibers have a singular core disclination of strength $s = -1/2$. This disclination line is located in the center of the triangular arrangement. The relation between disclination strength and fiber configuration (eqn.(4.12)) is fulfilled.

Figure 4-5 shows a computed visualization of the director field of the 4-fiber configuration extracted from the upper left square in Figure 4-3. The square array of fibers have an escaped core disclination of strength $s = -1$. The relation between disclination strength and fiber configuration (eqn.(4.12)) is fulfilled. As explained before the presence of a $s = -1$ disclination is due that fact this structure with an escaped core has a lower energy thus making it more stable thermodynamically.

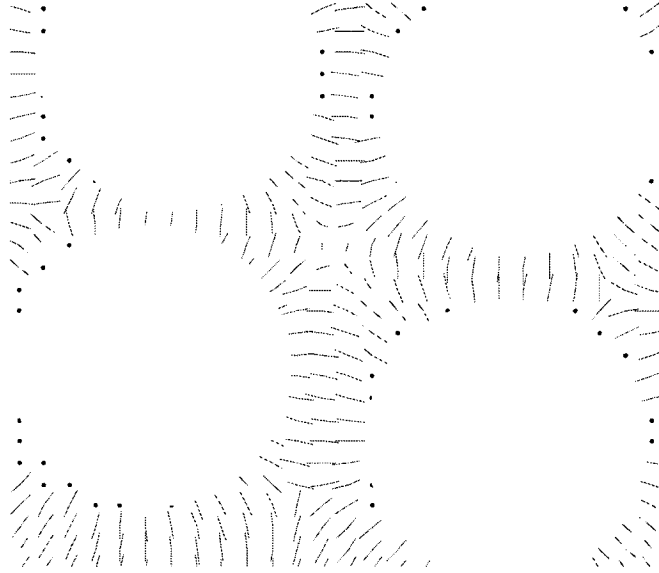


Figure 4-5: Computed director field for the square configuration extracted from fig.4-3b. The square configuration has a -2π ($s = -1$) disclination in the center with an escaped core.

In summary, the following experimental features have been captured in the simulations:

- (1) 4-fiber configuration lead to escaped core $s = -1$ disclinations,

- (2) 3-fiber configurations lead to singular $s=-1/2$ disclinations,
- (3) 7-fiber configuration leads to 5 singular $s=-1/2$ disclinations
- (4) The orientation distortions with strong face-on anchoring are strongest under close proximity of multiple fibers.

4.5 Conclusions

A computational and theoretical study of orientation processes in spatially heterogeneous carbon fiber-carbon mesophase composites reveals the principles that control textural processes. Micron sized fibers embedded in a mesophase create texture through strong anchoring. The property that governs this effect is the anchoring length, which is the ratio of the bulk elastic coefficient of the mesophase to the anchoring energy of the fiber-mesophase interface. When the fiber radius is greater than the anchoring length, texturing and disclination lines nucleate in the vicinity of the fiber-mesophase interface. For concentrated fiber suspensions, multiple fiber effects lead to specific disclination types. Three fiber configurations lead to singular $s=-1/2$ disclinations, while

Four fiber configurations lead to escaped core $s=-1$ disclinations. The number of 3, 4, 5, etc. fiber configurations will undoubtedly depend on the fiber density. For moderate packing fractions as shown in Figure 4-2, 3-fiber configurations dominate over 4-fiber configurations, and hence the most prevalent defects will be singular core of strength $s=-1/2$. The conceptual framework and computational modeling provide new insights in how to optimize and control textures in C/CM composites. Specifically, it has been shown that the texture T is a function of the fiber volume fraction and the dimensionless length scale ratio:

$$T = f \left(\varphi, \frac{R}{\ell_{extrapolation}} \right)$$

The dimensionless length scale ratio is a function of the fiber geometry (R), the temperature-dependent mesophase elasticity (K), and the fiber-mesophase interfacial tension (γ_{an}).

Hence for a given fiber loading, temperature and surface treatments are control variables to achieve specific textures.

4.6 Acknowledgments

This research was supported by a grant from Engineering Research Center program of National Science Foundation under award number EEC 9731680. GG gratefully acknowledges partial support from the Eugenie-Ulmer Lamothe Fund, Department of Chemical Engineering, McGill University.

4.7 References

- [1] Pierre D. *Fibers and Composites* , 1st edition. Taylor and Francis. 2003: 3-23.
- [2] Chung DDL. *Carbon Fiber Composites* . Washington: Butterworth-Heinemann. 1994
- [3] Buckley JD. *Carbon-carbon Composites* . In: Peter ST, editor. *Handbook of composites* (2nd Edition). London, U.K.: Kluwer Academic Publishers, 1997; 333-351.
- [4] Zimmer JE, White JL. *Disclination structure in the carbonaceous mesophase*. In: *Advances in Liquid Crystals* , 5 , 1982; 157-213.
- [5] Zimmer JE, White JL. *Mesophase alignment within carbon fiber bundles* . *Carbon* 1983; 21 (3): 323-324
- [6] Yan J, Rey AD. *Texture formation in carbonaceous mesophase fibers* . *Physical Review E* 2002; 65 : 031713-13
- [7] Hurt R, Krammer G, Crawford G, Jian KQ, Rulison C. *Polyaromatic assembly mechanisms and structure selection in carbon materials*. *Chemistry of Materials* 2002; 14 (11): 4558-4565.
- [8] de Gennes PG, Prost J. *The physics Of Liquid Crystals* , 2nd edition. Oxford: Clarendon Press. 1993.
- [9] Kleman M, Lavrentovich OD. *Soft Matter Physics* . New York: Springer-Verlag. 2003.
- [10] Gupta G, Hwang DK, and Rey AD. *Optical and structural modeling of disclination lattices in carbonaceous mesophases*. *Journal of Chemical Physics* 2005; 122 (3): 034902-11.
- [11] Yan J, Rey AD. *Modeling elastic and viscous effects on the texture of ribbon shaped carbon fibers*. *Carbon* 2003; 41 (1): 105-121.

- [12] Doi M . *Molecular dynamics and rheological properties of concentrated solutions of rodlike polymers in isotropic and liquid crystalline phases.* *J. Polym. Sci.:Pol. Phys. Ed.* 1981; **19** : 229-243
- [13] Femlab Version 3.0a, Comsol Inc.
- [14] Friedel J. *Dislocations.* Oxford: Pergamon. 1967.
- [15] Chandrasekhar FRS. *Liquid Crystals* , 2nd Edition. Cambridge: University Press. 1992.
- [16] Madhusudana NV, Pratibha R. *High Strength defects in nematic liquid crystals .* *Current Science* 1982; **51** : 877-881.
- [17] Zimmer JE, Weitz RL. *Disclinations in a graphite bundle. Extended abstracts 16th biennial conf. on carbon :* American Carbon Society, 1983; 92-93
- [18] Cladis PE and Kleman M. *Non-singular disclinations of strength $S=+1$ in nematics .* *Le Journal De Physique* 1972 ; **33** :591-598.
- [19] Meyer RB. *Existence of even indexed disclinations in nematic liquid-crystals.* *Phil. Mag.* 1973; **27** : 405

CHAPTER 5

Texture Rules for Concentrated Filled Nematics

5.1 Abstract

Defect textures in concentrated fiber-filled polygonal networks in nematic liquid crystals are analyzed using differential geometry and computational modeling based on Landau-de Gennes theory. Micron fibers exhibit singular cores of strength $-1/2$ for odd polygons and escaped cores of strength $-(N-2)/2$ for even polygons (N : number of sides), in agreement with experiments while simulations predict singular cores of strength $-1/2$ in submicron fibers. The computed textures satisfy physical and topological stability rules, and the total charge inside each polygon obeys the Poincaré-Brouwer theorem.

5.2 Introduction and Discussion

Filled nematics (FNs) [1], ferronematics [2], colloidal nematics [3], and carbon-mesophase carbon composites [4] are biphasic heterogeneous materials consisting of embedded particles, drops, and fibers in a nematic matrix, that have attracted much interest due to the need to develop new colloidal and composite science as well as for their potential applications. For random and ordered heterogeneous materials the emphasis is on the description of spatial organization [5]. On the other hand for FN, additional measures include distortions in the liquid crystal, and emergence of topological defects, which occur when the director is fixed at the liquid crystal-particle interface. Available theoretical descriptions include suspensions of spherical particles [6] and disks [7]. However, most of the work till now has focused on single or two particles. The problem of multiparticle becomes more involved since depending on the interactions of the particles inside the host, particles

can form long linear chains [8], periodically aligned chains of drops [9], or more complicated structures such as two dimensional hexagonal ordering of particles [10]. On the other hand, random heterogeneous filled nematics (RHFNs), such as carbon fiber-mesophase carbon (c/c) composites, are materials not covered in the existing theories of composites. A significant body of experimental literature indicates that the polygonal network as shown schematically in fig. 5-1a, obtained by joining the fiber centers in typical c/c composites includes triangles, rectangles, pentagons, and hexagons.

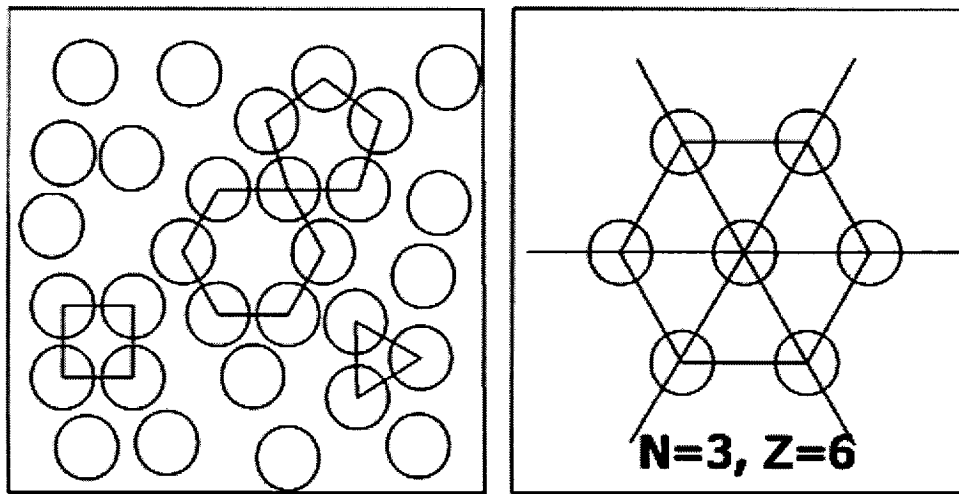


Figure 5-1: (a) Particle arrangements in a carbon fiber-mesophase carbon composites; the circles are cross-section of the carbon fibers. The outlined areas denote different polygonal networks: $N=3, 4, 5,$ and 6 . (b). Shows fibers in an infinite triangular lattice, here number of polygon sides $N=3$ and the coordination number for this lattice $Z=6$.

The origin of type of topological defects or super-disclinations (i.e. group of disclinations) that may arise within these polygons [11] is not well understood. The texture within the polygon of N sides τ^N can be characterized by

$$\tau^N = \Psi(n, D_c, C_h, R) \quad (5.1)$$

n is the number of wedge disclinations, D_c is the type of disclination core, C_h represents the total charge of the super-disclination, and R is the fiber radius. In nematic liquid crystals the defect core type can be singular or nonsingular (also known as escaped core [12]); in the former the defect core is characterized by a complex radial nano-scale gradient in the molecular order parameters, while in the latter the director escapes into the third dimension forming a macroscopic core region. A summary of experimental texture results [13] for c/c microcomposites is shown in Table I; the results indicate that the texture pattern is:

$$\tau^{N=\text{even}} = \Psi(n, D_c^E, -(N-2)/2, R \approx \mu m), \tau^{N=\text{odd}} = \Psi(n, D_c^S, -(N-2)/2, R \approx \mu m)$$

The objective of this letter is to use theory and simulation to explain the texture selection mechanisms, shown in Table I, and to establish the role of fiber size on texture selection: $\tau^N = \tau^N(R)$ in these multiple fiber arrangements. Although due to available experimental data [13] we focus on discotic nematic carbonaceous mesophases as the model material, the results are applicable to other uniaxial nematic materials.

Table 5-1: Experimental Textures [13] for c/c composites

Array	Strength	Core Structure
Triangular	-1/2	Singular
Square	-1	Escape
Pentagonal	-3/2	Singular
Hexagonal	-2	Escape

The number of disclinations in FNs is restricted by the Poincaré-Brouwer theorem, which dictates the number of singularities in polygonal planar vector fields [14]. The type of disclinations is governed by texture energies [15]. The minimization of texture energy proceeds by two mechanisms: (a) split of high strength singular core disclinations into multiple low strength singular core disclinations, and (b) instability of singular disclinations

of integral strength due to director escape into the third dimension; this mechanism drives the production of non-singular lines of integral strength. The presented computational results based on the Landau-de Gennes liquid crystal model allows to quantify the impact of these three rules in texture selection in real fiber-filled nematics [13], and show if the energy minimization process satisfies topological stability rules that state that for nematics, the only topological stable singular lines are of strength $s = \pm 1/2$

We start by using Poincaré-Brouwer theorem to establish $\tau^N = \Psi(C_h)$ and hence the relation between number of particles N and total charge C_h . The disclination charge of a planar director field within a polygon is equal to its Euler characteristic χ [14]:

$$\sum_i s_i = F_c - E + V = \chi \quad (5.2)$$

where s_i { $i=F_c, E, V$ } is the disclination strength, F_c the number of faces, E the number of edges, and V the number of vertices. For a network of N sides polygons and coordination number Z an example of which is shown schematically in fig. 5-1b, the relations $E=VZ/2$, $F_c=VZ/N$ hold. Using Euler's theorem in 2D ($F_c-E+V=1$) we find for an infinite polygonal network: $Z/N=2/(N-2)$. Replacing Z/N into eqn. (5.2) we find that for an infinite network in the absence of edge defects ($s_E = 0$): $s_{F_c} = -s_V (N - 2) / 2$. For the present homeotropic anchoring, each circular fiber has a charge $s_V=+1$, and hence $s_{F_c} = -(N - 2) / 2$, which explains the observed functionality between N and C_h . (See Table I and [13]). For example, for $N=5$, $s_{F_c} = -3/2$ [13]. This simple analysis shows that real textures [13] do obey the Poincaré-Brouwer theorem.

To establish how all the elements of the texture $\tau^N = \Psi(n, D_c, R)$ depend on the number of particles N we must use computational modeling. The model system consists of N cylinders of radius R suspended inside the liquid crystalline matrix. We only need to consider single polygonal lattices, $N=3, 4, 5, 6$, in conjunction with periodic boundary

conditions. The length scales are: fiber radius (R), center to center distance between two fibers (L), and the system size (H). We are interested in concentrated FNs, and use a constant and representative packing fraction of $L/R=2.3$. By varying R at constant L/R , the distance between the fibers changes but geometric self-similarity is preserved. Results for low and intermediate packing fractions are not discussed. It is well-known that for μm carbon fibers, strong homeotropic anchoring prevails [16, 17]. In addition it was demonstrated [18] that strong anchoring in these materials persists to approximately 100 nm glass cavities, and motivated by this result we retain the strong anchoring assumption in all our simulations. We recall that all experimental results are for μm fibers [13]. The nematic order of the mesophase is represented by the second order symmetric tensor order parameter $\mathbf{Q}(r, t)$ [19]. The eigenvectors or director triad $(\mathbf{n}, \mathbf{m}, \mathbf{l})$ describe macroscopic orientation, and eigenvalues of \mathbf{Q} are related to the uniaxial and biaxial molecular order parameters (S, P), which describe the degree of molecular order. The evolution of \mathbf{Q} in the absence of flow is determined by the Volterra variational derivative of the total free energy F with respect to the tensor order parameter:

$$-\gamma(\mathbf{Q})\frac{d\mathbf{Q}}{dt} = \left(\frac{\delta F}{\delta \mathbf{Q}}\right)^{[s]} \quad (5.3)$$

Here γ represents the rotational viscosity and [s] implies symmetric and traceless property. In Landau-de Gennes theory the dimensionless free energy density f^* can be expressed in terms of homogenous f_h^* and the gradient f_g^* contributions (under one constant assumption ($L_2=L_3=0$) for simplicity)

$$F^* = \int_{V^*} f^* dV^* = \int_{V^*} (R^{*3}f_h^* + R^*f_g^*) dV^* \quad (5.4)$$

$$f_h^* = \frac{1}{2} \left(1 - \frac{U}{3} \right) (\mathbf{Q} : \mathbf{Q}) - \frac{U}{3} \mathbf{Q} : (\mathbf{Q} \cdot \mathbf{Q}) + \frac{U}{4} (\mathbf{Q} : \mathbf{Q})^2 \quad (5.5)$$

$$f_g^* = \left(\frac{1}{2} \nabla_\alpha^* \mathbf{Q}_{\beta\gamma} \nabla_\alpha^* \mathbf{Q}_{\beta\gamma} \right) \quad (5.6)$$

where * indicates dimensionless quantities [20]. The coefficient U is a dimensionless temperature; $U=8/3$ corresponds to the isotropic-nematic transition. The correlation length $\xi = \sqrt{\frac{L_1}{\varphi k_B T}}$ is of molecular length size, L_1 is elastic constant [19] and T is the temperature. φ , k_B are number density of molecules and Boltzmann's constant respectively. The term $R^* = R/\xi$ is the dimensionless radius of the fiber. Since the value of ξ is of the order of $10 \sim 20nm$ [3] we choose R^* from 40 to 300 (representative of fiber radius $R = 400nm$ to $3\mu m$). We consider cylindrical fibers dispersed in the isotropic state $\mathbf{Q} \approx \mathbf{0}$, and then perform a thermal quench ($U < 8/3 \rightarrow U = 3.5$) to simulate texture formation. At all internal interfaces we impose strong anchoring: $\mathbf{Q}_0 = S_{eq}(\delta_r \delta_r - \frac{1}{3} \delta)$; here δ_r is the radial unit outward normal at the fiber surface and S_{eq} is the equilibrium scalar order parameter of the bulk nematic and in dimensionless units is expressed as $S_{eq} = \frac{1}{4} + \frac{3}{4} \sqrt{1 - \frac{8}{3U}}$ [20].

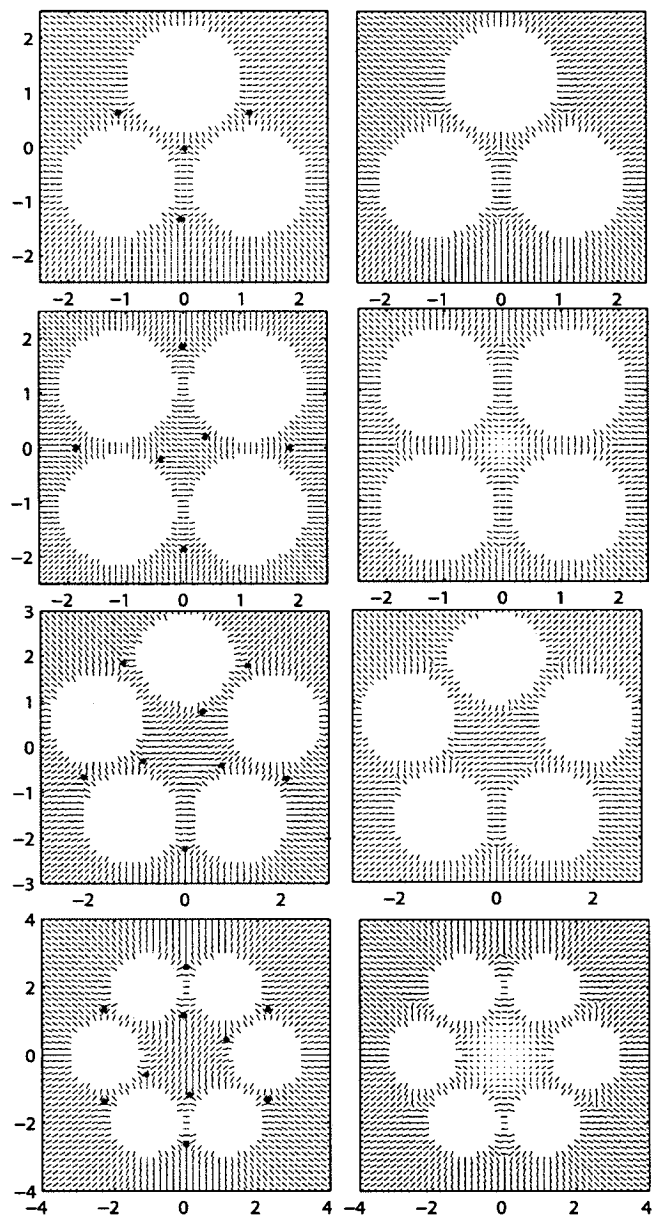


Figure 5-2: Summary of computational results for submicron (left column) and micron fiber results. Different scales are selected for clarity. See text.

A summary of representative numerical results are shown in Figure 5-2. The computed visualizations are for the director orientation (short arrows) which are superposed on the scalar order parameter S , given in terms of gray scale (white is $S=S_{eq}=0.616$, black is $S=0$); in all visualizations dark dots are singular defect cores and escaped non-singular cores show no changes in order parameter and therefore are white.

The left column corresponds to submicron fibers ($R/\xi < 100$) and the right column to micron fibers ($R/\xi > 100$). For submicron fibers we find:

$\tau^{\text{even}} = \tau^{\text{odd}} = \Psi(N-2, D_c^S, -(N-2)/2)$, the number of defects is $N-2$, all disclinations are singular, the total charge follows the Poincaré-Brouwer result of $(N-2)/2$, defect splitting removes high charge lines, and the topological stability rule is obeyed since only stable singular cores of $s=-1/2$ are observed. For micron fibers we find:

$$\tau^{\text{even}} \neq \tau^{\text{odd}}, \tau^{\text{even}} = \Psi(1, D_c^E, -(N-2)/2), \tau^{\text{odd}} = \Psi(N-2, D_c^S, -(N-2)/2)$$

For even number of particles there is a single defect with an escaped core, of charge $-(N-2)/2$; for example for six particle configuration the disclination has a charge of -2 . For odd number of particles, the $N-2$ disclinations have singular cores of strength $-1/2$ and the total charge is $-(N-2)/2$. For all micron fiber-based polygons, Poincaré-Brouwer theorem is obeyed, defect splitting operates for odd polygons, escape into third dimension removes singular cores of integral strength, and topological stability rules are fulfilled. The main distinction between submicron and micron fibers occurs for even number of particles, where the former displays $N-2$ singular core disclination and the latter a single escaped core high strength disclinations. To establish the texture selection driving force for even number of particles we compute the total gradient elasticity in the system (integral of eqn. (5-6)), since this energy will be responsible for transition between singular and escaped core disclinations [19]. Figure 5-3 shows a representative computation of the dimensionless gradient energy as a function of dimensionless fiber radius, for $N=4$; it

shows that submicron fibers display singular multiple $s = -1/2$ defects while micron fibers display one escape core $s = -1$ disclination; the cross-over is approximately $R^* = 120$. Our results are in excellent agreement with experiments [13] and with well-known geometry-driven transitions between singular and escape cores [19]. Using the instability theorem for integral lines for a capillary of radius R_c , the transition between escape-singular defect occurs at $R_c^* \sim 20$ [19]; computing an equivalent capillary radius from the inner circle tangent to the four fibers we find using the integral theorem that $R^* \sim 37$; this deviation is due to the more complex internal surface geometry of the present multi-fiber structure as opposed to the circular capillary geometry.

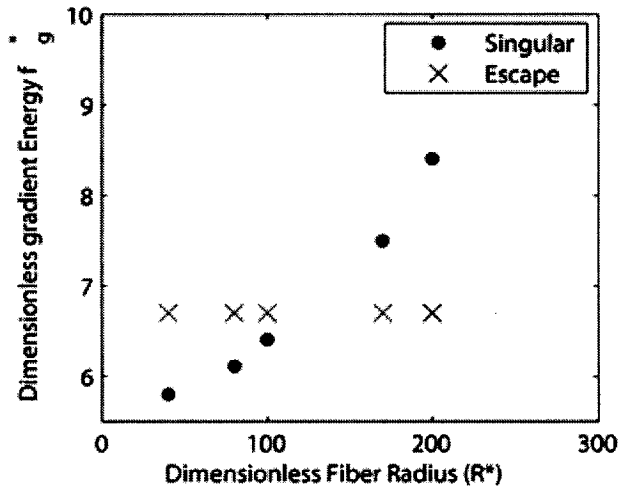


Figure 5-3: Dimensionless gradient elasticity as a function of dimensionless fiber radius R^* , for $N=4$, $U=3.5$. See text.

Experiments [13] shows that for $N=5$, high order $s = -3/2$ singular disclinations are observed, in contrast to our computational results (see third row, right column in Fig.(5.2)), which shows that the stable selected state are three $s=-1/2$ singular disclinations. Several

mechanisms may explain the presence of the $s = -3/2$ line at higher temperature, including saddle-splay energy [15], elastic anisotropy [19], viscosity divergence [17], and defect splitting kinetics for $s = -3/2(\textit{singular}) \rightarrow 3s = -1/2(\textit{singular})$. We note that heating carbonaceous mesophases at high temperatures produces a very viscous melt and eventually a solid phase [17]. The present model always predicts at the early stage, $s=-3/2$ defect is created, which subsequently splits. Figure 5-4 shows the increase of the computed dimensionless splitting time with increasing dimensionless temperature U , a kinetic effect that is compatible with the observed viscosity divergence [17].

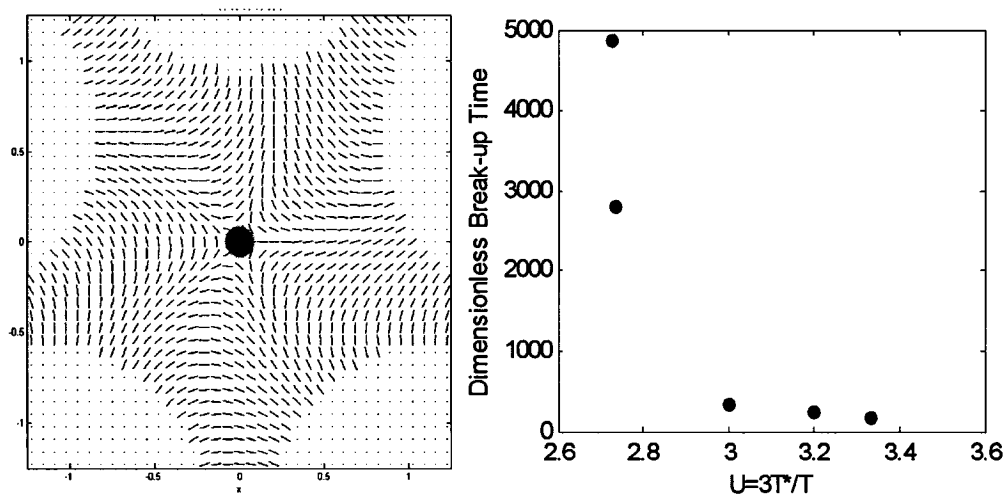


Figure 5-4: (a) Computed enlarged view of a $s = -3/2$ singular disclination line, for $N=5$, $U=3.5$, at intermediate time $t^* = 600$. See text. (b) Dimensionless splitting time as a function of nematic potential U . The slow-down is driven by proximity to the nematic-isotropic transition temperature.

In summary, we have used differential geometry and computational modeling to analyze texture selection rules in multi-fiber filled nematic mesophases. Three defect physics rules, including the Poincaré-Brouwer theorem, the instability theorem for integral lines

and energy minimization by defect-splitting are shown to operate in actual texture selection of c/c composites based on micron-sized fibers [13]. Computational predictions for submicron fibers show that regardless of packing geometry, only singular and topologically stable $-1/2$ will be observed. The findings provide a robust theoretical framework for a theory of composites involving oriented matrices.

The research was supported by a grant from Engineering Research Center program of National Science Foundation under award number EEC 9731680. The authors would like to thank Dr. J. Zimmer for providing experimental data to validate their results.

References

1. M. Kreuzer and R. Eidenschink, in *Liquid Crystals in Complex Geometries*, edited by G. P. Crawford and S. Zumer (Taylor and Francis, London, 1996), Chap. 15.
2. J. Rault, P.E. Cladis, and J. P. Burger, *Phys. Lett. A*, *32*, 199 (1970).
3. H. Stark. *Phys. Reports*, *351*, 387 (2001).
4. J. L. White, and P. M. Sheaffer, *Carbon* *27*, 697 (1989)
5. S. Torquato, *Random Heterogenous Materials: Microstructure and Macroscopic Porperties* (Springer-Verlag, New York, 2002).
6. O. Guzmán, E. B. Kim, S. Grollau, N. L. Abbott, and J. J. de Pablo, *Phys. Rev. Lett.* *91*, 235507 (2003).
7. N.M. Silvestre, P. Patricio, M. Tasinkevych, D. Andrienko, and M.M.T. da Gama, *J. Phys. Cond. Matter.* *16*, 19 (2004).
8. P. Poulin, H. Stark, T.C. Lubensky, and D.A. Weitz, *Science* *275*, 1770 (1997).
9. Y.Ch. Loudet, P. Barois, and P. Poulin, *Nature (London)* *407*, 611 (2000).
10. V.G. Nazarenko, A.B. Nych, and B.I. Lev, *Phys. Rev. Lett.* *87*, 075504 (2001)
11. P. Galatola, and J.B. Fournier, *Phys. Rev. Lett.* *86*, 3915 (2001).
12. P. E. Cladis, and M. Kleman, *Journal de Physique* *33*, 591 (1972); R. B. Meyer, *Phil. Mag.* *27*, 405 (1973).
13. J.E. Zimmer and R.L. Weitz, in *Extended Abstracts 16th Biennial Conference on Carbon. American Carbon Society*, 1983, p. 92.
14. R. S. Millman, and G. D. Parker, *Elements of Differential Geometry* (Prentice-Hall, Englewood Cliffs, NJ, 1997); R. D. Kamien, *Rev. Mod. Phys.*, *74*, 953 (2002).
15. M. Kleman, and O.D. Lavrentovich, *Soft Matter Physics* (Springer, New York, 2003).
16. R. H. Hurt and Z. Y. Chen, *Physics Today* *53*, 39-59 (March 2000).

17. J. E. Zimmer and J. L. White, *Advances in Liquid Crystals: Disclination structures in carbonaceous mesophase 5* , 157-213 (1982).
18. Christopher Chan et. al. *Carbon (in press)* .
19. P. G. de Gennes and J. Prost, *The Physics of Liquid Crystals* (Clarendon Press, Oxford, 1993).
20. G. Gupta, D. K. Hwang, and A. D. Rey, *J. Chem. Phys.* . 122, 034902 (2005).

CHAPTER 6

Conclusions

A model used to describe texture formation in carbon fiber /carbon mesophase composites has been formulated, solved and validated with existing experimental data. The computational and theoretical study based on the Landau de Gennes theory for liquid crystals is able to replicate commonly observed textures in these composites.

The model is able to predict the defect lattice structure observed in experiments done to manipulate mesophase texture. The model predicts the formation of a disclination network of square symmetry, composed of square lattice array of $+2\pi$ and an array of $-\pi$ disclinations that lie along the diagonals of the square lattice. A reflection polarized optical microscopy model was implemented and solved to validate the texture with experiments. A comparison between experiments and simulations show excellent quantitative agreement.

The model for CF/CM composite captures the texturing effect induced by micron-sized fibers embedded in the mesophase. A concentrated fiber regime study shows relation of the type of defect to specific fiber arrangement. Three fiber configuration leads to a $s = -\frac{1}{2}$ defect, while four fiber configuration lead to $s = -1$ defect. A detailed study of the effect of fiber configurations in high concentrated regime is also carried out. Three defect physics rules, including the Poincaré-Brouwer theorem, the instability theorem for integral lines and energy minimization by defect-splitting are shown to operate in actual texture selection of c/c composites based on micron-sized fibers. A study of submicron sized fibers indicates that only singular defects are created regardless of the fiber configuration.

The computational study performed in this thesis provides new and significant insights and a better fundamental understanding of the role of processing and geometric conditions

on texture formation in carbonaceous materials. The thesis shows that defect lattices can be long-lived structures that once formed remain in the system regardless of thermal processing. The thesis also shows that control of defect distributions in *c/c* composites is possible through fiber packing densities, fiber-matrix interfacial conditions, fiber sizes, and temperature. Large fibers at high packing fractions and sufficiently low temperatures tend to form textures with small number of singular defects. Nano-fibers at high packing fractions tend to produce large number of singular defects. Mechanical properties of *c/c* composites can then be manipulated through careful control of thermal and geometric conditions.

Future work should extend the simulations to other interfacial *c/c* conditions, other fiber size distributions, and other fiber densities. On the computational side, automatic remeshing, and optimized 3D simulation codes will provide a better understanding of texture formation in *c/c* composites.

APPENDIX A

This appendix is to summarize the constitutive equation and lists the parameters used in simulating the different cases studied in this thesis.

The dimensionless, coupled, time dependent, non-linear partial differential tensor equation that was solved using commercially available finite element software package FEMLAB[®] is:

$$\begin{aligned}
 -\gamma(\mathbf{Q}) \frac{dQ_{ij}}{dt} &= \left(1 - \frac{U}{3}\right) Q_{ij} - U Q_{i\alpha} Q_{j\alpha} + \frac{U}{3} Q_{\beta\alpha} Q_{\alpha\beta} \delta_{ij} + U Q_{\alpha\beta}^2 Q_{ij} \\
 &+ \frac{\xi^2 \kappa}{2H^2} \left(\nabla_i^* Q_{\gamma\delta} \nabla_j^* Q_{\gamma\delta} \right) - \frac{\xi^2 \kappa}{6H^2} \left(\nabla_o^* Q_{\gamma\delta} \nabla_o^* Q_{\gamma\delta} \right) \delta_{ij} - \nabla_l^* \frac{\xi^2}{H^2} \left(\nabla_l^* Q_{ij} \right) \\
 &- \nabla_l^* \frac{\xi^2 \vartheta}{2H^2} \left(\left(\nabla_\alpha^* Q_{\alpha j} \right) \delta_{li} + \left(\nabla_\alpha^* Q_{\alpha i} \right) \delta_{lj} \right) + \nabla_l^* \frac{\xi^2 \vartheta}{3H^2} \left(\left(\nabla_\alpha^* Q_{\alpha o} \right) \delta_{lo} \right) \delta_{ij} \\
 &\quad - \nabla_l^* \frac{\xi^2 \kappa}{H^2} \left(Q_{\alpha l} \nabla_\alpha^* Q_{ij} \right)
 \end{aligned} \tag{A-1}$$

The above equation was implemented in FEMLAB's general PDE mode. In this mode the partial differential equations have to be written in the form:

$$d_a \frac{\partial \mathbf{u}}{\partial t} = \nabla \cdot \mathbf{\Gamma} + F \tag{A-2}$$

Since \mathbf{Q} is symmetric and traceless, the dependent variables of the problem are the five components of tensor \mathbf{Q} . For FEMLAB implementation q_1, q_2, q_3, q_4, q_5 correspond to $Q_{11}, Q_{12}, Q_{13}, Q_{22}, Q_{23}$ components of the $\mathbf{Q}=\mathbf{u}$ tensor respectively. The expanded terms in FEMLAB then become:

$$\Gamma_{11X} = 1/3 * e h^2 * ((3+2 * v) * q_{1x} + 2 * v * q_{2y} + 3 * k * q_1 * q_{1x} + 3 * k * q_2 * q_{1y})$$

$$\Gamma_{11y} = 1/3 * e h^2 * (3 * q_{1y} - v * q_{2x} - v * q_{4y} + 3 * k * q_2 * q_{1x} + 3 * k * q_4 * q_{1y})$$

$$\Gamma_{12X} = 1/2 * e h^2 * ((2+v) * q_{2x} + v * q_{4y} + 2 * k * q_1 * q_{2x} + 2 * k * q_2 * q_{2y})$$

$$\Gamma_{12y} = 1/2*eh^2*(2*q2y+v*q1x+v*q2y+2*k*q2*q2x+2*k*q4*q2y)$$

$$\Gamma_{13X} = 1/2*eh^2*((2+v)*q3x+v*q5y+2*k*q1*q3x+2*k*q2*q3y)$$

$$\Gamma_{13y} = eh^2*(q3y+k*q2*q3x+k*q4*q3y)$$

$$\Gamma_{22X} = 1/3*eh^2*(3*q4x-v*q1x-v*q2y+3*k*q1*q4x+3*k*q2*q4y)$$

$$\Gamma_{22y} = 1/3*eh^2*(2*v*q2x+(3+2*v)*q4y+3*k*q2*q4x+3*k*q4*q4y)$$

$$\Gamma_{23X} = eh^2*q5x+eh^2*k*(q1*q5x+q2*q5y)$$

$$\Gamma_{23y} = 1/2*eh^2*(2*q5y+v*q3x+v*q5y+2*k*q2*q5x+2*k*q4*q5y)$$

The corresponding F terms are:

$$\begin{aligned} F11 = & (q1-1/3*q1*U-1/3*U*q1^2-1/3*U*q2^2-1/3*U*q3^2 \\ & +2/3*U*q4^2+2/3*U*q1*q4+2/3*U*q5^2+2*U*(q1^2 \\ & +q4^2+q1*q4+q2^2+q3^2+q5^2)*q1-1/3*eh^2*k*(-2*q1x^2 \\ & -2*q1x*q4x-2*q4x^2-2*q2x^2-2*q3x^2-2*q5x^2+q1y^2 \\ & +q4y^2+q1y*q4y+q2y^2+q3y^2+q5y^2)) \end{aligned}$$

$$\begin{aligned} F12 = & ((1-1/3*U)*q2-U*(q1*q2+q2*q4+q3*q5)+2*U*(q1^2+q4^2+q1*q4+q2^2 \\ & +q3^2+q5^2)*q2-1/2*eh^2*k*(2*q1y*q1x+2*q4x*q4y+q1x*q4y+q1y*q4x \\ & +2*q2x*q2y+2*q5x*q5y+2*q3x*q3y)) \end{aligned}$$

$$F13 = (q3-1/3*q3*U-U*q2*q5+U*q3*q4+2*U*(q1^2+q4^2+q1*q4+q2^2+q3^2+q5^2)*q3)$$

$$\begin{aligned} F22 = & (q4-1/3*q4*U-1/3*U*q2^2-1/3*U*q4^2-1/3*U*q5^2+2/3*U*q1^2+2/3*U*q1*q4 \\ & +2/3*U*q3^2+2*U*(q1^2+q4^2+q1*q4+q2^2+q3^2+q5^2)*q4+1/3*eh^2*k*(2*q1y^2 \\ & +2*q4y^2+2*q1y*q4y+2*q2y^2+2*q5y^2+2*q3y^2-q1x^2-q1x*q4x-q4x^2 \end{aligned}$$

$$-q2x^2-q3x^2-q5x^2))$$

$$F23=(q5-1/3*q5*U-U*q3*q2+U*q5*q1+2*U*(q1^2+q4^2+q1*q4+q2^2+q3^2+q5^2)*q5)$$

The parameters chosen to simulate the cases studied in this thesis are as follows:

1. Study of Periodic disclination Lattices in Carbonaceous Mesophase(Chapter 3):

$$\text{Equilibrium Scalar Order Parameter: } S_{eq} = 0.62$$

$$\text{Initial Scalar Order Parameter: } S_0 = 1^{-10}$$

$$\text{Biaxial Order Parameter: } P = 0$$

$$\text{Nematic Potential: } U=3.5$$

$$\text{Dimensionless Radius (R*): } \frac{\xi^2}{H^2} = 0.01$$

$$\text{Dimensionless Elastic Constants: } \vartheta, \kappa = 0$$

$$\text{Rotational Viscosity: } \gamma(\mathbf{Q}) = 1$$

2. Defect study in C/C Composites (Chapter 4)

$$S_0 = 1^{-10}$$

$$P = 0$$

$$U=3.5$$

$$\frac{\xi^2}{H^2} = 0.01$$

$$\vartheta, \kappa = 0$$

3. Defect study of concentrated Filled Nematics (Chapter 5)

$$S_0 = 1^{-10}$$

$$P = 0$$

$U=3.5$

from $\frac{\xi^2}{H^2} = 0.0033$ (for micron sized fibers); $\frac{\xi^2}{H^2} = 0.025$ (for nano sized fibers)

$\vartheta, \kappa = 0$